UNIVERSITY OF CALIFORNIA, SAN DIEGO

Diagnostic Structural Health Assessment Through Layered Integration of Non-destructive Imaging Data

A dissertation submitted in partial satisfaction of the
requirements for the degree
Doctor of Philosophy

in

Structural Engineering

by

Michael Robert Hess

Committee in charge:

Falko Kuester, Chair
Tara C. Hutchinson
Ryan Kastner
Dominique A. Rissolo
Michael D. Todd
Mohan M. Trivedi

2018

The Dissertation of Michael Robert Hess is approved, and it is acceptable in quality and form for publication on microfilm and electronically:

Chair

University of California, San Diego

2018

DEDICATION

For my parents:

TABLE OF CONTENTS

LIST OF FIGURES

LIST OF TABLES

NOMENCLATURE

The following section provides a list of variables and parameters used in this dissertation, in alphabetical order. Note that the base dimensions include: mass (M), force (F), length (L), and time (T).

Symbol	**Description**	**Base Units**
E	Young's modulus of elasticity	F/L^2
G	Shear modulus	F/L^2
ν	Poisson's Ratio	Dimensionless
ρ	Mass density of a material	M/L^3
σ_y	Yield stress	F/L^2

ACKNOWLEDGEMENTS

The research and experiments presented in this dissertation were supported by numerous individuals and organizations. First, I would like to express my sincere gratitude to my advisor, Professor Falko Kuester, for the granting me the flexibility and opportunity to pursue research into such an interdisciplinary field. With his support, I have been able to travel nationally and internationally to present my research as well as to conduct fieldwork in Italy and Mexico. I would also like to thank my committee members, Professors Tara C. Hutchinson, Michael Todd, Mohan Trivedi and Ryan Kastner, for their time, feedback and guidance throughout my research process.

The fieldwork conducted as a part of this dissertation were made possible by dedication and support of many individuals and organizations including Alex Hubenko and Vanessa Pool of UC San Diego, Dr. Maurizio Seracini in Florence, Italy, Dr. Dominique Rissolo, Centro INAH Quintana Roo, Adriana Velazquez Morlet, Opera di Santa Maria del Fiore and President Franco Lucchesi. Also at UC San Diego, I would like to thank my classmates and fellow researchers for their help and support including Mr. Vid Petrovic, Ms. Ashley Richter, Mr. Dominique Meyer, Ms. Rebecca Napolitano, Mr. Eric Lo, Mr. John Mangan, Dr. Christine Wittich, Dr. Michael Yeager, Ms. Michelle Chen, Dr. Chris Trautner and Mr. Frank Beckwith.

Last, but certainly not the least, I would like to thank my family for their unending support, including my fiancé Emily, my parents Rick and Michelle, my brother Tommy, and my sisters Carisa and Susan. I would especially like to thank Emily for coming with me on this crazy journey to San Diego to pursue a graduate degree, for the love and support though this whole process, and for being an incredible inspiration, partner, role model, and friend. And of course, mom and dad, this dissertation is ultimately dedicated to you because without your love, guidance and support for twenty-eight years, I would not be where I am today. Thank you for everything.

The research program described in this dissertation was financially supported by the National Science Foundation under IGERT Award #DGE-0966375, "Training, Research, and Education in Engineering for Cultural Heritage Diagnostics." Additional support for this research included the National Science Foundation under award #CNS-1338192, "MRI: Development of Advanced Visualization Instrumentation for the Collaborative Exploration of Big Data," the UC San Diego Academic Senate, the Qualcomm Institute at UC San Diego, the Friends of CISA3, and the World Cultural Heritage Society. Opinions, findings, and conclusions are those of the author and do not reflect those of the sponsoring agencies.

Multiple sections and chapters of this dissertation have been published or will be submitted for potential publication in technical journals or conference proceedings. The dissertation author was the first author and primary investigator for each of these publications. Each is summarized in the following paragraphs.

Chapter 3, in part, is a reprint of the material as it appears in the Journal of Structure and Infrastructure Engineering. Hess, M., Petrovic, V., Yeager, M. and Kuester, F. (2017). "Terrestrial laser scanning for the comprehensive structural health assessment of the Baptistery di San Giovanni in Florence, Italy: an integrative methodology for repeatable data acquisition, visualization and analysis" *Structure and Infrastructure Engineering*, 1-17.

Section 3.2.3 in part, is a reprint of the material as it appears in the International Archives of the Photogrammetry, Remote Sensing & Spatial Information Sciences. Hess, M., Petrovic, V., & Kuester, F. (2017). "Interactive Classification of Construction Materials: Feedback Driven Framework For Annotation and Analysis of 3D Point Clouds" *International Archives of the Photogrammetry, Remote Sensing & Spatial Information Sciences*, (Vol. 42, pp. 343-347).

Chapter 4, in part, is a reprint of the material as it appears in the Journal of Infrared Physics & Technology. Hess, M., Vanoni, D., Petrovic, V. and Kuester, F. (2015). "High-resolution thermal imaging methodology for non-destructive evaluation of historic structures" *Infrared Physics & Technology*, 73, 219-225.

Chapter 5, in part, is a reprint of the material as it appears in the Proceedings of the 2014 IEEE International Conference on Imaging Systems and Techniques (IST). Hess, M., Kuester, F. and Trivedi, M. (2014). "Multimodal registration of high-resolution thermal image mosaics for the non-destructive evaluation of structures." In *Imaging Systems and Techniques (IST), 2014 IEEE International Conference on*, 216-221.

Chapter 6, in part, is a reprint of the material as it appears in Digital Heritage, 2015. Vol. 2. Hess, M., Petrovic, V., Meyer, D., Rissolo, D. and Kuester, F. (2015). "Fusion of multimodal three-dimensional data for comprehensive digital documentation of cultural heritage sites." In *Digital Heritage, 2015*, vol. 2, 595-602.

VITA

EDUCATION

2012	B.S., Civil Engineering, cum laude Northeastern University, Boston, MA
2014	M.S., Structural Engineering University of California, San Diego, La Jolla, CA
2016-2017	Teaching Assistant, Department of Structural Engineering University of California, San Diego, La Jolla, CA
2018	Ph.D., Structural Engineering University of California, San Diego, La Jolla, CA

AWARDS & FELLOWSHIPS

2013-2016	NSF-IGERT Fellowship
2017	PWC Research Support
2018	US Army Core of Engineers Support

FIELDWORK

2013	Florence, Italy: Baptistery di San Giovanni, Palazzo Vecchio, Palazzo Rucellai
2013	Calabria, Italy: Castello Svevo, Santuario di Santa Maria di Anglona
2014	Quintana Roo, Mexico: 16th Century church, Cave shrine
2014	San Diego, CA USA: Museum of Man
2014	Florence, Italy: Baptistery di San Giovanni, Santa Maria del Fiore Cathedral
2016	Yucatan, Mexico: Site of Oxkintok, Tzat Tun Tzat Labyrinth

PUBLICATIONS

Journal Papers (In Print)

Hess, M., Petrovic, V., Yeager, M., & Kuester, F. (2017). Terrestrial laser scanning for the comprehensive structural health assessment of the Baptistery di San Giovanni in Florence, Italy: an integrative methodology for repeatable data acquisition, visualization and analysis. Structure and Infrastructure Engineering, 1-17.

Hess, M., Vanoni, D., Petrovic, V., & Kuester, F. (2015). High-resolution thermal imaging methodology for non-destructive evaluation of historic structures. Infrared Physics & Technology, 73, 219-225.

Refereed Conference Proceedings

Hess, M., Petrovic, V., & Kuester, F. (2017). Interactive Classification of Construction Materials: Feedback Driven Framework For Annotation and Analysis of 3D Point

Clouds. *International Archives of the Photogrammetry, Remote Sensing & Spatial Information Sciences*, (Vol. 42, pp. 343-347).

Rissolo, D., Lo, E., **Hess, M.**, Meyer, D. E., & Amador, F. E. (2017). DIGITAL PRESERVATION OF ANCIENT MAYA CAVE ARCHITECTURE: RECENT FIELD EFFORTS IN QUINTANA ROO, MEXICO. *International Archives of the Photogrammetry, Remote Sensing & Spatial Information Sciences*, (Vol. 42, pp. 613-616).

Bianchini, C., **Hess, M.**, Inglese, C., & Ippolito, A. (2017). Quality or Quantity: The Role of Representation in Archaeological Architecture. *In New Activities for Cultural Heritage* (pp. 150-157). Springer, Cham.

Rissolo, D., **Hess, M.**, Hoff, A., Meyer, D., Amador, F., Morlet, A. V., Petrovic, V., & Kuester, F. (2016). Imaging and Visualizing Maya Cave Shrines in Northern Quintana Roo, Mexico. *In 8th International congress on archaeology, computer graphics, cultural heritage and innovation* (pp. 382-384). Editorial Universitat Politècnica de València.

Hess, M., Petrovic, V., Meyer, D., Rissolo, D., & Kuester, F. (2015, September). Fusion of multimodal three-dimensional data for comprehensive digital documentation of cultural heritage sites. In Digital Heritage, 2015 (Vol. 2, pp. 595-602). IEEE.

Mangan, J., **Hess, M.,** & Kuester, F. (2015, September). A role-based methodology for data-driven workflows, and Nephelai: A scalable infrastructure which enables it. In Digital Heritage, 2015 (Vol. 2, pp. 413-416). IEEE.

Meyer, D., **Hess, M.,** Lo, E., Wittich, C. E., Hutchinson, T. C., & Kuester, F. (2015, September). UAV-based post disaster assessment of cultural heritage sites following the 2014 South Napa Earthquake. In Digital Heritage, 2015 (Vol. 2, pp. 421-424). IEEE.

Hess, M., Kuester, F., & Trivedi, M. (2014, October). Multimodal registration of high-resolution thermal image mosaics for the non-destructive evaluation of structures. In Imaging Systems and Techniques (IST), 2014 IEEE International Conference on (pp. 216-221). IEEE.

Hess, M., Meyer, D., Hoff, A., Rissolo, D., Guillermo, L. L., & Kuester, F. (2014, November). Informing historical preservation with the use of non-destructive diagnostic techniques: a case study at Ecab, Quintana Roo, Mexico. In Euro-Mediterranean Conference (pp. 659-668). Springer, Cham.

Presentations

Hess, M., Petrovic, V., & Kuester, F. (2017, August). Interactive Classification of Construction Materials: Feedback Driven Framework for Annotation and Analysis of 3D Point Clouds. Paper presented at: CIPA 2017. International Committee of Architectural Photogrammetry (CIPA), Ottawa, Canada.

Hess, M. (2017, March). Non-Destructive Techniques for the Structural Health Assessment of Historic Buildings. Paper presented at: CAA 2017. Computer Applications and Quantitative Methods in Archaeology (CAA), Atlanta, GA, USA.

Meyer, D., Guerra, G., Lo, E., **Hess, M.,** Forcellini, D., and Kuester F. (2017, March). Comparing Measured Frequency Responses of the Third Tower of San Marino to Simulation Derived Frequency Responses from a Photogrammetry and LIDAR Acquired 3D Model. Paper

presented at: CAA 2017. Computer Applications and Quantitative Methods in Archaeology (CAA), Atlanta, GA, USA.

Hess, M. (2016, May). Informing Historical Preservation with the Use of 2D and 3D Non-destructive Imaging Techniques: A Case Study at the Site of Ecab, Quintana Roo, Mexico. Paper presented at: AACCP 2016. Architecture, Archaeology and Contemporary City Planning (AACCP), Cancun, Mexico.

Hess, M., Yeager, M., Petrovic, V., and Kuester, F. (2016, March). Fusion of 2D and 3D Imaging Data for the Non-Destructive Assessment of the Baptistery di San Giovanni in Florence, Italy. Paper presented at: CAA 2016. Computer Applications and Quantitative Methods in Archaeology (CAA), Oslo, Norway.

Meyer, D. E., Hodgkins, J., Negrino, F., Miller, C. E., Orr, C. M., Kuester, F., Benazzi, S., Peresani, M., Riel-Salvatore, J., Strait, D., Czechowski, M., Smirnova, V., **Hess, M.** (2016, March). Optimization in the Co-Registration of Large Point Clouds for Archaeological Visualization. Paper presented at: CAA 2016. Computer Applications and Quantitative Methods in Archaeology (CAA), Oslo, Norway.

Hess, M., Petrovic, V., Rissolo, D., & Kuester, F. (2016, January). Multimodal Diagnosis of Historic Baptistery di San Giovanni in Florence, Italy. Paper presented at: SHA 2016. 49th Annual Conference on Historical and Underwater Archaeology, Washington, D.C., USA.

Hess, M., Petrovic, V., Rissolo, D., & Kuester, F. (2015, September). Fusion of Multimodal Three-dimensional Data for Comprehensive Digital Documentation of Cultural Heritage Sites. Paper presented at: Digital Heritage 2015. 2nd Digital Heritage International Congress, Granada, Spain.

Mangan, J., **Hess, M.,** & Kuester, F. (2015, September). A role-based methodology for data-driven workflows, and Nephelai: A scalable infrastructure which enables it. Paper presented at: Digital Heritage 2015. 2nd Digital Heritage International Congress, Granada, Spain.

Meyer, D., **Hess, M.,** Lo, E., Wittich, C. E., Hutchinson, T. C., & Kuester, F. (2015, September). UAV-based post disaster assessment of cultural heritage sites following the 2014 South Napa Earthquake. Paper presented at: Digital Heritage 2015. 2nd Digital Heritage International Congress, Granada, Spain.

Hess, M., Hoff, A. R., Meyer, D. E., Rissolo, D., Guillermo, L., Glover, J. B., Amador, F. E., Vaughn, A., & Kuester, F. (2015, January). Digital Documentation and Assessment of the Remote Colonial Church at Ecab, Quintana Roo, Mexico. Paper presented at: SHA 2015. 48th Annual Conference on Historical and Underwater Archaeology, Seattle, WA, USA.

ABSTRACT OF THE DISSERTATION

Diagnostic Structural Health Assessment Through Layered Integration of Non-destructive Imaging Data

by

Michael Robert Hess

Doctor of Philosophy in Structural Engineering

University of California, San Diego, 2018

Professor Falko Kuester, Chair

Much of the built infrastructure that exists today has outlived its designed life and the unknown health of these structures poses safety and life-time maintenance concerns. The lack of reliable understanding as to a structure's current state of health, oftentimes results in the expensive demolition and replacement of entire structures. If professionals were instead equipped with a comprehensive structural health assessment that provides actionable data describing an existing structure, they could then make more informed decisions with potential for less expensive remedies.

For historical structures the need for structural assessment methods is even more critical, because replacement is not an option due to their economic, social and cultural impacts.

This dissertation presents methods to non-destructively acquire data describing the existing state of a given structure to inform future analyses and structural health assessments. The first objective is to identify the types of information that should be documented, and the techniques utilized to acquire those data. Emphasis here is placed on collecting information pertaining to geometry (at the surface, subsurface and volumetric levels), appearance, and context. These data are then integrated into a holistic digital model, or an as-built information model, to enhance interpretation and understanding by correlating results from different modalities in time and space.

The culmination of this dissertation is a repeatable methodology for the creation of as-built information models which ultimately serve as a data repository and the core hub for processing, analysis, dissemination and decision-making processes. Professionals and stakeholders will make more informed decisions if equipped with a reliable digital documentation record that captures a structure's history, flaws and damages both at the surface and internally. These sources are then used to inform diagnostic assessments of the structure's state of health as well as informing future predictive analyses and lifecycle maintenance. Though the initial scope highlights applications for historical structures, the developed methods for assessment and analysis can be extended to any existing structure at any scale. The ability to generate these models efficiently can greatly improve the investigation and maintenance of built infrastructure all over the world.

Chapter 1 Introduction

1.1 Motivation

Aging built infrastructure poses safety and lifetime maintenance issues that are often addressed by expensive replacement of entire structures in the absence of a thorough understanding of the structure's current condition. If professionals were instead equipped with a structural health assessment that provides actionable data describing an existing structure, they could make more informed decisions with potential for less expensive remedies. The underlying problem addressed in this dissertation is the treatment of symptoms instead of understanding and treating a root cause. Historical structures were chosen as the main focus of this research because replacement, or even a simple pragmatic solution, are not an option due to their economic, social and cultural impacts. Though the initial scope highlights applications with historical structures, the developed methods for assessment and analysis can be extended to any existing structure at any scale.

Proposed here is the creation of an integrative methodology that leverages the acquisition of multiple data streams that are then inputs for processing, analysis, and dissemination pipelines. Relevant diagnostic imaging technologies exist but are not yet leveraged to their fullest potential for the application of structural health assessment. The engineer's toolkit for simulation and analysis have progressed rapidly with technology, but until now the way in which data is collected and used to inform the input models has not progressed with it. Input data can be used to streamline geometry creation for existing structures as well as contribute information not visible at the surface that may have great impacts on the final analysis.

The presented acquisition techniques contribute information at the surface, sub-surface and volumetric levels with the goal of digitally documenting and reconstructing all existing components of the structure in a single holistic, digital representation. Additional techniques not presented here

could also be added to the workflow if supplementary details about the structure are needed, but the overall methodology for acquisition, processing, analysis and dissemination will be the same.

Many of the acquisition techniques have been proven effective individually for structural health assessment, but the diagnostic value of the data can be increased if combined into a multi-dimensional layered model. The layered nature of this digital model enhances interpretation and understanding by correlating results from different modalities in time and space. Professionals and stakeholders can make more informed decisions if equipped with an accurate digital documentation record that captures flaws and damages both at the surface and internally. This digital model can serve as the core hub for processing, analysis, dissemination and decision-making processes.

The ability to generate these models efficiently can greatly improve the investigation and maintenance of built infrastructure all over the world. In the United States specifically, there is a dire need to address problems with crumbling civil infrastructure and all over the world there are common problems associated with the life-time maintenance and stewardship of historical structures. The culmination of this dissertation is a repeatable methodology for the creation of as-built information models that serve to inform professionals and stakeholders about a given structure's state of health. The creation of these information models must be repeatable in order to gather vital temporal changes. Benefits of building information modeling (BIM) have been documented and quantified for new construction, but an approach to generate these records from existing structures has not been created.

1.2 Scope of Research

This dissertation aims to address three primary research objectives with the ultimate goal of attaining a better understanding of and approach towards the structural assessment of existing structures. The first objective is to identify data acquisition modalities aimed at measuring and analyzing surface, subsurface and volumetric information at building scale. The second objective

is to develop a methodology for the integration of these data into one holistic as-built information model. The final objective of this dissertation is to utilize these as-built information models to make more informed structural health assessments and decisions.

1.2.1 Scope of Non-destructive Imaging at Building Scale

The first objective of this dissertation is to explore the application of multiple non-destructive imaging techniques at the scale of entire buildings. As will be detailed in Chapter 2, previous works have studied the utility of individual imaging techniques for small scale structural health assessments and analyses. Motivated by these previous small-scale studies, this chapter will detail how to methodologically scale the acquisition of these data to document entire structures with the end goal of creating comprehensive as-built information models.

Specific emphases are placed on the acquisition methodology to be repeatable, comprehensive, and accurate. For the purposes of structural health assessment and monitoring, any methodology that does not meet these three criteria will not withstand the test of time and will be rendered unusable for scientific investigation. If a methodology is repeatable, it can be performed in subsequent documentation campaigns and used to monitor changes over time. Additionally, repeatability is important in respects to utility of emerging technologies; this is to say that a methodology should not be limited to technology that exists today, but open to welcome new technology by focusing on the output information. A methodology must be comprehensive to guarantee stakeholders and future users of the data that any damages, deficiencies and changes have been captured. Finally, accuracy is paramount to the success of surveying existing structures to ensure an overall reliability of the generated data.

The goal of the presented integrative methodology (Figure 1.1) is to perform an overall structural health assessment on existing structures using non-destructive imaging techniques. The final output is a comprehensive digital model that describes a structure's makeup as completely as

possible enabling users to generate and validate hypotheses concerning a given building without invasive techniques or the need to visit the site physically. This notion unlocks powerful collaboration opportunities in which domain experts can all make assessments of the same structure from anywhere in the world using the digital representation.

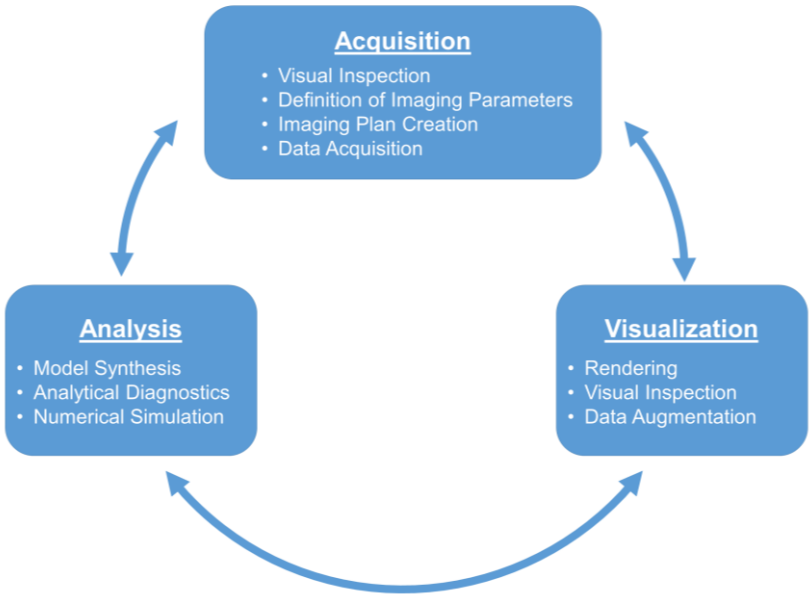

Figure 1.1 Integrative diagnostics methodology for acquisition, visualization and analysis of non-destructive imaging data (Hess, Petrovic, Yeager, & Kuester, 2017).

With an understanding of the output requirements, the approach to data acquisition can be detailed to encompass existing technologies as well as leaving the framework open to future technological advancements. These first chapters will detail acquisition strategies for four non-destructive imaging techniques which can also serve as templates that could be used to incorporate future technologies. Terrestrial laser scanning (TLS) and photogrammetry are featured as the methods of geometric documentation. Methods for high-resolution thermal imaging are then presented to demonstrate the acquisition of surface and subsurface data which may not be visible to the naked eye. Finally, ground penetrating radar (GPR) is offered as an example for volumetric data capture. There are many other geophysical and tomographic techniques that can provide

complementary data and it is encouraged that these and other data types be integrated as well following the presented approaches.

1.2.2 Scope of As-built Information Modeling

The output of the presented large-scale data acquisition methodologies will be a comprehensive as-built information model. For purposes of this dissertation, an as-built information model is defined as a high dimensional digital surrogate of an existing structure that captures, as accurately and completely as possible, the existing state of a structure at the surface, subsurface, and volumetric levels. To ensure the greatest diagnostic value, the data contained in the digital surrogate should ideally maintain full resolution and not be subsampled, simplified or approximated. Finally, an as-built information model could be used to augment or update an existing BIM as well as generate a new BIM for a structure with no previous records.

Previous studies have expressed the need for better documentation of existing structures to replace or supplement the typical practice of generating idealized computer-aided design (CAD) representations. Imperfections within existing buildings can be symptoms of underlying problems, so, a high level of detail is required, especially in historical buildings, to capture discrepancies from idealized conditions such as level floors and square corners. However, the need for better input data streams extends far beyond records of surface geometry. There are many other data layers that augment, complement and enhance the pure geometry of an existing structure. Presented in this dissertation is a methodological approach for combining multi-dimensional datasets into one holistic information model. The utility of the generated information models is not limited to engineers, but also beneficial to historians, restorers, architects, government entities, and the public, so the scope of documentation should not be limited by the surveyor's hypotheses or incoming objectives.

1.2.3 Scope of As-built Information Model Utilization

Next generation structural health monitoring will rely on interactive, predictive models for buildings and other structures in combination with a decision-making framework, enabling day-to-day life-cycle management and rapid assessment and response following extreme events. This requires a digital surrogate, or an information model, of a structure that encapsulates its geometry, material characteristics and current state-of-health. To be effective for rapid creation of actionable information, the digital surrogate must also be adaptable to injection of newly emerging data and insights. Presented here is a larger vision of as-built structural health assessment that pushes toward a BIM logic approach of creating comprehensive models that dynamically integrate data and can be used for decision making and analysis.

The benefits of BIM for new construction have been demonstrated and quantified. The last objective of this dissertation is to demonstrate how as-built information models can be used to make more accurate and meaningful assessments of existing structures. Primarily through numerical simulations, the benefits of more accurate documentation records are shown to alter the diagnosis, interpretation and prediction of a structure's state of health. Through the combination of non-destructive imaging data, assumptions concerning a building's construction can be minimized or avoided which in turn can prevent misinforming professionals and stakeholders.

1.3 Organization of Dissertation

This dissertation consists of eight chapters. This chapter motivates the study of existing structures and outlines the primary research objectives as well as the scope and organization of the dissertation. Chapter 2 provides a review of the literature focusing on data acquisition for structural health assessment, multimodal data integration, and combination of multi-dimensional data for assessment of structures. Chapter 3 presents research concerning data acquisition techniques for geometric documentation and analysis. Chapter 4 presents both instrumentation and a methodology

created to address building scale acquisition of thermal images. Chapter 5 begins to address the combination of imaging modalities with a method for automated fusion of visible and thermal images. Chapter 6 continues to address multimodal fusion with an example of the combination of 3D geometric techniques. Chapter 7 summarizes the combination of n-dimensional data modalities for the creation of as-built information models and presents how as-built information models can be used for more informed analysis of existing structures. 7.7 concludes this dissertation with a summary of the primary contributions and recommended future research directions.

Chapter 2 Research Background and Prior Work

There has been a recent surge in studying the uses of non-destructive imaging technologies and how they may be applied towards buildings and other built structures. Most previous studies only scratch the surface of the overall utility of the generated data with limited focus on small proof of concept examples. The work to date has demonstrated some great use cases for these imaging techniques, but there are much larger applications for more accurate, detailed and holistic representations of existing structures for the study of past, present and future loading scenarios. This chapter will highlight previous uses of laser scanning, photogrammetry, thermal imaging and tomography for documentation and analysis of existing structures. The last section of this chapter summarizes what is missing from the presented prior works and how this dissertation aims to fill these knowledge gaps.

2.1 Non-Destructive Imaging Techniques for Structures

This section discusses previous works that apply non-destructive imaging techniques individually for documenting and analyzing existing structures. Each technique will first be discussed for its independent utility. Then in Section 2.2, previous works highlighting combined uses of non-destructive techniques in the area of information modeling. Finally, Section 2.3 will briefly cover previous studies performing experimental and numerical testing on masonry structures. The presented literature review will cover the background of the technologies, applications for imaging structures, and how the imaging data can be used to derive meaningful conclusions about a structure's state of health.

2.1.1 Terrestrial Laser Scanning

To acquire geometry at the surface, terrestrial laser scanning (TLS), or light detection and ranging (LiDAR), is a well proven technology with trusted accuracy and repeatability for 3D

documentation of existing structures. Laser scanners reflect a laser off a rotating mirror in order to acquire a sphere of measurements from one central point of view. To calculate a distance, scanners either use a time of flight measurement technique that calculates distance based on the time it takes for the laser to return from a surface or a phase shift method that compares the emitted and received phases of the laser (Lemmens, 2011). TLS, is a surveying technique that can provide accurate 3D geometry, with millimeter accuracy (FARO, 2017), of all surfaces visible from the scanner's point of view. This imaging modality is a line-of-sight technique, which means that the device only records measurements from the first surface it sees and nothing beyond that. For 3D environments, multiple imaging positions are therefore required in order to realize a complete digital 3D representation. Though identifying survey positions may be time consuming, once the positions are chosen, laser scanning will reliably return measurement points at a known resolution from every surface the laser hits.

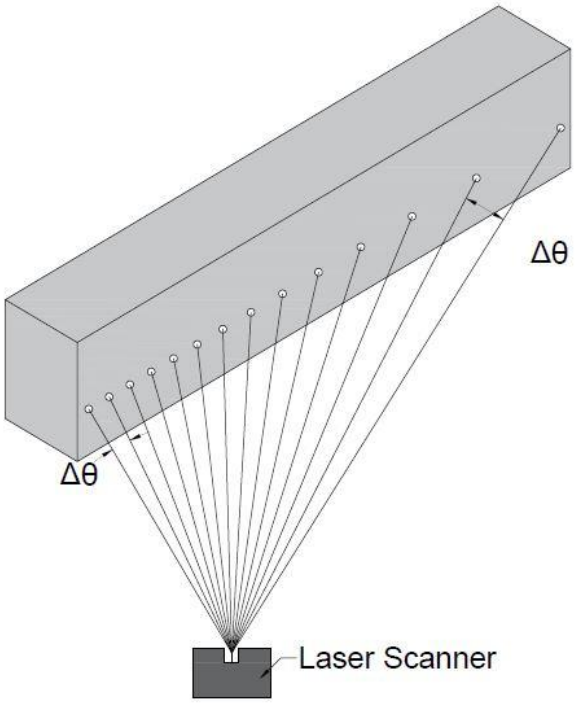

Figure 2.1 Demonstration of the radial resolution behavior of laser scanners and how linear resolution varies with distance from the scanner (Hess, Petrovic, Yeager, & Kuester, 2017)

The duration of each scan varies based on the desired scan quality and resolution, with the scan duration increasing as a function of both. Increasing the quality of the scan increases the duration because each point is sampled multiple times in order to reduce noise in the resulting data set. Scans durations can range from seconds to hours and resolutions range from one millimeter to fifty millimeters (FARO, 2017). In this context, resolution is defined as the linear space between measurement points. The laser originates from one central point and the laser trajectories diverge as they travel away from the scanner (Figure 2.1). For this reason, manufacturers normally specify resolution at a particular radius from the scanner and beyond that distance, the points will be spaced farther apart. The radially-controlled behavior warrants careful consideration when determining the resolution required to resolve target features (Laefer, Truong-Hong, Carr, & Singh, 2014).

Advances in TLS technology have been driven by fields like the automotive and aerospace industries that are looking to perform reverse engineering as well as applications in Building Information Modeling (BIM) for the assessment of new and as-built systems (Volk, Stengel, & Schultmann, 2014; Bosche, Ahmed, Turkan, Haas, & Haas, 2015; Huber, et al., 2011). The most important tool in the preservation of buildings is an accurate geometric record of the existing structure. Previous studies have expressed the need for better documentation of existing structures to replace or supplement the typical practice of generating idealized CAD representations (Tang, Huber, Akinci, Lipman, & Lytle, 2010). The imperfect nature of existing buildings, especially historical buildings, requires a high level of detail to capture discrepancies from idealized level floors and square corners which in many cases can be symptoms of underlying problems.

Establishing accurate geometry is just one step towards describing a structure's state of health, but there are many ways in which this one data stream can provide a wealth of insight. In the context of structural assessment, laser scanning has been used to achieve different objectives, but the literature still lacks an overall methodology to repeatably document entire structures for

general evaluation by various professions. General TLS methodology variants have been tested, but often the studies are limited in scope to address very specific outcome deliverables. The U.S. General Services Administration (US, 2009) and Olsen (Olsen, Kuester, Chang, & Hutchinson, 2009) outline the challenges of TLS implementation, but still do not present a full methodology for the execution and offer a narrow vision of the extent to which these data can be used.

The specific process of TLS technology is well documented (Bernardini & Rushmeier, 2002; Lemmens, 2011) and the importance of collaboration between engineers, conservators, and restoration experts has been highlighted in the context of historical building documentation (Arias, Herraez, Lorenzo, & Ordonez, 2005; Haddad, 2007). Tang and Akinci (2012) conducted bridge surveys to achieve specific objectives through extracting cross sections from scanning data. Taking a thin planar slice of points describing a structure can yield what looks to be engineering drawings that capture any variability measured in the surfaces of the scanned structure. This study, however, concludes that data quality issues caused by occlusions can significantly impact the outcome of surveying objectives.

2.1.2 Photogrammetry

Photogrammetry, or the field of making measurements from photographs, has been around for over a century, but has recently gained a lot of attention due to advances in computing technology. The field is extremely broad and now encompasses many areas of computer vision, specifically multi-view geometry. Structure from Motion (SfM) is a photogrammetric technique that uses two-dimensional images taken from multiple viewpoints to compute a 3D representation of the scene being surveyed (Bolles, Baker, & Marimont, 1987). Mutual features are detected in images of the same scene taken from different perspectives. This process is repeated for many overlapping images and the positions and orientations of the acquiring cameras is estimated. With

an estimate of the camera locations, the matching features from different images are projected into 3D space and where the rays intersect is a three-dimensional coordinate in space.

Without other knowledge, the technique is only useful for relative measurements, but if a reference scale is captured in the imaging scene, then accurate dimensions can be assigned to the resulting coordinate system. Photogrammetry like TLS is a line-of-sight approach, meaning that the user must ensure that images are acquired from enough viewpoints to eliminate any issues of occlusion. The resulting coordinates can be associated colors from the input images and the result, as in laser scanning, is a 3D point cloud describing a target structure, site or landscape. Photogrammetry techniques are extremely flexible and can provide resolutions ranging from kilometers to micrometers (Bianchini, Ippolito, & Bartolomei, 2015; Bourke, 2014; Brunetaud, Luca, Janvier-Badosa, Beck, & Al-Mukhtar, 2012; Hess, et al., 2014). In addition to the relative geometry generated by photogrammetric techniques, the images themselves can be used to provide high-resolution photorealistic textures to the target being studied.

The field of cultural heritage documentation has greatly benefited from advances in SfM processing and there is still room for growth in application of the resulting data. Use of these 3D data have progressed from simple documentation for posterity (Guarnieri, Vettore, El-Hakim, & Gonzo, 2004; Ikeuchi, Nakazawa, Hasegawa, & Ohishi, 2003) all the way to numerical structural simulations of entire complex structures. Photogrammetry techniques can be used in a wide range of cultural heritage applications such as topographic site mapping (Westoby, Brasington, Glasser, Hambrey, & Reynolds, 2012; Fonstad, Dietrich, Courville, Jensen, & Carbonneau, 2013), three-dimensional digitization (Grun, Remondino, & Zhang, 2004; Pavlidis, Koutsoudis, Arnaoutoglou, Tsioukas, & Chamzas, 2007), and for analyzing heritage structures (Arias, Herraez, Lorenzo, & Ordonez, 2005; Yilmaz, Yakar, Gulec, & Dulgerler, 2007). One of the reasons for the adoption of SfM methodologies in cultural heritage contexts is the speed at which the surveys can be conducted.

The processing time can range from hours to weeks depending on the number of images and available computing power, but time on-site can be limited and fit within common constraints of cultural heritage site access.

2.1.3 Thermal Imaging

Infrared thermography is an imaging technique that measures the radiation emitted by a surface in the long wave infrared range of the electromagnetic spectrum. Infrared waves have longer wavelengths than visible light, ranging from 0.78 to 1000 μm (Vollmer & Mollmann, 2010), but can be captured with infrared cameras and subsequently displayed in the visible spectrum. Infrared cameras that are sensitive to different wavelengths exist and wavelengths ranging from 7 to 14μlm are typically captured with thermographic camera sensors. These wavelengths shift with the temperature of the surface where the observed infrared wavelength decreases as temperature increases. When the emissive properties of the surface are known the camera can be calibrated to convert the observed wavelengths to emitted temperature. The set of recorded temperatures is then mapped to a range of colors in the visible spectrum in order to display the results against a scale that correlates each color to a temperature value.

Thermography is classified into two categories, passive thermography and active thermography. Passive thermography uses the ambient or natural heating and cooling of the specimen to measure differences in heat transfer. On the other hand, active thermography utilizes a controlled external heating or cooling source in order to record the heat flux, or rate of thermal energy transfer, across the target surface (Vollmer & Mollmann, 2010). The main difference in the two methods is that passive thermography is a snapshot that gives a qualitative evaluation of the target structure while active thermography is a sequence of images that can also yield quantitative results because the external heat source is defined with a known time and strength (Avdelidis &

Moropoulou, 2004). For example, with a controlled heat source, the material and structural characteristics of the specimen can be calculated (Shull, 2002).

In structural engineering, passive thermography is the preferred technique to use in situ because it is not practical to have external sources that apply heat evenly to entire surfaces at building scale. In these areas of application, thermography can be used to monitor energy losses, map areas of moisture, and detect delamination and cracks. These inspection techniques are well documented (Balaras & Argiriou, 2002; Grinzato, Bison, & Marinetti, 2002; Ljungberg, 1994) and extremely important, especially as structures age; it is crucial to monitor structures to detect damage and flaws early and take corrective actions before the damage has progressed or significant energy is wasted. Thermography presents a non-destructive approach for detecting warning signs and identifying issues that may not be visible to the human eye (Ljungberg, 1994). A fast thermal surveying methodology will be vital to efficiently monitor the natural aging and decay of the entire built infrastructure.

One of the most important applications for thermal imaging in NDE is detecting structural details and damage. Grinzato et al. (Grinzato, Bison, & Marinetti, 2002), Hess et al. (Hess, et al., 2014), and Imposa (Imposa, 2010) explain how thermal image mosaics can be acquired and used towards determining what types of modifications have occurred over the history of the structure. Grinzato outlines the importance of knowing the history of structural modifications and any anomalies within the structure in general, highlighting that accurate structural evaluation and identification of construction details is vital for a proper conservation plan (Grinzato, Bison, & Marinetti, 2002). Thermal imaging is extremely useful in these situations because it is a non-intrusive technique that reveals information about features that are not visible without opening walls or damaging the existing structure in any way.

Balaras and Argiriou (Balaras & Argiriou, 2002) explain how thermography can be used in the context of building diagnostics, specifically looking at building energy audits. This application uses thermography to detect areas where heating or cooling is escaping, insulation is missing, or areas where thermal bridges exist. All of these findings are then reported in order to develop a plan to address the issues that were found. The examples in (Balaras & Argiriou, 2002) reveal some detail in the thermograms, but no context for the area. Grinzato et al (Grinzato, Bison, & Marinetti, 2002) explain how thermal image mosaics can be acquired and used towards determining what types of modifications have occurred over the history of the structure as well as documenting cracks and areas of moisture. Thermal imaging is extremely important in these situations because it is a non-intrusive technique that provides information about features that are not visible without opening damaging the existing structure in any way.

2.1.4 Ground Penetrating Radar

Ground penetrating radar (GPR) is a well-established approach that emits radar pulses from a source antenna which travel through the surveyed material until they are reflected back to a receiving antenna at the surface. Reflections are caused when there is a boundary between materials with different permittivity. The higher the frequency of the electromagnetic waves emitted, the shallower the depth of penetration into the material. Lower frequency waves will penetrate deeper into a material, but will be more limited in terms of the size of anomalies that can be detected.

The processing of the reflected signals is the most complicated aspect of GPR surveys. In order to localize where the reflections originated there must be knowledge of the material the wave was traveling through. Knowing or estimating the material, the velocity of the wave through that material can be used to convert the time between emitted and received pulses to a distance to the anomaly. The processing is difficult still, because wave propagation is not linear, so the direction of the anomaly is unknown. This ultimately leads to a large optimization problem with variables of

wave velocity, noise and anomaly depth. When GPR samples are collected along a path or multiple parallel paths, they can all be analyzed together to help accurately localize the detected features.

GPR equipment has been commercially produced since the 1970's, but the early versions were very bulky and not portable (Davis & Annan, 1989). From the beginning, GPR has been widely used in the geotechnical fields for measuring features such as ice thickness, water table levels, and fractures. GPR can be used from the surface as well as from within boreholes to characterize subsurface conditions (Sander, Olhoeft, & Lucius, 1992). More recently, GPR has been used to map utilities, analyze deterioration of bridge decks, and create 3-D models to map concrete structural components (Alani, Aboutalebi, & Kilic, Applications of ground penetrating radar (GPR) in bridge deck monitoring and assessment, 2013; Maierhofer, 2003; Maser, 1996).

GPR has also been used in previous studies to study structures of historical and archaeological importance. Previous works have highlighted the need for tomographic techniques to detect and measure hidden structural features that optical techniques cannot address (Solla, González-Jorge, Álvarez, & Arias, 2012). GPR has been used to investigate the wooden elements in the slabs and pillars of historical buildings. GPR works very well with wood that is very old and deteriorated because it is essentially a dust that creates a high permittivity contrast (Lualdi & Zanzi, 2002). The capability of GPR to study structures beneath the floors and in vaults of historical buildings has also been demonstrated (Cardarelli, et al., 2002; Orlando & Slob, 2009).

There are many uses for GPR data and different methodologies have been evaluated previously. The clear message here is that GPR can be an extremely useful tool in the field of structural health assessment to provide information that is hidden beneath the surface out of scope for other imaging techniques. There are also many other tomographic techniques that can provide complimentary and supplementary benefits. Seismic tomography, ultrasonic tomography, acoustic emission, and electrical resistivity tomography have also shown promising results for applications

in structural assessment (Carpinteri & Lacidogna, 2006; Cosentino, Capizzi, Martorana, Messina, & Schiavone, 2011; Flint, Jackson, & McCann, 1999).

2.2 Information Modeling

Existing structures, especially historical ones, are complex constructions that prove to be difficult to understand and diagnose when problems arise. Previous studies have highlighted the potential benefits of providing better diagnostic tools and data to inform structural health assessments (Alani, Aboutalebi, & Kilic, Integrated health assessment strategy using NDT for reinforced concrete bridges, 2014; Kilic, 2015; Woo, Wilsmann, & Kang, 2010). Though there is recognition as to the needs of these data and the benefits they would bring, few have paved the way for integrating multivariate and multidimensional data over a structure's lifetime. Presented here are previous works that introduce historical information modeling (HBIM) as well as some that have begun to utilize multiple imaging techniques.

The National BIM Standard-United States (NBIMS-US) defines BIM as "the digital representation of physical and functional characteristics of a facility. As such it serves as a shared knowledge resource for information about a facility, forming a reliable basis for decisions during its life cycle from inception onwards." BIM is currently being implemented for new construction (inception), but has not yet extended to accurately model structures that already exist. Structural health assessment is a decision-making process based upon data that describe an existing structure's current state of health, and BIM has been shown to be a "reliable basis" for these data driven decisions. Previous studies have quantified the benefits for new construction and similar benefits could be mirrored in the management of existing structures (Barlish & Sullivan, 2012; Leite, Akcamete, Akinci, Atasoy, & Kiziltas, 2011).

Recent studies have been conducted to address the recognized need for BIM techniques for historical structures in what is now referred to as HBIM (Brumana, Oreni, Raimondi,

Georgopoulos, & Bregianni, 2013; Oreni, Brumana, & Cuca, Towards a methodology for 3D content models: The reconstruction of ancient vaults for maintenance and structural behaviour in the logic of BIM management, 2012). The content models presented in these previous works are a great initial step that will certainly enable better management of cultural heritage sites and structures. The main challenge with historical structures are their extremely complicated and vague baseline conditions upon which all other assessments or interpretations are built (Woo, Wilsmann, & Kang, 2010).

BIM frameworks are generally not very flexible with input geometries and different imaging modalities. To this point, previous HBIM approaches have simplified existing conditions in order to conform to typical BIM practices. For an enhanced state of knowledge concerning a building's stability or remaining life, assumptions should not be made when accurate data of baseline conditions can be gathered. However, some have started to address the issues associated with converting complex geometry captured with TLS into parametric models that will conform to typical BIM operations (Banfi, 2016; Barazzetti L. , et al., 2015; Oreni D. , et al., 2014).

The combination of data from multiple imaging modalities has been shown to improve understanding of complex historical constructions. Visual inspections can provide an initial pulse for a quick determination of a structure's state of health, but only though the additional input from techniques like thermal imaging and GPR can one gain a true understanding of the existing structural state (Kilic, 2015; Barazzetti L. , et al., 2015). Many researchers and practitioners are beginning to utilize data from multiple imaging modalities to diagnose and restore structures (Oreni, Brumana, & Cuca, 2012; Bosiljkov, Uranjek, Žarnić, & Bokan-Bosiljkov, 2010). However, there is still much work to be done in how these different data streams connect, interact, and most importantly, how they are used together to inform structural analysis and preservation.

2.3 Masonry Testing and Simulation

Beyond the data acquisition and integration lies the future of all building analysis and management. The ultimate goal of structural engineering is the ability to accurately simulate structures under different loading scenarios to predict their responses and assess any apparent risk. Steel and concrete structures are understood far better than ever before through research and testing all over the world. With data from experimental testing, it is possible to validate results from numerical simulations. Most historical structures however, do not conform to straightforward structural analysis procedures. Constructed hundreds of years ago with unknown materials in unknown sequences, these buildings are some of the most complex structures to diagnose structural integrity.

Historic structures are complex and heterogeneous structures which function discontinuously due to disparities in the material properties. If one is looking for an understanding as to how a structure came to be in a certain state or what the possible load capacity is under current circumstances, then capturing the true nature of the existing materials and boundary conditions is crucial. Many numerical approaches have been tested to characterize structural response of unreinforced masonry structures (Giordano, Mele, & De Luca, 2002; Lourenço, Krakowiak, Fernandes, & Ramos, 2007), however none have claimed to be the ultimate solution for accurate prediction of complex masonry constructions.

As opposed to focusing entirely on the numerical methods, presented here are examples that demonstrate the necessity of accurate documentation of existing conditions. Through experimental testing of masonry specimen, previous works have studied the effects that simply varying mortar bed joint thickness can have on the ultimate capacity of a masonry wall. In these cases, the compressive capacities of masonry walls were tested with different mortar bed joint thicknesses (Francis, Horman, & Jerrems, 1971; Reddy, Lal, & Rao, 2009; Stang, Parsons, &

McBurney, 1929; Zavalis, Jonaitis, & Lourenço, 2014). The reported results clearly show that overall compressive strength of the masonry system decreases as mortar thickness is increased. This is an extremely important observation given that many simplified numerical simulation methods do not consider mortar geometry.

Even if the mortar thickness is accounted for, numerical simulation can still prove to be very complicated. The elastic modulus of a mortar cube or core is not necessarily a true representation of a mortar joint in its context. Previous authors have shown that the calibrated elastic modulus of the mortar in the context of being a bed joint in a masonry wall can be up to ten times less than that of a raw mortar core (Zavalis, Jonaitis, & Lourenço, 2014).

More important still is that many historical structure do not have regular homogeneous masonry patterns with consistent stone and mortar dimensions (Valero, Bosché, Forster, Wilson, & Leslie, 2017). More experiments, physical testing and numerical simulations must be completed to definitively conclude the best method for predicting the accurate response of masonry structures, especially historical structures. Reflecting on the mentioned previous works which demonstrate the effects of mortar thickness, it can be seen that even when all variables are known, predictive simulations of masonry structures are extremely complex. One of the goals of this dissertation is to gather as much information as possible from existing masonry structures in order feed the complex task of diagnostic and predictive modeling.

2.4 Summary

Existing structures, especially cultural heritage structures, are in dire need of better solutions for the documentation, analysis and assessment of their state of health. Previous works have touched on the fact that there are imaging technologies and techniques that can aid in adding small pieces to the overall puzzle. There has not yet been research done to demonstrate how these

techniques can be used together in order to generate a complete and holistic record of an existing structure.

This dissertation aims to detail the approach of using non-destructive imaging techniques to better diagnose historical structures. The first objective is to provide the knowledge of how these imaging techniques, and others like them, can be performed at building scale in a way that is trusted and repeatable. The second objective is to integrate all of these dissimilar, but complementary data, into one holistic as-built information model. The final and ultimate goal of this dissertation is to evaluate how these multi-modal digital surrogates can better inform the preservation and life-cycle management of existing structures as a whole.

Chapter 3 Geometric Documentation and Analysis

This Chapter discusses large-scale acquisition of geometric data to comprehensively measure an entire structure's surface geometry. This aspect represents the skeletal structure for the final as-built information model. An accurate geometric record of an existing structure is vital for all future data streams to be referenced to. Image textures, thermal information and volumetric data can all be projected onto and added to the geometric model later, but first an accurate geometric record must be established. The two methods for geometric reconstruction presented here are TLS and SfM.

While being a critical piece for the alignment and referencing of other data, the geometric record is also extremely useful on its own for assessment and analysis ranging in scale from millimetric details to numerical simulations of entire buildings. It will be demonstrated here that even when objectives are not formed prior to a survey, comprehensive data sets of high quality and reliability will enable meaningful structural health assessments. With a reliable comprehensive baseline model in place, it can be annotated, qualitatively analyzed and recurring surveys can be conducted to track changes and damages throughout time.

3.1 Terrestrial Laser Scanning

The first method presented here is terrestrial laser scanning (TLS), also known as light detection and ranging (LiDAR). TLS is a technique that reflects a laser off a rotating mirror in order to acquire a sphere of measurements from one central point of view. Instruments use either a time of flight measurement technique that calculates distance based on the time it takes for the laser to return from a surface or a phase shift method that compares the emitted and received phases of the laser (Lemmens, 2011). This surveying technique can provide accurate 3D geometry, with millimeter accuracy (FARO, 2017), of all surfaces visible from the scanner's point of view. In order

to effectively leverage this technology in the field, all objectives and constraints must be understood and appropriately addressed. TLS is widely understood and is a trusted means of acquiring geometric information, but a comprehensive methodology for large scale acquisition for measurement of existing structures has not been developed. The ultimate goal of this work is to present a methodology for the creation of comprehensive interpretive models used for as-built structural health assessment; the resulting model will enable a wide range of analysis objectives and also accommodate the study of future damages and changes.

Repeatability is vital to the presented methodology because analysis of temporal data is crucial to monitoring and understanding damage patterns, and the results are only valid if the two datasets are of comparable quality, accuracy and reliability. Changes over time as well as existing and new damage locations cannot always be predicted, so the methodology must be repeatable, comprehensive and detailed in order to detect and characterize them in the future. It is important to have a clear definition of a practical, field-ready documentation approach that ensures the generation of quality data from which informed decisions can be made, especially in fields where this technology is a new addition to the traditional practices and operators may not have extensive experience. The proposed integrative diagnostics methodology demonstrates that these repeatable acquisition, visualization, and analytical workflows can revolutionize the preservation and management of historical structures.

For large scale structural health assessment, the objective is to capture accurate geometric data of an entire structure that can then be used to enable the visualization, location and quantification of any structural deficiencies. The most critical constraints of TLS surveys that must be considered are time, occlusions, overlapping regions of the scans, physical placement of equipment and the specifications of the scanner. Typically, with historical structures the most

difficult challenges with data acquisition are access to the building and the total amount of allotted time on-site.

3.1.1 Case Study: Baptistery of San Giovanni

The goal of the case study was to perform an overall structural health assessment on the Baptistery di San Giovanni in Florence Italy. The scope of the investigation was very broad because a diagnostic study had not been conducted on the building so there were no specific objectives other than a general assessment of the structural integrity and construction methods. The work at the Baptistery demonstrates how TLS data can be methodologically acquired, visualized and analyzed to generate and validate hypotheses concerning the structural integrity of a given building (see Figure 3.1).

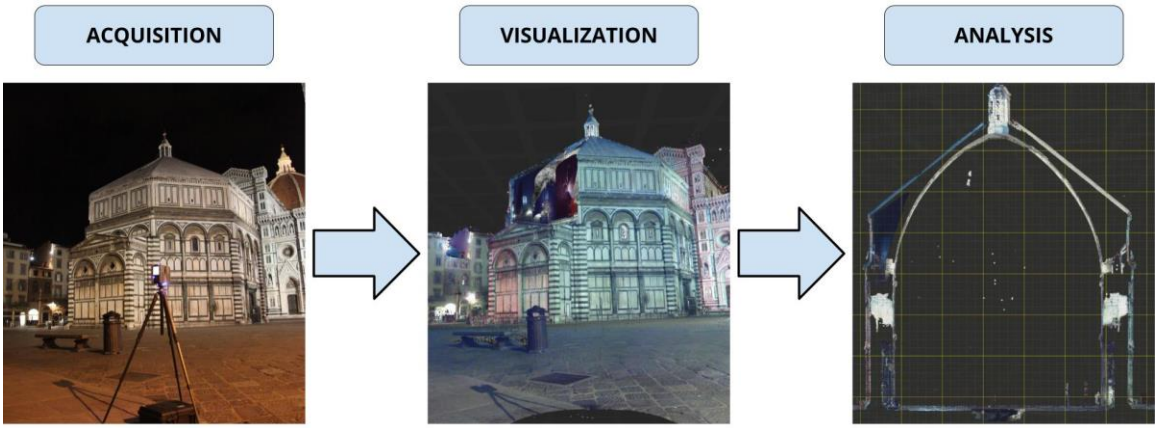

Figure 3.1 Methodological approach to traverse from acquisition to visualization and analysis.

The Baptistery di San Giovanni is located in the heart of Florence, Italy. While dwarfed in size and fame by the adjacent Santa Maria del Fiore (Duomo) Cathedral, the Baptistery's history and cultural significance equal, if not surpass, the Duomo's. The earliest historical reference to the Baptistery occurs in 897AD, long before Florence's renowned renaissance, and the construction of the Duomo, had begun. However, the foundation of the building is much older. The ecclesiastical edifice rests upon the remains of earlier structures, whose use and intention have been cause for

much debate over the centuries. Legend holds that the site of the Baptistery originally featured a Roman temple dedicated to Mars. Excavations beneath the Baptistery in the early 20th century revealed that its walls do indeed rest upon Roman constructions that date to the 3rd century AD. The excavations disproved the theory of a temple to Mars, but their findings did validate the antiquity of the Baptistery's foundation and excitingly expanded the already rich history of the site. The building was named the city's official Baptistery in 1128 (Arletti, et al., 2011), and for centuries most Florentine citizens were baptized within its walls, and still to this day religious services are held inside the monument. The Baptistery now serves as one of the most popular tourist attractions in Florence situated adjacent to the front entrance of the Duomo Cathedral. For more information about the history of the site and other studies conducted, see (Arletti, et al., 2011; Fratini, Pieraccini, Atzeni, Betti, & Bartoli, 2011; Cardarelli, et al., 2002; Giusti, 2000; Williams, 1994).

The Baptistery is an octagonal masonry structure with an eight-sided dome which measures just over forty meters in height. The 666 square meter interior of the building does not have any central supporting structure and the weight of the dome rests upon its eight walls. The dome itself has a dual shell construction, as seen in Figure 3.2, where the exterior shell, which is constructed of large cut stones, helps to support the thrust of the interior dome as well as protect against environmental conditions like rain, snow, wind and i.e. The interior shell is constructed of smaller, rough masonry and the curved interior surface of the dome is richly decorated with glass mosaic tiles. The entire exterior and most of the interior vertical walls are also covered with marble slab facades, hiding the structural masonry walls. The 'scarsella', or apse, is a rectangular addition on the West side of the structure serving as the one deviation from octagonal symmetry. The previously mentioned excavations beneath the Baptistery begin beneath the 'scarsella' and continue under one third of the Baptistery's footprint. It is also important to note that the areas above the excavations are now supported with a modern reinforced concrete slab – a decision that may have caused unintentional, but irreversible damages to the structure. Its cultural significance and age,

unique geometry, materials, structural and non-structural components, combined with being a heavily visited tourist attraction, create a demanding case study environment for structural health assessment.

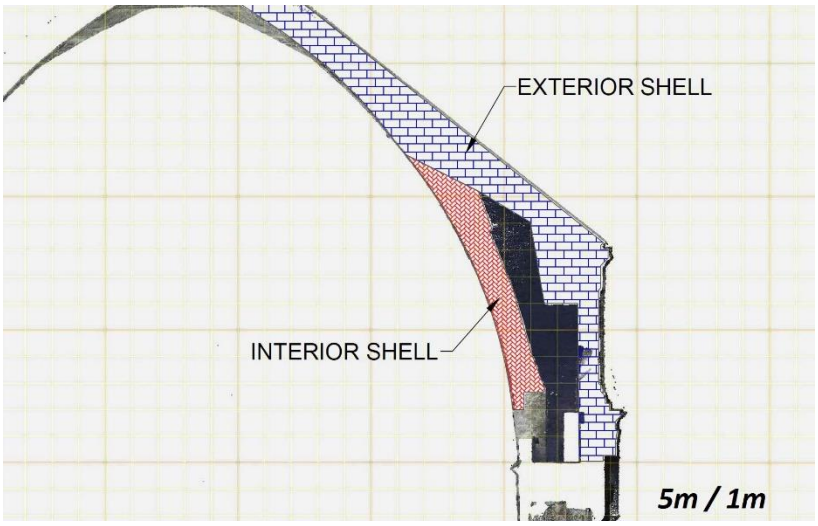

Figure 3.2 Section cut of the laser scanning data showing details of the dome's dual shell construction.

The adjacent Duomo Cathedral has been instrumented since 1955 to sense environmental conditions, track crack progression and to study why the structure is experiencing damages. Mechanical deformometers installed in 1955 have provided over 50 years of quarterly measurements of crack width along with internal and external temperature measurements. In addition, a digital system consisting of 166 instruments (72 displacement transistors and an assortment of thermometers, piezometers, and levelometers) has 5 million recorded measurements from 1987 to 2007 (Ottoni, Coïsson, & Blasi, 2010), but so far all of these data have yet to provide insight into the cause of the structural deficiencies that can be visually observed. Upon visual inspection, the Baptistery is constructed in a similar manner and is experiencing cracking in similar locations as the Duomo. While the Baptistery has not been instrumented with sensors, its 3D surface geometry can provide a wealth of information pertaining to what areas warrant further investigation as well as setting an accurate as-is record of the structure. The working hypothesis of this paper is that a rapid TLS-based investigation can create a preliminary digital surrogate with immediate

diagnostic value, enabling visually observed deficiencies of its ground floor slab, foundation, arches and dome to be studied and quantified.

3.1.1.1 Acquisition

This section details the acquisition workflow (outlined in Figure 3.3) for comprehensive TLS documentation of a structure. The most difficult challenges with the data acquisition at the Baptistery was access to the building and the total amount of time on-site allotted to the study. Preliminary walkthroughs of the exterior as well as the publicly accessible portion of the Baptistery were conducted in order to formulate imaging plans for the spaces. The primary decision to be made was how many scans were required to acquire data from the proper viewpoints on all visible surfaces. In order to make this decision, any occlusions, physical constraints, range and sufficient overlap needed to be taken into account in a systematic scanning plan. The presence of line-of-sight occlusions, where one surface prevents data collection on another surface beyond it, necessitate additional scans from alternate angles in order to realize a comprehensive model of the space. Furthermore, the scans cannot simply capture each surface exclusively, but must also have sufficient overlap with adjacent scans to enable accurate alignment of the scans during data post-processing. Often, physical 2D and 3D targets, such as checkerboard placards and spheres, are placed in the target space to aid in co-locating overlapping datasets, but the targets must ideally remain stationary for the entirety of the scanning survey. Due to the abundance of surface details present on the stone surfaces and mosaics and without the ability to leave physical targets in the space between access windows, it was decided that physical targets were not needed to register the scans to each other.

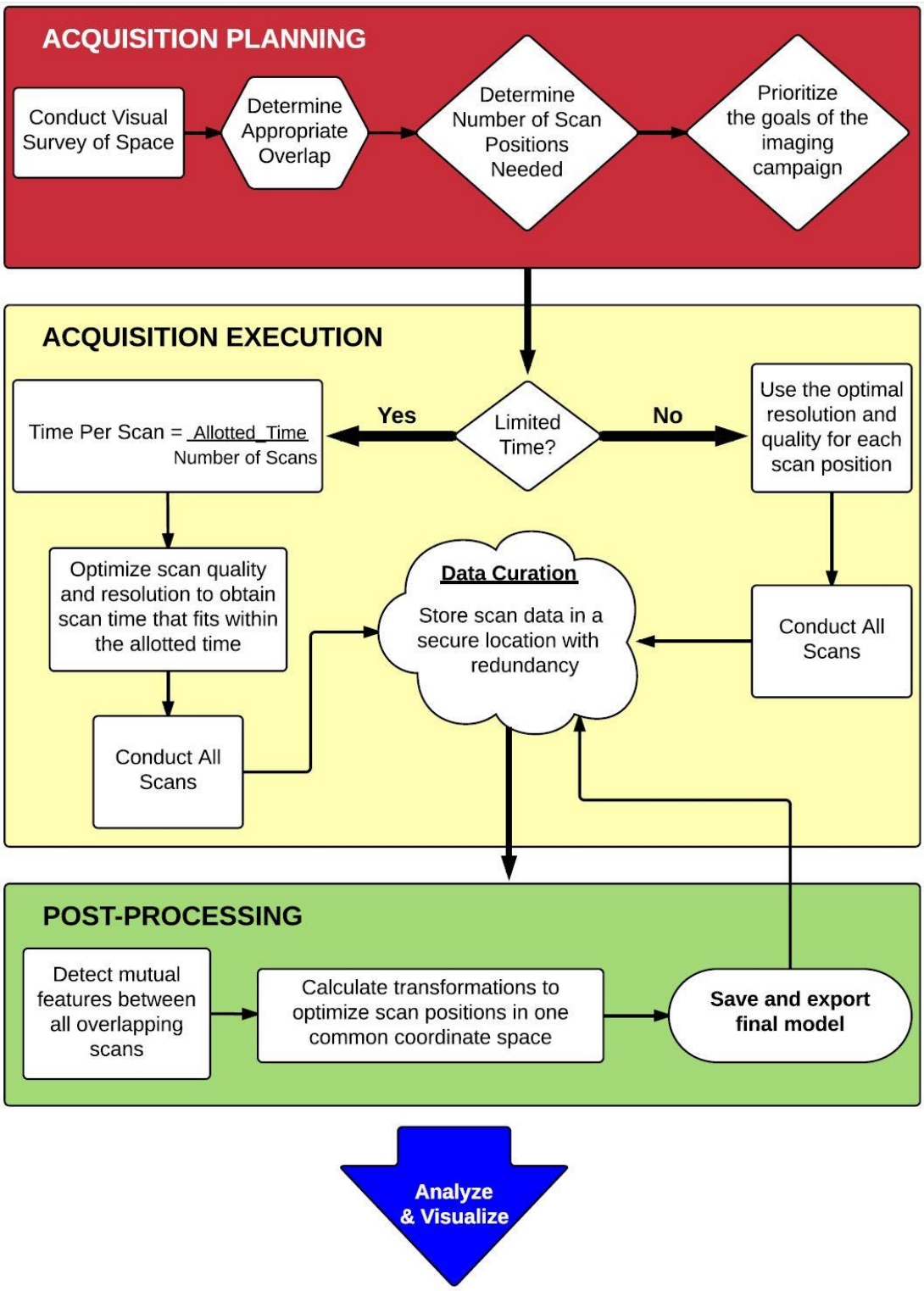

Figure 3.3 Proposed methodology for the acquisition of TLS data.

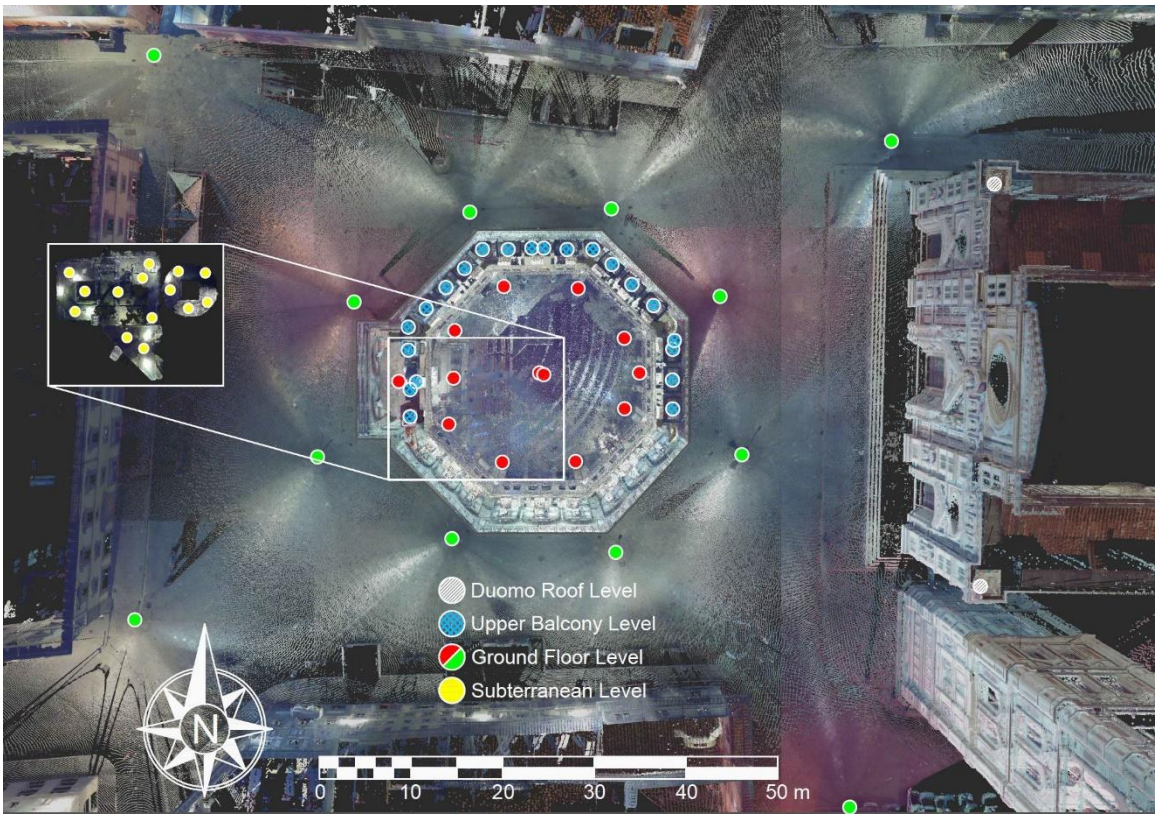

Figure 3.4 Plan view of the site showing the positions for the scans for the exterior (green), interior (red), excavation site (yellow) and upper hallways between the two shells of the dome (blue).

The exterior of the Baptistery required the least amount of spatial planning for occlusion mitigation and the scans were completed from each corner of the structure in addition to scans placed farther away in order to capture the geometry of the roof. Due to the absence of central support systems in the main interior space, there were few occlusions and most of the scans were amply overlapped. As seen in Figure 3.4, most scans in the main interior space were located in the corners of the octagonal structure in order to reconcile minor occlusions generated by the supporting columns located close to the walls. The third scanning phase was located on the third story of the structure in the narrow space between the inner and outer shells of the dome. This space was extremely important to document due to its complex construction and overall impact on the understanding of the dome's structural behavior. Due to the narrow, hallway-like nature of this space, the scans required close proximity in order to ensure data overlap adequate for scan

alignment. Finally, the excavated portion below the Baptistery was visually surveyed in order to plan for the narrow fields of view. The most difficult aspect of planning the scanning of the excavation space was ensuring the accurate alignment to the interior scans above through the small opening of the access door. Detailed attention was placed on a scanning positioned at the base of the stairs to the excavation that would capture a both the excavation and a significant portion of the apse above.

With the number of scanning locations drafted, the next step was to determine how much time could be allotted to each scan. The exterior scanning was easier for time budgeting because there was no scheduling necessary in order to scan outside the building. The only time related constraint was the presence of tourists who would cause occlusions in the data as they walked by during the day, so for this reason, it was concluded that the exterior scanning would be completed late at night when there was very little foot traffic by the monument. The interior scanning would prove challenging because the Baptistery is open to tourists during the day, and scanning could not fall within normal operating hours. In order to gain access to the space outside of business hours, special permissions and staff supervision were requested from the Opera di Santa Maria del Fiore (OPA), which is the entity responsible for both the Duomo Cathedral and the Baptistery. Access was generously granted for three mornings and one evening, limiting interior access to ten hours. The finite amount of time allotted inside the monument affirmed the need for scanning to be organized and efficient. As a result of different time constraints, spatial limitations and requirements, separate scanning campaigns were planned for the exterior, interior, excavation and upper hallway spaces, as highlighted by the different markers in Figure 3.4.

For this study, the scanning was performed using a Faro Focus 3D laser scanner, which is a lightweight scanner with the ability to capture points with an accuracy of plus or minus two millimeters (FARO, 2017). The duration of each scan varies based on the desired scan quality and

resolution, with the scan duration increasing as a function of both. Increasing the quality of the scan increases the duration because each point is sampled multiple times in order to reduce noise in the resulting data set. Resolution in this context represents the space between measurement points, so a higher resolution scan will produce more total points because they are spaced closer together. The laser originates from one central point and the rays diverge as they travel away from the scanner (Figure 2.1). For this reason, resolution is normally defined at a specific radius from the scanner and beyond that distance, the points will be spaced farther apart. The radially-controlled behavior warrants careful consideration when determining the resolution required to resolve the features in question (Laefer, Truong-Hong, Carr, & Singh, 2014). The duration, resolution and quality of the scans must be optimized to ensure full coverage of the structure in the allotted time on site. Scans durations can range from seconds to hours and resolutions range from one millimeter to fifty millimeters, so there needs to be a proper balance that produces a complete survey that is of acceptable quality (FARO, 2017).

As there was no time constraint for the exterior scanning and higher range was desired, a higher quality setting was used to reduce noise at longer ranges yielding longer scan durations. The interior spaces on the other hand had to at least halve the scan time. The interior space was a very controlled environment so there would be no concerns of noise in the data and a lower quality setting could be used to speed up the scans while still achieving a higher resolution compared to the exterior. Due to the close proximity of all surfaces in the small excavation space, fast scans with lower resolution and quality settings provided enough measurement detail throughout the space. The lower resolution is characterized by the angle increments in which the scanner acquires points; this means that though the resolution (which is defined as a point spacing at ten meters away) is lower, in tight spaces, the points will be denser. In order to align the scans in the hallways between the shells of the dome with the interior of the Baptistery, high quality points needed to be measured through small windows that looked into the interior of the building. Utilizing high quality scans in

the upper hallway necessitated lower resolution scans in order to complete the survey in the allotted time. Table 3.1 shows the number of scans conducted for each space as well as the average time, resolution, and number of points per scan in each area.

Table 3.1 Baptistery laser scanning statistics.

Space	Number of Scans	Average time per scan	Average number of points per scan
Exterior	14	27:45	28,083,564
Interior	13	13:53	43,798,216
Excavation	14	8:32	31,191,672
Between Shells	21	11:07	7,005,528
		Total points	**1,592,625,490**

With the on-site systematic scanning campaign completed, the individual scans must be aligned together to produce a comprehensive model of the building. Post-processing of the scans is included here as an acquisition step because the data are most useful as a complete model of the structure as opposed to individual fragments. Point cloud alignment can be completed in many ways ranging from more manual techniques like target based alignment (Scaioni, 2005) to fully automatic quaternion based methods (Benjemaa & Schmitt, 1998; Huber & Hebert, 2003; Tang, Huber, Akinci, Lipman, & Lytle, 2010). Automated cloud-to-cloud alignment is an efficient way to simultaneously align all scans while minimizing and homogeneously distributing the residual alignment error (Benjemaa & Schmitt, 1998).

The post-processing of the data required a considerable amount of computing power, user interaction and patience in order to obtain a final model that accurately stitches all of the separate scans together with a minimized alignment error. In this study, the scanner's proprietary software, FARO Scene, was used to perform both target based alignment and automatic scan-to-scan

alignment (Benjemaa & Schmitt, 1998; Scaioni, 2005). Initial alignment was achieved by manually identifying mutual features between overlapping scans. Once the scans were generally well positioned, automatic cloud-to-cloud alignment was performed to simultaneously align all scans thereby reducing the residual registration error.

Each point cloud is compared with the adjacent cloud with the most overlap and the distance between datasets is calculated point by point to determine the alignment error. These errors, or scan point tensions, are calculated and minimized during cloud-to-cloud alignment in the FARO Scene point cloud software. The alignment results, summarized in Table 3.2, show that the average point to point error in the entire dataset is under four millimeters. The survey succeeded in obtaining 3D measurements detailing almost every visible surface of the structure. The resulting data set is composed from sixty-two individual scans and totals over one and a half billion 3D data points. No sub-sampling or decimation of the point data was performed in order to retain all measured data points. Maintaining the full resolution data set enables more precise measurements and also aids in assessing the quality of scan alignment.

Table 3.2 Baptistery laser scanning alignment results.

	Mean scan point tension (mm)	**% < 4mm**	**% Overlap**
Interior average	2.98	63.3	84.1
Between shells average	2.45	69.0	33.8
Total interior avg.	2.71	66.1	59.0
Excavation Average	4.48	53.9	51.3
Exterior average	4.72	46.0	63.9
Total average	3.65	58.0	58.3

3.1.1.2 Visualization

With the sixty-two individual data sets from the Baptistery now aligned, the natural first application of the visualization system is to visit the site digitally and virtually (Figure 3.5). This crucial first step – the visualization of the data – informs and facilitates analysis, aids in the interpretation of results, promotes individual and collaborative exploration, and helps in planning future work to be done, whether analysis or further data acquisition. Effective diagnostics requires the means to create and refine models by flexibly synthesizing, layering, and augmenting trusted data – in this case, the one and a half billion data points acquired with calibrated surveying instruments. The interactive visualization system provides an environment for performing these tasks, and serves as a hub for the acquisition and analysis workflows.

Figure 3.5 TLS data set for the Baptistery di San Giovanni showing the surrounding structures as well as the internal dual shell construction.

In order for the interactive visualization system to effectively serve this role, the visualization framework must offer both performance, to deal interactively with billions of data

points, and flexibility, to minimize friction involved in data organization and exchange. To this end, a custom algorithm was developed (Petrovic, et al., 2011; Petrovic, Vanoni, Richter, Levy, & Kuester, 2014) using an adaptively and progressively refining rendering strategy that loads data on the fly as required (a technique commonly referred to as out-of-core.) The algorithm leverages a GPU-based pointbuffer to decouple the interactive performance of visualization from the costs of streaming data from disk or a network server. On-demand loading of data is fully feedback-driven, governed by real-time estimates of the contributions the various data subsets make to the rendering. This paradigm allows data assets, regardless of size, to be dynamically added, removed, interactively repositioned and otherwise transformed, while maintaining interactive visualization performance – enabling the real-time exploration of billions of data points, and allowing the user to flexibly inspect the complete virtual site surrogate.

The visualization system enables the direct visual inspection of the site surrogate 'as-scanned' in full, without concealing evidence of data quality issues, such as scan noise, gaps in coverage and alignment errors – letting the entirety of the recorded evidence be taken into account when making measurements or interpretations, or when contemplating corrective action or a need for additional scanning. It is important to note the interdependent, complementary and iterative nature of the visualization, analysis, and acquisition workflows, as seen in Figure 1.1. Visualization and analysis are used to reveal areas in the digital model that require more data to be acquired, whether to correct data quality issues, or to provide more detail for focused systematic, interactive visual inspection can directly yield analytical results enabling collaborators to form hypotheses, some of which would not be possible without the digital data, as well as aid in designing and planning non-interactive analyses to perform, such as the finite element modeling described in Section 3.1.1.3.

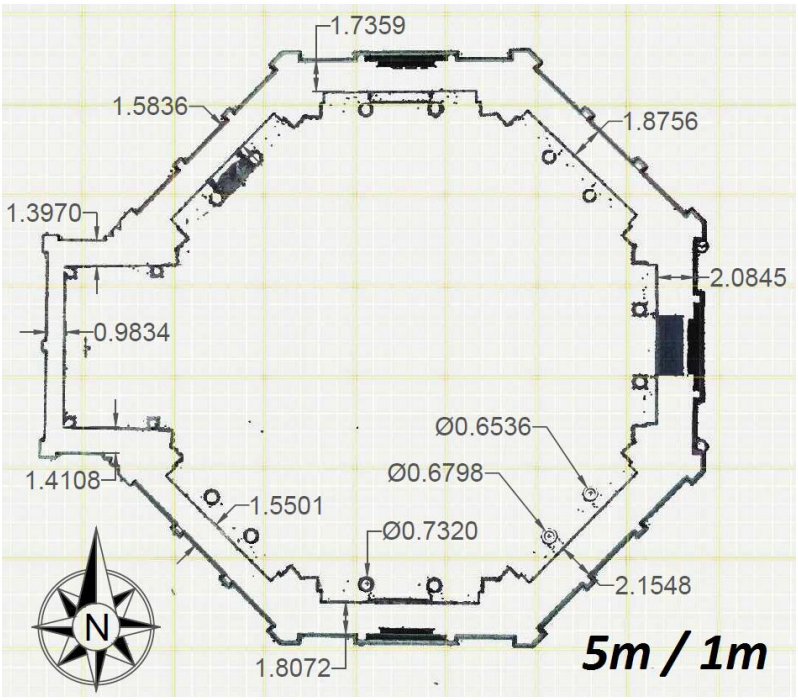

Figure 3.6 Example of a plan view extracted from the TLS data to highlight wall and column measurements.

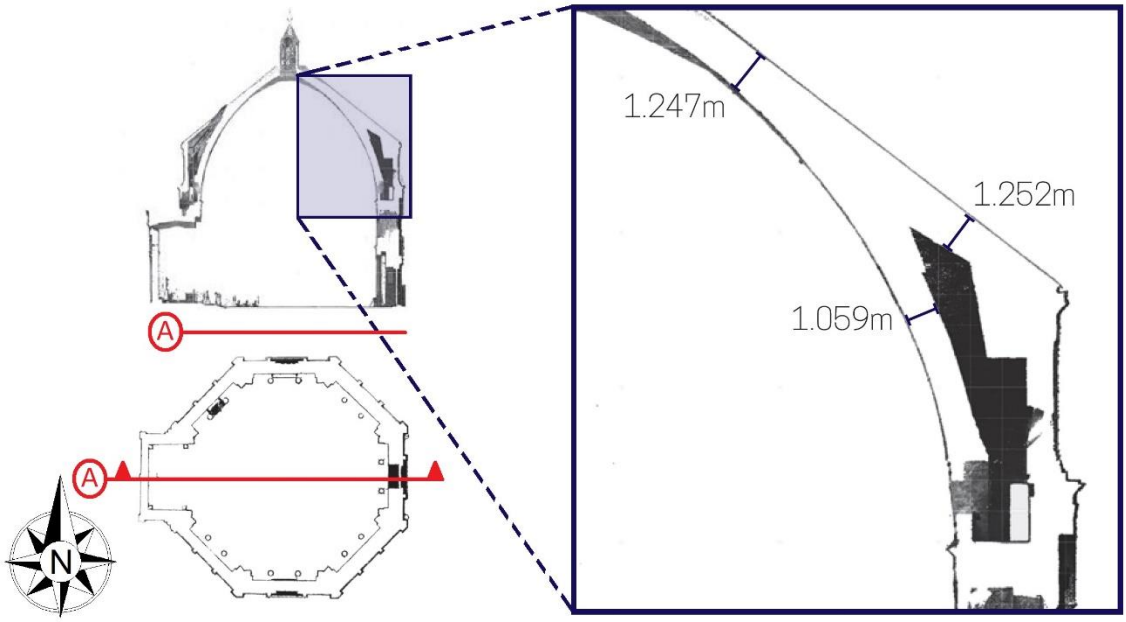

Figure 3.7 Example of a section view extracted from the TLS data measure the thickness of different sections of the dome.

Using the presented approach, derivative data products including cross-sections and floor-plans are computed and visualized at interactive rates from the data points describing the as-built condition of the structure (see Figure 3.6 and Figure 3.7). Creation of these derivative products is supported through a user scriptable interface, allowing for the rapid addition of new strategies for data representation.

The flexibility of the system provides the opportunity for collaborators to work in parallel with the ability to later integrate and compare multiple interpretations within a common digital space. The visualization system serves as a hub for both acquisition and analysis. The visualization system makes import, export, manipulation, alteration and updating of data straightforward, effectively providing a central environment for planning and preparation (e.g. by selecting and exporting sub-regions for further processing) of analyses such as those described in Section 3.1.1.3, evaluation of analysis results and tracking of site documentation progress. Finally, the products of any analyses can be incorporated within the context of the entire virtual surrogate (as in the deviation analyses described in Section 3.1.1.3 and shown in Figure 3.8 and Figure 3.10) for an enhanced understanding of how the analysis results describe the structure's state of health.

The implemented approach allows users to freely inspect the complete virtual site surrogate on hardware ranging from a laptop, to a cluster-driven immersive display environment (e.g. CAVE (DeFanti, et al., 2009), WAVE (Fox, 2013), or tiled display (Yamaoka, Doerr, & Kuester, 2011)). The use of each of these visualization environments provided different benefits. A laptop can be taken on site or to a stakeholder to inspect and present both raw data and results. The ability to transport and manipulate billions of data points describing an entire building is extremely useful in a range of analysis, presentation, and collaboration scenarios. CAVEs provide the ability for a user to be immersed in three-dimensional datasets which provides a digital surrogate of the site being

analyzed. This enables people who were not able to visit the physical site to experience it in a way that is still very close to reality. Tiled display walls and WAVE environments open the data to collaborative exploration and interpretation; these spaces are extremely useful for group investigations of the data in 2D for tiled display walls and in immersive 3D for WAVE displays.

3.1.1.3 Analysis

TLS provides enough accuracy and resolution to make measurements down to a millimeter (FARO, 2017) which can be utilized to perform analyses ranging in size from defects, like cracks, to the global scale of entire buildings. The following examples demonstrate the varying utilities of the comprehensive structural health assessment data set. In this case study it is important to note that none of the presented analyses were intended or predetermined objectives, but stemmed from inspection of the digital record, which highlights the importance of having a reliable method to generate a comprehensive data set.

Due to the nature of TLS data sets, the initial utility is to take measurements between coordinate points. Measurements can be easily extracted from any region of interest with a calculation using the distance formula between two 3D points, as shown in Equation (3.1).

$$d(P_1, P_2) = \sqrt{(x_2 - x_1)^2 + (y_2 - y_1)^2 + (z_2 - z_1)^2} \tag{3.1}$$

Though this is the simplest use for 3D data sets, the ability to compute precise measurements can be extremely beneficial when measuring damages like cracks and structural components like columns. Assessments stemming from this basic application can be observations like crack width, skewed walls, and varying wall thicknesses. An example of the latter is shown in Figure 3.6 where a small slice of the TLS data has been used to measure differences in wall thickness and column diameter.

Another two-dimensional product of the TLS data can be typical engineering drawings like section cuts and plan views of the structure. Figure 3.7 demonstrates an example of a section cut taken from the laser scanning data of the Baptistery in which three example dimensions are highlighted to exhibit the level of precision contained in the data. These deliverables are very useful for planning purposes, especially for historical buildings, where stakeholders typically lack any previous construction records. Without a comprehensive digital model, the provided engineering drawings would be an incomplete misrepresentation of the existing structure.

Beyond providing the ability for singular measurements and engineering drawings, collections of the three-dimensional data can be processed to analyze deviation patterns that exist in a structure. These deviations can be signs of larger problems due to events that have occurred, or are in the process of occurring, and can help inform preservation decisions. Two examples are presented here in order to demonstrate how TLS data can be analyzed to compare existing conditions to idealized conditions.

First, the floor of the Baptistery was studied in order to reveal any topographic deformations that could be due to settling. In other words, this study is a comparison between an idealized level plane and the existing marble surface of the floor. The 3D data of the floor was extracted from the overall model of the Baptistery and analyzed to calculate the variability in the surface. The z-value for every point was normalized over the entire set in order to determine a comparative displacement. Based on the deviation analysis, the points were assigned a color to visualize the deformation where the color correlates to a relative difference in height. The result of this analysis, shown in Figure 3.8, shows a total difference of over sixteen centimeters from the highest point of the floor to the lowest visualized as white and black respectively. This extreme deviation from an idealized level plane could contribute to a worsened structural response of the building to a given loading scenario. Excavation induced settlement causes an increase in lateral

strains in a structure leading to increased vulnerability to differential settlement, cracking, and a decrease in the building's stiffness (Boscardin & Cording, 1989; Son & Cording, 2005). Large scale assessments of this type can lead to more in depth studies that investigate the cause of the observed deviations.

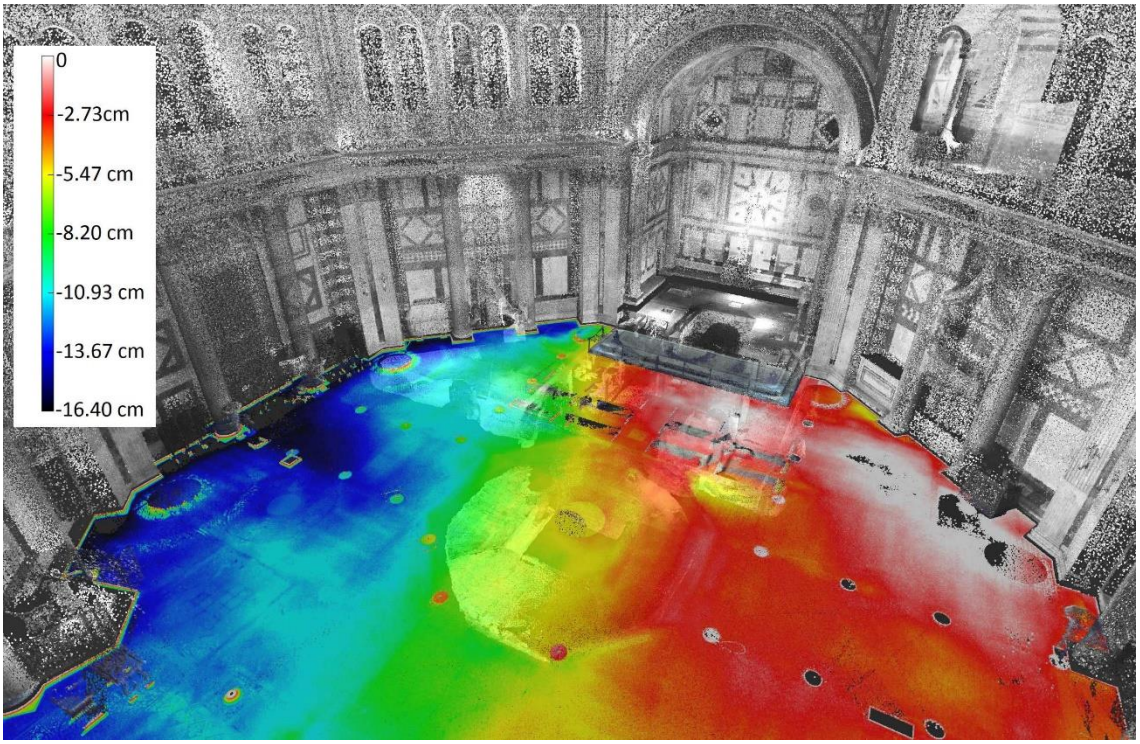

Figure 3.8 The analyzed scanning data of the floor layered on the original data of the Baptistery.

A second analysis was performed on the cupola, or domed ceiling, of the Baptistery. The dome is constructed of eight sides each having a catenary construction. This type of dome construction is depicted in Figure 3.9 showing that it is not hemispherical, but composed of intersecting cylindrical surfaces coming to more of a point. In order to calculate the deviation from an idealized surface, the surface must first be defined. This was accomplished by calculating a best-fit cylinder for the data points in each of the eight sides of the cupola.

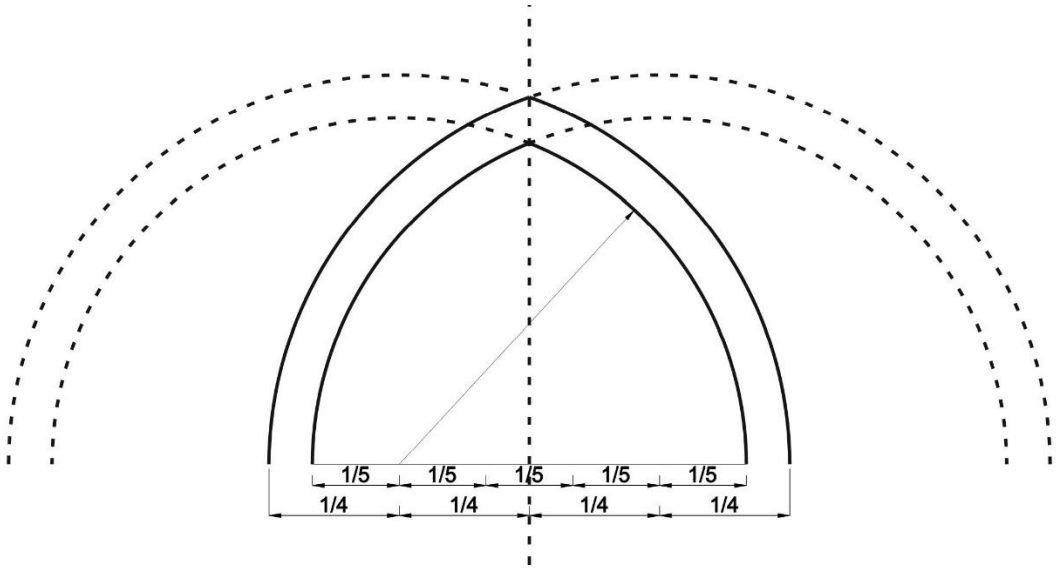

Figure 3.9 Catenary dome construction.

Due to the cylindrical shape of the catenary construction, the analysis could be simplified into a two-dimensional problem. For each of the eight sides, the points describing the dome were transformed to align the centerline of the cylindrical shape perpendicular with the x-y plane. The two-dimensional simplification comes from the shared centerline of the cylinder becoming a common center of a best fit circle when aligned perpendicular to a reference x-y plane. The values to be calculated are the center of the circle (x_c, y_c) and the radius (r) in the following:

$$(x_i - x_c)^2 + (y_i - y_c)^2 = r^2 \tag{3.2}$$

Through elaboration of Equation (3.2), equation of the best fit circle can be linearized and represented as $x^2 + y^2 = Ax + By + C$, where $x_c = -A/2$, $y_c = -B/2$ and $r = \sqrt{4C + A^2 + B^2}/2$. Using least squares regression, Equation (3.3) is minimized by solving the system $\frac{\partial F}{\partial x_c} = 0$, $\frac{\partial F}{\partial y_c} = 0$, and $\frac{\partial F}{\partial r} = 0$. The matrix equation for the least squares regression of points the (x_i, y_i) is shown in Equation (3.4) where n is the total number of points describing the existing dome. Once the least squares regression is performed to calculate A, B, and C, the original three variables x_c, y_c, and r can be determined for the best fit of the data.

$$F(x_c, y_c, r) = \sum [(x_i - x_c)^2 + (y_i - y_c)^2 - r^2]^2 \tag{3.3}$$

$$\begin{bmatrix} \sum x_i^2 & \sum x_i y_i & \sum x_i \\ \sum x_i y_i & \sum y_i^2 & \sum y_i \\ \sum x_i & \sum y_i & n \end{bmatrix} \begin{bmatrix} A \\ B \\ C \end{bmatrix} = \begin{bmatrix} \sum x_i (x_i^2 + y_i^2) \\ \sum y_i (x_i^2 + y_i^2) \\ \sum x_i^2 + y_i^2 \end{bmatrix} \tag{3.4}$$

With the best-fit cylindrical surface calculated, the existing data points for each side of the dome are compared to the idealized shape by measuring each point's distance from the best fit shape. As in the study of the floor, the calculated deviations were then assigned correlated color values and written into the 3D point data in order to visualize the analysis results within the context of the overall model. In the results from the cupola analysis, as shown in Figure 3.10, red represents deviation away from the ideal surface, or bulging, whereas blue depicts deviation on the inside of the cylindrical surface, or caving in.

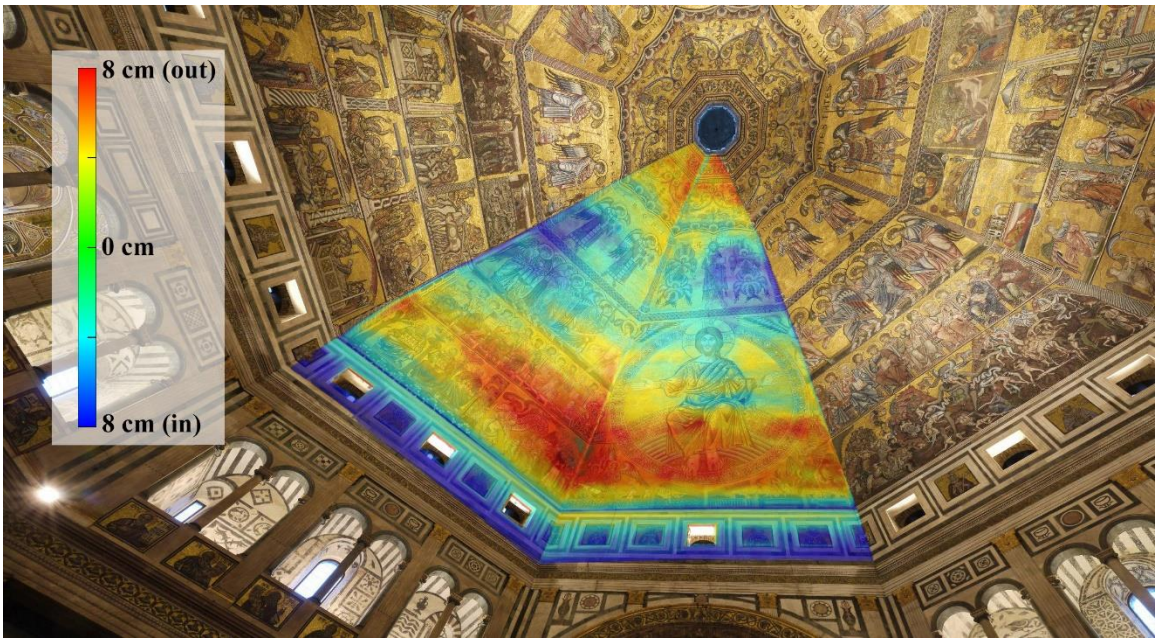

Figure 3.10 The analyzed data of the interior dome layered on a high-resolution image.

The goal of this type of application would be to perform these surveys on recurring schedule so any changes can be detected and tracked through time. If another comprehensive survey

was performed, the time-varying data could be compared using the same comparison methods to identify areas of change which will lead to a greater understanding of the underlying causes of damage. In these two analyses, the comparison data was artificially generated based on idealized assumptions, but the main emphasis is that any newly acquired data can be compared against reference data. The presented methodology ensures that any subsequent surveys will be a reliable basis for comparison.

When the analyzed data are viewed in the overall context of the holistic model, visualization can inform analysis and interpretation of cause-effect relationships. Four example hypotheses from the Baptistery are discussed here to show how comprehensive laser scanning data acquisition, visualization and analysis can enable resolution of difficult engineering problems.

First, the floor deformation is stated in hypothesis form to understand possible causes. The hypothesis is that the excavation activities beneath half of the Baptistery affected the settling of the structure. To gain a better understanding of the relationship between the excavation and the settling patterns the results of the floor analysis are visualized in the context of the rest of the structure. As shown in Figure 3.8 a significant drop in elevation exists at the boundary of the excavation beneath the floor of the Baptistery. The inference here is that the process and outcomes of the excavation led to a change in the floor's response to settling. When the archaeological site was excavated, a modern reinforced concrete slab was constructed to support the floor of the Baptistery above. The consequence of this action seems to be an increased stiffness of only the Northwest portion of the floor which in turn changed the rate at which that portion of the structure now settles. A differing rate of settlement over time will lead to even larger differential settlements and likely damages that will propagate up the structure (Boscardin & Cording, 1989; Son & Cording, 2005). One may not have been able to connect these facts without seeing the floor deformation results in the overall

context of the structure and substructure. The lesson learned here is that modern retrofit actions can lead to unintended consequences, which can alter a historical masterpiece forever.

The cupola analysis is also an excellent example of how the 3D data alone can serve to validate hypotheses because it illustrates the hoop stresses that act at in the lower portion of domed structures. Hoop stress is the resulting horizontal thrust generated by domed and arched structures. The concept has been demonstrated mathematically (Flügge, 2013), but in this case, it has been quantified for an existing historical dome and the results can be visualized in the context of the entire structure.

For the two deformation analyses the argument could be made that the structures may have always looked exactly as they do now, but the more realistic likelihood is that they were constructed closer to the idealized shapes and deformed over time. This holds two important notions: (1) that the structures are far from the idealized shapes and (2) that there was likely deformation and damage that occurred over time to cause these deviations. The existing surfaces not only deviate from ideal shapes, but the changes that caused the deviations may also cause deviation from ideal mechanical responses of the construction materials. Again, it is important to note, that the ideal surfaces that were used for comparison here were created from assumptions, but if future surveys were to be completed in the same comprehensive manner, the new data could be compared against the presented data to help further validate hypotheses with irrefutable evidence.

To expand on propagating damages, two more hypotheses are explored. The first is that the cracks visible above the main doors of the structure may have propagated throughout the structure and may also be indications of further damage. To test this theory, a high-resolution scan was conducted above the North door, seen in Figure 3.11, in order to document and measure the damages that exist. In the highlighted section of Figure 3.11 a crack in an arch located one story above the North door is shown and measured; the crack has propagated from above the North door,

through a floor slab and through the archway shown. These precise measurements are important to document the existing damages in the structure. Now that this digital documentation record exists, these cracks can be monitored over time by completing subsequent laser scanning surveys of the balcony.

Figure 3.11 Scanning data highlighting the dimensions of a crack above the North door.

The last hypothesis again concerns the substructure of the Baptistery. Viewing the damage patterns in the foundation wall (Figure 3.12) in the context of the supporting structure above shows that the diagonal cracking occurs directly below a main supporting column. It seems that when the substructure was emptied, more of the weight to be supported was transferred to the foundation wall. Without the context provided by the digital viewport shown in Figure 3.12 the damage in the foundation wall may seem arbitrary; with the overall context provided by the comprehensive model, one can see that the column above rests directly above the cracking damage.

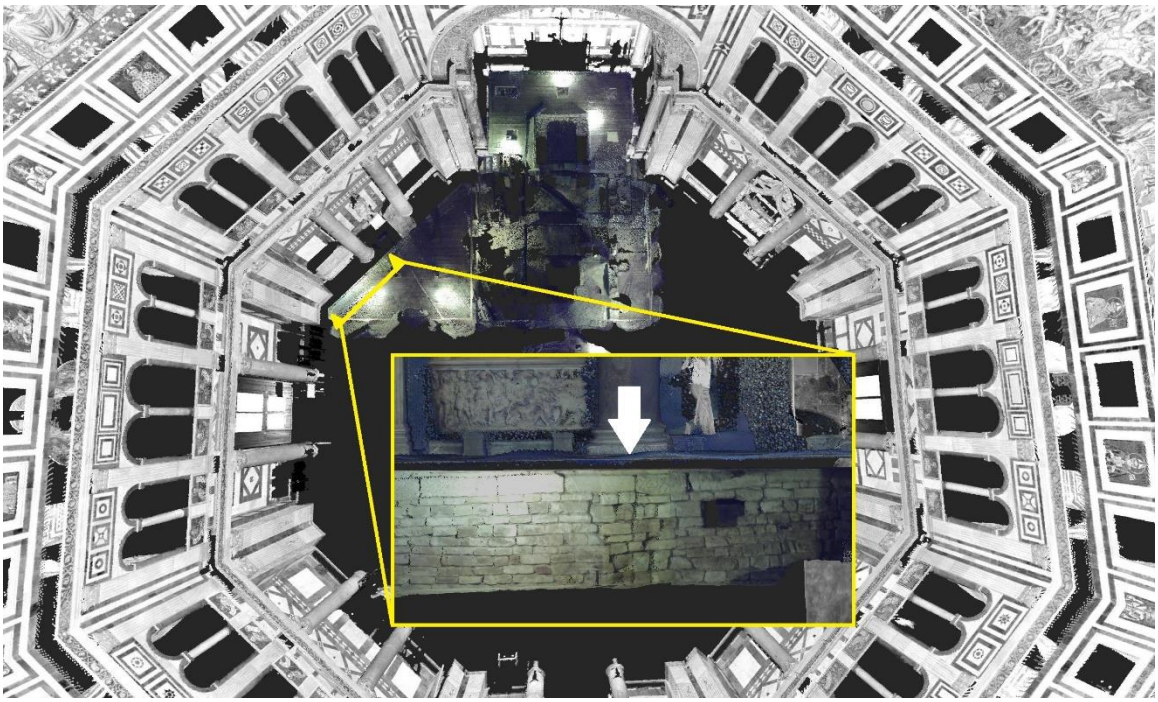

Figure 3.12 Digital viewport showing a supporting column that rests above a cracked foundation wall.

With accurate geometry measured everywhere in the structure, more detailed numerical analysis can be performed to accurately characterize the internal forces and structural performance of the building. For the Baptistery, initial numerical simulations were conducted to further study the damages observed in the foundation wall. First, the laser scanning data was used to guide the modeling and simulation of one of the Baptistery walls. Section cuts and dimensions were extracted from the final model in order to calculate the volume of masonry material that exists in one of the eight sides of the dome. This volume calculation enabled very realistic estimation of the forces acting on the supporting walls and columns. Autodesk Inventor was then used to perform the following analyses (Kim, Kim, Park, & Kim, 2010).

Wall models with and without a door were created and simulated in order to calculate the reaction force at the base of the columns on the first floor. This calculation was done in order to

transfer the resulting column load to a numerical model of the foundation wall beneath in order to understand if the force of the column above the wall could be a cause of the observed cracking pattern. The numerical modeling strategy used for the main supporting wall was a smeared macro-modeling approach where the masonry units and mortar are modeled as a continuous, isotropic material with one set of material properties across the entire model (Betti & Vignoli, 2011). The material properties used in the analysis were those from the ETH Zurich walls (Facconi, Plizzari, & Vecchio, 2013; Ganz & Thürlimann, 1984; Ghiassi, Soltani, & Tasnimi, 2012). The calculated weight of over thirteen hundred tons was distributed over the top surface of the model while the bottom surface was fixed, and a static analysis was performed in order to obtain the reaction forces at the base of the columns. The results from the simulation, shown in Figure 3.13, concluded that in the walls without a door each column carries approximately sixty-four thousand pounds.

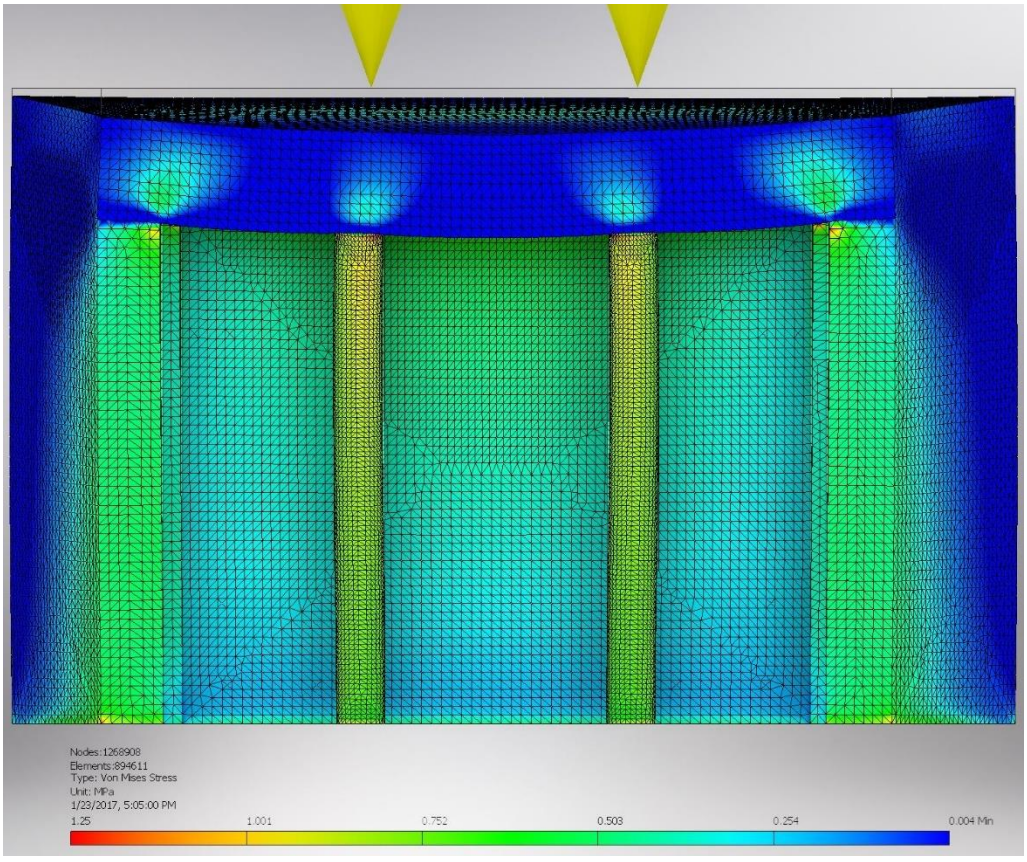

Figure 3.13 Numerical simulation of the Baptistery wall showing the resulting stress.

Table 3.3 Material properties used to simulate granite stones.

E (ksi)	ν	G (ksi)	ρ (lbs/in3)	σy (ksi)
7977	0.25	3916	0.098	5.656

The foundation wall was then modeled from the TLS data to capture the irregular distribution pattern of the masonry stones and mortar. It is important to note that the simulated foundation wall was assumed to have all of its mortar joints intact to resemble the wall before damage. The mortar material properties were the same as used in the previous simulation, but in this analysis the stones were modeled individually and given properties to resemble cut granite stone (Table 3.3). The reaction force calculated in the previous simulation was applied as a

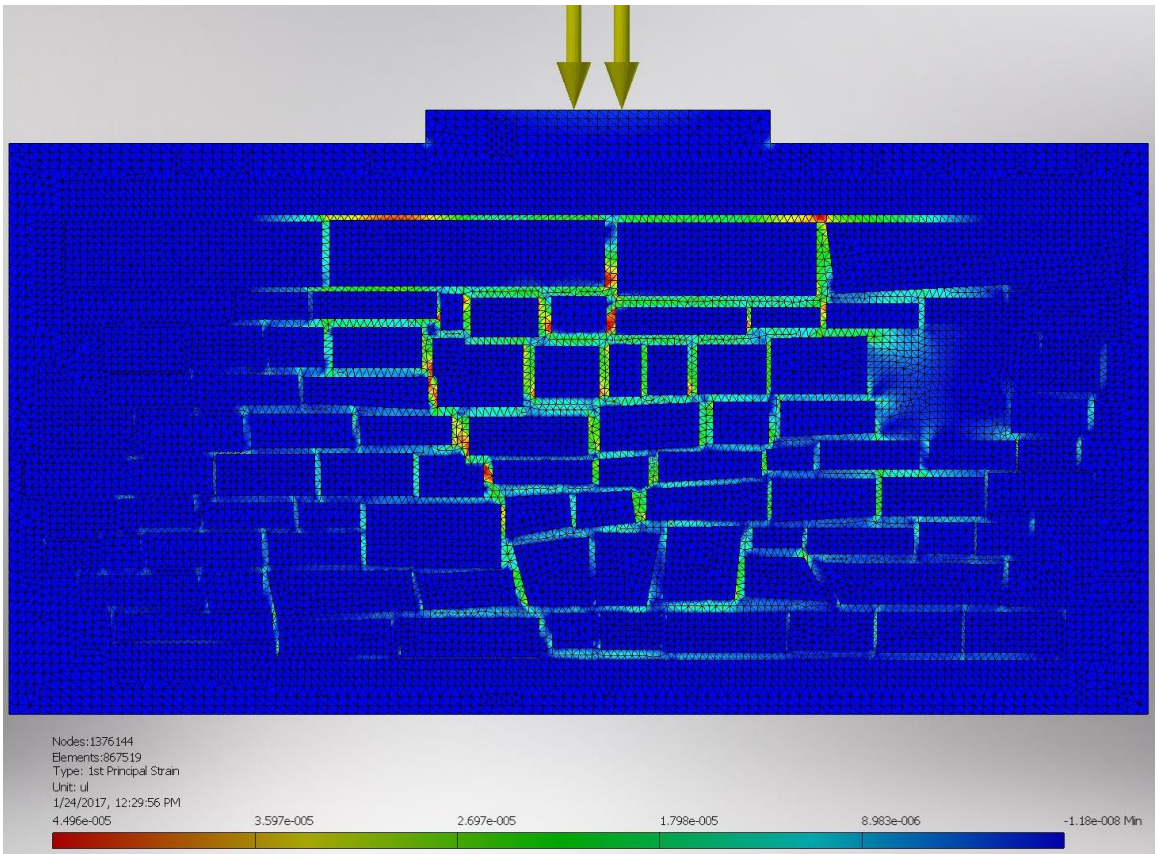

Figure 3.14 Results from the numerical simulation of the existing foundation wall showing the first principal strain.

pressure on the column's base while keeping the bottom of the foundation wall fixed. In this initial simulation shown in Figure 3.14, it can be seen that the principal strain is concentrated in exactly the areas of observed cracking. More complex simulation and interpretation are required to determine the root cause of the cracks as well as future response of the wall with the existing cracks defined and accounted for. These follow-up investigations are possible through the use of the integrated data acquired in the survey campaign.

3.1.2 Conclusions

Historical structures have endured both man-made and natural disasters as well as other actions that may have caused unintended consequences along the way. Many structures have survived through these decaying processes, but preventative actions must be taken in order to prolong their life further into the future for more generations to experience. Structural health assessment is an imperative step towards proper management of these priceless cultural landmarks. Through structural health assessments professionals can learn what deficiencies exist now, possibly how they occurred, and most importantly how to slow or stop the decaying processes in the future.

A structural health assessment was undertaken to study one of the most iconic monuments in Florence, Italy, the Baptistery di San Giovanni. Without specific outcomes or objectives established before the documentation campaign, the goal was to generate a comprehensive geometric record of the entire building. In order to guarantee a comprehensive survey of the entire building, a specific methodological approach was required. The presented approach considers the limitations of TLS technology as well as the challenges and circumstances presented by the structure being studied. The survey of the Baptistery presented challenges of time, limited access, delicacy, and cultural significance which were all taken into account along with issues of occlusions, sufficient overlap and required resolution inherent in TLS documentation. These challenges provided boundary conditions for the formulation of a complete structural health

assessment methodology. The diagnostic value of a repeatable integrative methodology has been presented through this case study at the Baptistery wherein data acquisition, visualization and analysis informed the structural health assessment of an iconic historical monument.

The TLS survey of the Baptistery acquired 3D measurements detailing almost every visible surface of the structure resulting in over one and a half billion 3D data points. Several analyses were performed on the raw data in order to inform stakeholders as to the Baptistery's structural integrity. Two examples are presented in which the acquired laser scanning data has been compared against reference geometry to assess deformation patterns. The deviation analyses presented here demonstrate the capability for initial assessments based on ideal conditions, but in the future, the same methodology can be used to study temporal TLS datasets in order to detect new damages and structural changes. This work also demonstrates the ability to form and test hypotheses from TLS data of an existing structure. Utilizing the feedback driven visualization system, analysis can be performed iteratively with the ability to export selected portions of the dataset for analyses like finite element modeling. To accentuate this capability, finite element analysis was conducted on two connected wall systems in the Baptistery to study the potential cause of observed damages.

By following the comprehensive acquisition, visualization and analysis workflows presented in this paper, significant observations can be made and in some cases quantified analysis can be performed enabling better management and preservation of historical structures. Through the presented methodology, the assessment objectives need not be known in advance of the survey and in this way, a more comprehensive survey can be expected with no bias given towards areas being investigated. The goal of this work is to show that with thorough geometric documentation, powerful diagnostic analysis can be performed from data which was not initially intended to be used for any specific investigation. Many previous works have presented specific studies that can

be conducted from TLS data and here we emphasize that this methodology enables the incorporation of all analyses in one integrative, dynamic, interpretive model.

For the results of TLS surveys to have an impact on the preservation of structures, they must be communicated in the proper manner to the entities with the power to take action. The flexible visualization environment outlined here is able to not just communicate the conclusions already made, but also allow stakeholders and other necessary professionals to explore the data, make their own conclusions, and perform their own analyses. Next steps will include the integration of complementary data streams generated by other techniques such as thermal imaging and ground penetrating radar. The incorporation of these additional data into the comprehensive model will enable more analyses to be performed in one collaborative environment and also enhance understanding and management of historical structures.

3.2 Photogrammetry

The previous section detailed some of the powerful uses of detailed digital geometric data acquired with laser based techniques. This section explores alternate methods for geometry creation through the use of 2D imagery. Photogrammetry techniques like structure from motion (SfM) are being used more often due to the exponential increase in available computing power and the advancement of high-resolution cameras. As discussed in 2.1.2 the approach processes photos taken of a target from different points-of-view in order to triangulate common features and project them into three-dimensional space. In addition to the 3D point clouds that can result from dense feature matching in the images, the images contain the photorealistic texture that produce a visually compelling representation of the target. Recall that photogrammetry is a line-of-sight approach, so the user must ensure that images are acquired from enough viewpoints to eliminate any issues of occlusion. SfM techniques are often unsuccessful when attempting to reconstruct an interior space like a room, therefore interior building surveys are not typically completed solely with

photogrammetry. The resulting point cloud on its own is also not a reliable source of absolute measurements unless a reference scale is specified to transform the points into accurate world coordinates.

There are certain procedures to follow when generating photos for SfM models. Experience with the process has given way to learning the things to do and not to do. Generating a truly photorealistic model of an outdoor structure can be difficult because of unpredictable changes in natural lighting and the size of the target structure, which requires many camera angles, some of which cannot be obtained from the ground. Through studying the process as well as results obtained from many trials, a better understanding has been achieved. Through this detailed understanding of the underlying computer vision techniques and expected operating conditions, a methodology of how to generate high quality photos for SfM applications has been developed.

Presented in this Section are three areas of application where photogrammetry was used in accordance with the developed best practice methodologies in order to achieve different goals. First is an example of geometry creation for site documentation for an at risk cultural heritage site. Next, photogrammetry is discussed in regard to its utility for disaster response, reconnaissance, and analysis. Discussed in the last section is the use of the photogrammetric point clouds for more detailed analysis of structures using interactive point cloud visualization and annotation. The field of cultural heritage documentation has greatly benefited from advances in SfM processing and there is still room for growth in the application of the resulting data.

3.2.1 Geometry Creation

One of the reasons for the adoption of SfM methodologies in cultural heritage contexts is the speed at which the surveys can be conducted. The processing time can range from hours to weeks depending on the number of images and available computing power, but time on-site can be limited and fit within common constraints of cultural heritage site access. To give some perspective

of the amount of post-processing required, a computer with 128 gigabytes of RAM ran for two weeks processing 5000 images in SFM software (Agisoft PhotoScan) in order to generate a point cloud of the church at the site of Ecab seen in Figure 3.15 which totaled 130 million points (Hess, et al., 2014). From two short days on site, ground based high-resolution images were combined with aerial images acquired with a drone to generate this 3D model through the use of SfM.

One of the fastest emerging technologies right now is remote imaging platforms, specifically aerial drones. Our team brought its own fleet of remote control, multirotor drones that have been designed or purchased for airborne imaging applications. A pilot stands on the ground controlling the drone and monitors the battery levels, altitude, orientation, etc. while simultaneously capturing images of a target below. Lightweight imaging drones are not often deployed to the field because the level of expertise required and the treacherous flying environment, such as dense vegetation and water. Aerial imagery obtained from satellites can be low quality and not helpful for detailed applications while renting aircrafts that can capture the desired image quality is very expensive, so small remote imaging drones are an extremely attractive option. Images taken from the sky provide context of the site and generate viewpoints that would not otherwise be available.

In the survey campaign, a high-resolution, Sony QX100, camera was attached to a small quadcopter and flown over the site to capture images. The aerial images give an amazing perspective of the structures and their surroundings with a high level of detail. Ground based photography was also used to acquire thousands of images. The high-resolution images can be combined with the aerial images and processed using SfM in order to render a photorealistic model of the structures and site. For the site of Ecab, three separate SfM models were created. The photogrammetric point clouds of the two structures seen in Figure 3.15 were created individually and then placed in their overall context of world coordinates using the last dataset which details the overall site geometry.

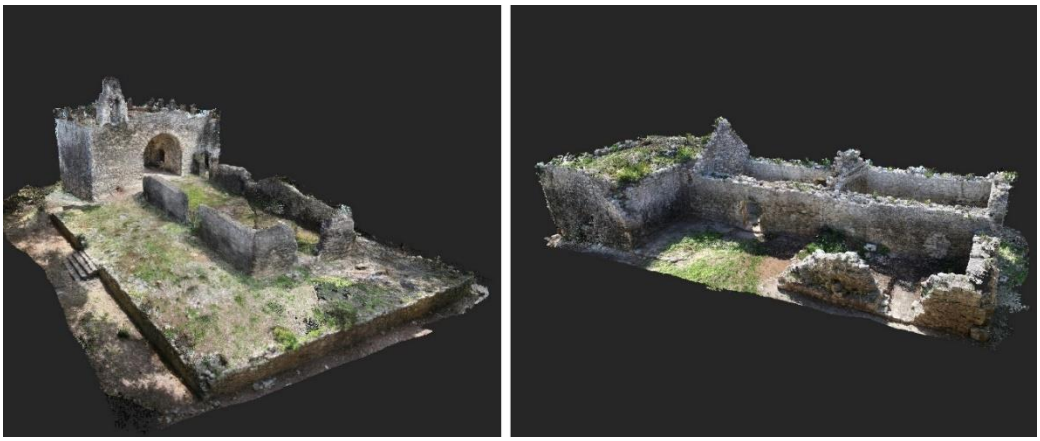

Figure 3.15 SfM point clouds of the Church (Left) and Casa Cural (Right).

These models exemplify the utility of photogrammetry techniques for the documentation of cultural heritage structures. These 3D models comprising of point clouds which contain hundreds of millions of 3D data points can now be used for future preservation and restoration planning. Mexico's National Institute of Anthropology and History (INAH) is the government entity serving as the stakeholder and decision makers for this historically significant site. These data records are extremely useful for posterity as well as detailed planning for this remote archaeological site that is at risk situated on the coast of an area of Mexico that is often at risk of experiencing hurricanes.

3.2.2 Disaster Response

The capabilities for disaster response and documentation has been tested in a handful of real world disaster scenarios as well as a simulated earthquake on a modern full-scale building. Following earthquakes in South Napa, California, Taiwan and Mexico City, a rapid response team was sent to document the damages incurred in the disaster. The goal of the documentation efforts being to learn why some structures failed and other did not. Insights made after studying events like these have been vital to the field of earthquake engineering.

Included in these response team were UAV pilots who were there to acquire aerial photographs for use in planning on the ground and for use in photogrammetry processing pipelines.

The latter is of interest here because the photogrammetry results provide geometric snapshots in time for areas that are rapidly changing as responders work to clean, demolish and rebuild after a disaster. One example from the South Napa Valley earthquake in 2014, shown in Figure 3.16 depicts a historical family vineyard that was damaged (Wittich, Hutchinson, Lo, Meyer, & Kuester, 2014). This is an excellent example of acquiring perishable data; due to large non-structural stainless-steel tanks that had fallen and were now leaning on the interior wall, the building was deforming more and more every day. Captured in the point cloud of the damaged building are the construction loader vehicles that were used to reinforce the right side of the structure which was deforming at a rapid pace.

Figure 3.16 Photograph (left) and SfM point cloud (right) of the damaged vineyard structure.

The simulated earthquake testing achieved a wide variety of structural engineering objectives (Hoehler, et al., 2017; Wang, et al., 2016). Discussed here is again the capability of rapid post-disaster documentation. Again, aerial imaging platforms were used to acquire photographs of the structure both before and after each earthquake event (Figure 3.19). This resulted in an array of pre- and post-disaster datasets which could be used for damage identification, change detection and

deformation measurement. These geometric snapshots can now be used in tandem with other physical sensor data to extract building characteristics and performance insights.

Figure 3.17 Photograph (left) and SfM point cloud (right) of building tested on the outdoor shake table.

3.2.3 Point Cloud Classification

The increasing use of photogrammetry techniques for the digital documentation of cultural heritage structures has led to an abundance of 3D point clouds that describe historical architecture. However, tools to analyze and interact with these 3D datasets are far less abundant. Demonstrated in this section is how these extremely rich geometric records can be analyzed and utilized to accomplish user defined tasks.

Existing structures, especially historical architecture which have existed for centuries, may have undergone undocumented transformations including damages, floor plan modifications, and alterations to original building materials. Photogrammetry techniques like SfM are being utilized more and more for the acquisition of accurate 3D geometry describing cultural heritage sites and structures. Initially, these 3D data records are great to visualize and gain digital perspectives of a

given target. More important though is the potential for analytical workflows and detailed assessment of structures using these dense point cloud records.

Presented in this section is just one of the countless objectives that can be achieved through the acquisition, visualization and analysis of photogrammetric point cloud data. Explored here is how to bridge the gap from digital documentation towards Historical Building Information Models (HBIM) (Oreni D. , Brumana, Della Torre, Banfi, & Previtali, 2014; Quattrini, Malinverni, Clini, Nespeca, & Orlietti, 2015) that not only capture the overall geometry of a structure, but also break down the virtual structure into its components. A vast majority of historical structures that still exist today are masonry constructions, so the focus of this work is to achieve the classification of the observed masonry materials through the analysis of 3D data derived from laser scanning or photogrammetric techniques.

Just as an architect traditionally annotates engineering drawings of a building, these 3D point cloud models should be annotated to provide additional information that will aid in the interpretation of the structure's construction, history, state of health, as well as decisions concerning its future preservation. A useful first step in this annotation process is to classify a structure's construction materials into different categories. The specific focus of this section is the classification of masonry materials into its individual components with the goal of building more accurate as-built models of historical structures. In the presented approach varying user defined functions have been tested within an interactive, feedback driven point cloud visualization framework (Petrovic, et al., 2011; Petrovic, Vanoni, Richter, Levy, & Kuester, 2014) to evaluate automated and semi-automated classification of 3D point cloud data. These functions can include decisions based on observed color, laser intensity, normal vector or local surface geometry.

Automatic classification of point cloud features is not always an accurate or straightforward process. The presented approach leverages interactive user, or subject matter

expert, inputs in order to classify building geometry more accurately and efficiently. Users have the ability create their own functions in JavaScript and the functions will be executed on top of the point cloud visualization engine. The visualization system handles the organization and queries to the point data and the user's function will execute on an identified selection of points. With the ability to manipulate and analyze billions of points in real time on available hardware, the visualization framework enables the swift addition of metadata to the 3D geometric model. Extremely important to the presented approach is that the raw point data are not altered; instead, tags are associated with the points with the ability for a point to have multiple tags as well as dynamically changing tags.

The operating scenario considers a subject matter expert as the user and the functions are designed by the user to achieve their prescribed objectives. Utilizing the expert's guided input, the system then performs automated routines to refine the classification. This semi-automated hybrid approach to classification allows more complicated features to be extracted and annotated through interactive feedback. The visual feedback achieved through the visualization system, allows for the user to more accurately refine the functions being executed to optimize the automated portion of the process.

The example presented here demonstrates the flexibility and utility of the presented point cloud visualization framework to achieve classification objectives. The goal of this work is the classification of construction materials used in cultural heritage structures. Specifically, this work demonstrates multiple approaches to automatically and semi-automatically classify masonry structures into their stone and mortar counterparts. The accurate geometric classification of existing masonry materials will aid in more realistic numerical simulations of a structure in order to plan for preservation and restoration actions.

Observations that can be quantified through masonry classification include the average sizes of masonry units and mortar joints, variation and distribution of those dimensions, in addition to overall masonry patterning. The goal of this study is to discourage general assumptions that can be made concerning the local geometry and uniformity of masonry constructions. In other words, highlighted here is a methodology to capture the as-built structural state. Although, in some cases, assumptions concerning masonry geometry may not lead to vastly different conclusions, the capability to accurately document the geometry exists and should become standard practice in order to more precisely assess a structure's state of health.

3.2.3.1 Point Classification Approach

The goal of the presented approach is to utilize a user's valuable expert intuition and input in order to classify 3D masonry material faster and more accurately. Through the presented flexible visualization system the user can dynamically annotate massive point clouds in real-time. The ability to manipulate the point cloud model in 3D space makes the job of annotating much easier with the ability to alter one's perspective with ease. The visualization engine enables the interactive manipulation of large point clouds that can be derived through laser scanning or image-based techniques. The heavy lifting of the visualization operations is handled by the underlying engine.

The example model used, as seen in Figure 3.18, is a point cloud derived through photogrammetric processing of images in order to render a geometric model. This structure was used due to the different phases of construction as well as the varying styles and colors used in the execution of the masonry facade. The approach uses an intelligent "paint brush", as seen in Figure 3.19, that interactively operates on a spherical selection of points. The size of the sphere used to query the points is adjustable and can be changed in real-time. The operations and functions that are executed within the brushing sphere are designed through a real-time updated JavaScript framework that communicates with the visualization engine in order to pass and execute the point

data queries. Attributes of the points such as coordinates, color, normal and intensity can each be accessed and utilized in the JavaScript functions.

Figure 3.18 Photogrammetric point cloud of a damaged masonry structure.

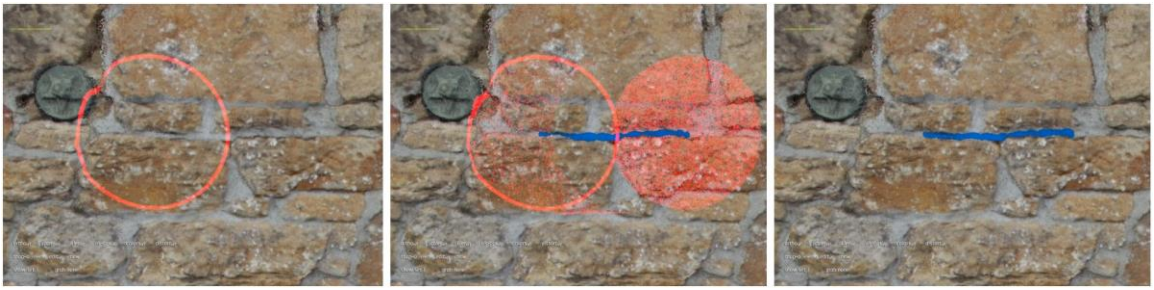

Figure 3.19 Intelligent point selection tool for interactive annotation of point clouds.

The first step of the presented example was to create a ground truth to compare our semi-automated tests against. The mortar in the front and the side of the building were manually annotated, or tagged, with pink and green respectively (seen in Figure 3.20). This ground truth tagging has three areas of style and color that each present their own challenges. The lower portion of the side wall is very irregular in pattern, constructed with stones that have a very different color than the mortar material and the topography of the mortar is very well defined. The topography of

the mortar in the upper portion of the side wall is also reasonably well defined, but the colors of the stone and mortar are very similar. As for the front of the building, the construction is very regular with small mortar joints that as similar in color and do not have a very pronounced geometric pattern. Even though this ground truth creation required two and a half hours, the interactive manipulation of the point cloud made it extremely easy to select neighborhoods of points corresponding to mortar. The resulting annotation is an extremely accurate classification of the existing mortar pattern and 3D geometry. Although this initial process was completely manual, when compared to traditional drafting techniques, the time spent was not significant and the accuracy achieved is much greater.

Figure 3.20 Manual ground truth annotation of mortar joints.

Next, a semi-automatic JavaScript function was developed and tested in order to make annotation of the mortar easier for the used by adding some intelligence to the interactive brush. The initial iteration of the mortar brush utilizes the color and normal of the points in order to make decisions based on local statistics. This method assumes that the center of the initial brush click, or seed point, is what the user desires to be tagged. With the initial seed point, the user queries the

core system and sends the location in the coordinate space and a search radius. The visualization system processes that query and returns a ball of points consisting of the nearest neighboring points to the specified coordinate within the given search radius ordered by distance from the center of the searching sphere. The ordered list of points that is passed from the visualization engine to the JavaScript function contains the attributes of each point: position (x, y and z coordinates), color (red, green and blue channels), point normals (x, y and z components), current tag or layer, as well as any other attributes associated with the point data.

The JavaScript first loops through a chosen number of closest points (fifty points in this test) to calculate the reference mean and standard deviation of each color channel and normal component in the area of the seed point. The script then steps out from the seed location point-by-point and compares each point's normal and color to the reference color and normal calculated in the first step. The classification strategy or selection criteria is flexible per user, but in this case the decisions were based on the variation from reference normal and distance in RGB space.

$$Normal\ Deviation = [N_{x,ref} \quad N_{y,ref} \quad N_{z,ref}] \cdot [N_x \quad N_y \quad N_z] > \cos\theta_{threshold} \tag{3.5}$$

$$RGB\ Distance = \sqrt{(R_{mean} - R)^2 + (G_{mean} - G)^2 + (B_{mean} - B)^2} \tag{3.6}$$

The presented normal variation criterion depends heavily on the surface indentation of mortar joints and accurate calculation of point normals to represent the changes in local surface geometry. The classification boundary is halted when a steep incline is detected indicating the transition out of the mortar valley to the stone surface or vice-versa. In particular, a normal is accepted if its dot product with the reference normal is greater than the cosine of the threshold angle as in Equation 3.5. The color attributes of the points are used to further enhance the accuracy of the classification. The color criterion considers RGB color space as a cartesian coordinate system and calculates the RGB distance of each point from the reference color. The threshold for the color distance is defined as a multiplier of the standard deviation of the RGB distances.

3.2.3.2 Results

Through testing, initial parameters were chosen so that mortar was classified if the color and normal thresholds were both satisfied. For the color constraint, the current point must be within two and a half standard deviations from the initial point color, based on the local neighborhood statistics. Given the initial reference normal direction and a maximum permissible deviation angle, a candidate point is accepted if the angle between its normal and the reference direction is smaller than the threshold deviation angle. In particular, a normal is accepted if its dot product with the reference normal is greater than the cosine of the threshold angle, which in this case is 53.13°.

Figure 3.21 Semi-automated annotation of mortar joints.

As seen in Figure 3.19, although many points are queried, only the points corresponding to mortar material are tagged due to the thresholding function defined in the JavaScript. This brush was utilized in three areas with the three different construction styles previously mentioned in order to compare the performance of the brush function under varying colors and normal values. Ten minutes was allocated for each test in which the user classified as much mortar material as possible with the scripted brush. The real-time feedback of the visualization system, which colors the tagged points, allows the user to revisit areas that have not been sufficiently tagged.

The resulting annotated mortar points, seen in Figure 3.22, were then compared with the ground truth data in order to identify false positive and false negative classifications. The overall results are summarized in Figure 3.22 detailing the percentages of false positives and negatives as well as the average distance of each false to a classified positive. The last distance comparison is to qualify how far off these false classifications were. For all of the tests, fifty percent of the misclassified points were less than nine millimeters away from a true classified point. This is to say that though the percentages may seem high, the accuracy of the classification was still acceptable. Also to be noted is the comparison in time where each of the three tests was executed in just ten minutes whereas the initial ground truth classification took two and a half hours.

Test	False Positives (FP)	False Negatives (FN)	Avg. distance of FP from true positive	Avg. distance of FN from tagged positive
Lower side	26%	30%	0.0102 m	0.0155 m
Upper side	23%	53%	0.0119 m	0.0137 m
Front	46%	28%	0.0095 m	0.0106 m

Figure 3.22 False negative and positive percentages for initial annotation test.

The initial implementation of the presented semi-automated interactive classification of masonry point clouds was effective in speeding up the process with limited repercussions in terms of accuracy. Improvements will be made in the future to minimize the number of false positives classified in the process as well as decrease the number of false negatives that are not classified along the way. Future efforts will be directed towards the integration of other methods and additional point attributes such as laser intensity when handling point clouds generating through laser scanning techniques. The flexibility of the scripting framework and its integration with the point cloud visualization system will have much broader implications and the presented case study

is relatively simple example of the utility of such a robust system. The JavaScript for the presented work is included in Appendix A.

3.3 Conclusions

This Chapter discusses the acquisition of large-scale geometric data through both laser scanning and photogrammetric techniques. Accurate surface geometry represents the vital scaffolding structure for all other data formats to be registered to and draped upon. Both TLS and SfM techniques have proven capable of performing rapid comprehensive documentation in the face of real world obstacles and limitations. Through the examples presented here, it is demonstrated that the geometric data alone can also be extremely useful for different diagnostic and analytical tasks. Comprehensive geometric data capture, regardless of the intended use, is crucial for effective creation and elaboration of an as-built information model. With a reliable comprehensive baseline model in place, it can be annotated, qualitatively analyzed and recurring surveys can be conducted to track changes and damages throughout time.

3.4 Acknowledgements

This work was supported by the National Science Foundation under award #DGE-0966375, 'Training, Research and Education in Engineering for Cultural Heritage Diagnostics,' and award #CNS-1338192, 'MRI: Development of Advanced Visualization Instrumentation for the Collaborative Exploration of Big Data.' Additional support was provided by the Kinsella Fund, the Qualcomm Institute at UC San Diego, the Friends of CISA3, and the World Cultural Heritage Society. The authors would like to thank the city of Florence, Maurizio Seracini, the Opera di Santa Maria del Fiore and President Franco Lucchesi for the opportunity to study the Baptistery di San Giovanni. The authors would also like to thank Centro INAH Quintana Roo, Adriana Velazquez Morlet, Enrique Terrones, Sandra Elizalde, Alexandra Hubenko, Vanessa Pool, Fabio Esteban

Amador, Jeffrey Glover, Andrew Vaughn, Roberto Echeverria, Manuel Joya, Reymundo Joya, Carlos Basto, and Marcia Kirby. Opinions, findings, and conclusions from this study are those of the authors and do not necessarily reflect the opinions of the research sponsors.

This chapter, in part, is a reprint of the material as it appears in the Journal of Structure and Infrastructure Engineering. Hess, M., Petrovic, V., Yeager, M. and Kuester, F. (2017). "Terrestrial laser scanning for the comprehensive structural health assessment of the Baptistery di San Giovanni in Florence, Italy: an integrative methodology for repeatable data acquisition, visualization and analysis" *Structure and Infrastructure Engineering*, 1-17. The dissertation author was the primary investigator and first author of this publication.

Section 3.2.3 in part, is a reprint of the material as it appears in the International Archives of the Photogrammetry, Remote Sensing & Spatial Information Sciences. Hess, M., Petrovic, V., & Kuester, F. (2017). "Interactive Classification of Construction Materials: Feedback Driven Framework for Annotation and Analysis of 3D Point Clouds" *International Archives of the Photogrammetry, Remote Sensing & Spatial Information Sciences*, (Vol. 42, pp. 343-347). The dissertation author was the primary investigator and first author of this publication.

Chapter 4 Subsurface Documentation: High-Resolution Thermal Imaging

Infrared thermography, which captures a combination of surface and subsurface information, can measure spatio-temporal ambient signals, from a distance, accomplishing multiple non-destructive evaluation (NDE) objectives. As discussed in 2.1.3, common application domains of this multi-purpose diagnostics tool include energy audits (Balaras & Argiriou, 2002; Titman, 2001)which establish the thermal envelope of a structure, detection of pests, moisture, and mold (Grinzato, Bison, & Marinetti, 2002), structural deficiency and integrity assessment focused on detecting cracks, delamination, as well as material characterization. The ability to characterize materials can aid in creating a baseline as-built record showing construction details and modifications of structures as in Figure 4.1. This is especially useful when surveying historic structures because they often lack these construction records.

Building-scale structural health assessment requires accurate and detailed measurements at the macro and micro scale, providing a holistic view of the structure, establishing the overall context, as well as the data needed to study small scale characteristics, deficiencies and damage patterns. Given the necessary resolution, instrumentation, time complexity and cost this is rarely done for thermographic surveys. The most advanced thermal cameras currently only achieve one-megapixel resolution (FLIR Systems Inc., 2014) and they come with a high price tag. When used in the field at building scale, different lenses may be used, a wide field of view lens providing context, but no detail, and a narrow field of view lens providing detail, but no context. With the available time budgets for site surveys, this often results in just a few spot surveys being performed.

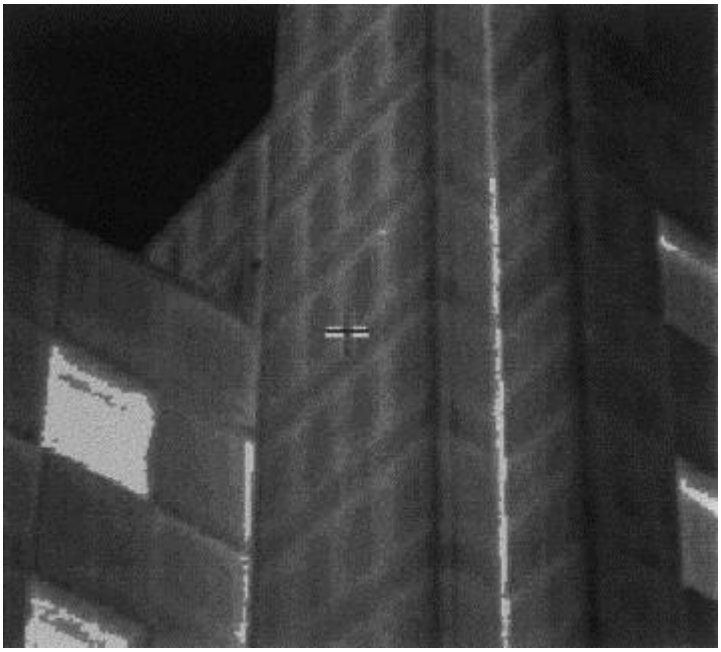

Figure 4.1 Traditional spot survey of a precast reinforced concrete building heated internally. Hot (bright) vertical lines indicate heat loss at return joints throughout height of the building (Titman, 2001).

In order to mitigate the issue of limited camera resolution, a methodology and optimized workflow are required to facilitate the rapid acquisition of building-scale thermal images. To fill a need for gigapixel imaging, robotic camera platforms have emerged (GigaPan Systems, 2015) to aid in acquisition and stitching of spatially accurate digital image panoramas. Now with the idea being well-established for digital photography, it seems reasonable that this approach should also extend to thermography to address its inherent limitations in spatial resolution. Thermography is a widely used technology in many disciplines, but there are still limitations in image resolution when it comes to diagnostic surveys on the scale of buildings.

This Chapter presents a methodology that leverages a low-cost, automated portable thermography (APT) system, designed to increase the spatial resolution of thermal images by performing rapid acquisition of thermal image mosaics. The target application for the APT methodology is passive building-scale surveys aiming to assist in monitoring energy losses,

mapping areas of moisture, revealing structural features, and detecting damage such as delamination and cracking. Automating the process is a step towards a standardized methodology that provides consistency and accuracy in the acquired data and metadata independent of site or operator. The APT workflow aims to be repeatable, provide the necessary setup to ensure accuracy, as well as save time on acquisition and post-processing.

The methodology, composed of the APT instrumentation, its sensors, workflow, and imaging results are presented to highlight how high-resolution thermal data can be accurately acquired for large surface areas using the proposed methodological approach. The methods for interpretation of the data will not change, but the quality of the data will be much higher allowing for more precise analysis conducted by domain experts. The presented methodology is repeatable regardless of the user, and the workflow ensures accuracy and consistent post-processing of the images using recorded metadata. With the presented methodology, the whole context can be displayed while maintaining the same level of detail within the high resolution thermal image. The presented approach also allows for the creation of important baseline records for evaluating a building's thermal efficiency and pinpointing sources of heat losses and other undesirable anomalies. The methodology, composed of the APT instrumentation, its sensors, workflow, and imaging results are presented as part of a case study conducted on buildings in Florence, Italy.

4.1 APT Instrumentation

The instrument consists of a robotic platform and remote imaging payload modules. The platform controls the imaging payload orientation with the ability to measure data such as position, heading, acceleration and vibration, humidity, and ambient temperature. The platform and the imaging payloads are responsible for the acquisition of the thermal images, while the additional sensor measurements from the platform enhance accurate post processing, analysis, and metadata creation used to geospatially anchor the survey. For example, a GPS sensor can be utilized to

geospatially locate the imaging data and a digital compass sensor used to provide the heading of the surface being imaged. Camera movement and vibrations can also be inferred from accelerometers placed on the platform, which can inform automated stitching of the images in post-processing stages and suggest if images are out of focus when captured. The efficiency of the system depends on the resolution of the imaging device, the presence of a focusing motor and the sensitivity of the thermal imaging sensors and robotic platform motors. Requirements and performance of the imaging system will depend on the application and the practitioner's available technology, but the methodology should remain effective.

With the parameters of the instrumentation well defined, the control system should offer a user interface that aids in the automated image acquisition as well as the storage of metadata relevant to the survey. Metadata can include the name of the project, file names, distance from the structure, time of day the image was taken, air temperature, etc. Automated metadata recording saves the surveyor's time recording data separately and assures a consistent digital workflow. Most importantly, the system must be robust and portable so it can easily be moved and operated on-site.

Figure 4.2 Annotated APT instrument (left) and the APT instrument deployed in the field (right).

Table 4.1 Implemented instrumentation specifications.

Thermal camera: FLIR A615 (FLIR Systems Inc., 2014)	
IR resolution	640 x 480 pixels
Thermal sensitivity	< 0.05 °C @ +30 °C/50 mK
Spectral range	7.5–14 µm
Accuracy	± 2°C or ± 2% of reading
Field of view	15° x 11° (19° diagonal)
Focal length	41.3 mm
Acquisition rate	50 Hz
Laser distance meter: AG FLS-C10 (Dimetix AG, 2015)	
Range	0.05–65 m
Accuracy	± 1 mm
Repeatability	± 0.3 mm
Acquisition rate	200 Hz

The implemented APT imaging payload and robotic platform are shown in Figure 4.2. The main component of the imaging payload is a GigE Vision compliant FLIR A615 thermal camera (FLIR Systems Inc., 2014) and the second component is a Dimetix AG FLS-C10 (Dimetix AG, 2015) laser distance sensor which is mounted above the camera in order to measure accurate distances at every camera position (see Table 4.1 for specifications). The distance measurements are used to focus the thermal camera properly and provide additional information about the position of the instrumentation setup. The motion platform is a pan and tilt system (PT785-S from ServoCity) driven by two servos and controlled with an Arduino Uno R3 microcontroller board. The implemented robotic platform allows for full 360° panning and 180° tilting enabling acquisition of a spherical panorama. The entire APT assembly is then mounted on a tripod for

stationary stability and leveling. The presented system uses MATLAB for controlling image acquisition and user input because of its ability to communicate with GigE Vision cameras.

4.2 APT Workflow

The proposed APT workflow consists of setup, acquisition, and post-processing stages which can be further augmented with additional sensors and processes to expand the scope of the survey being performed (see system diagram in Figure 4.3).

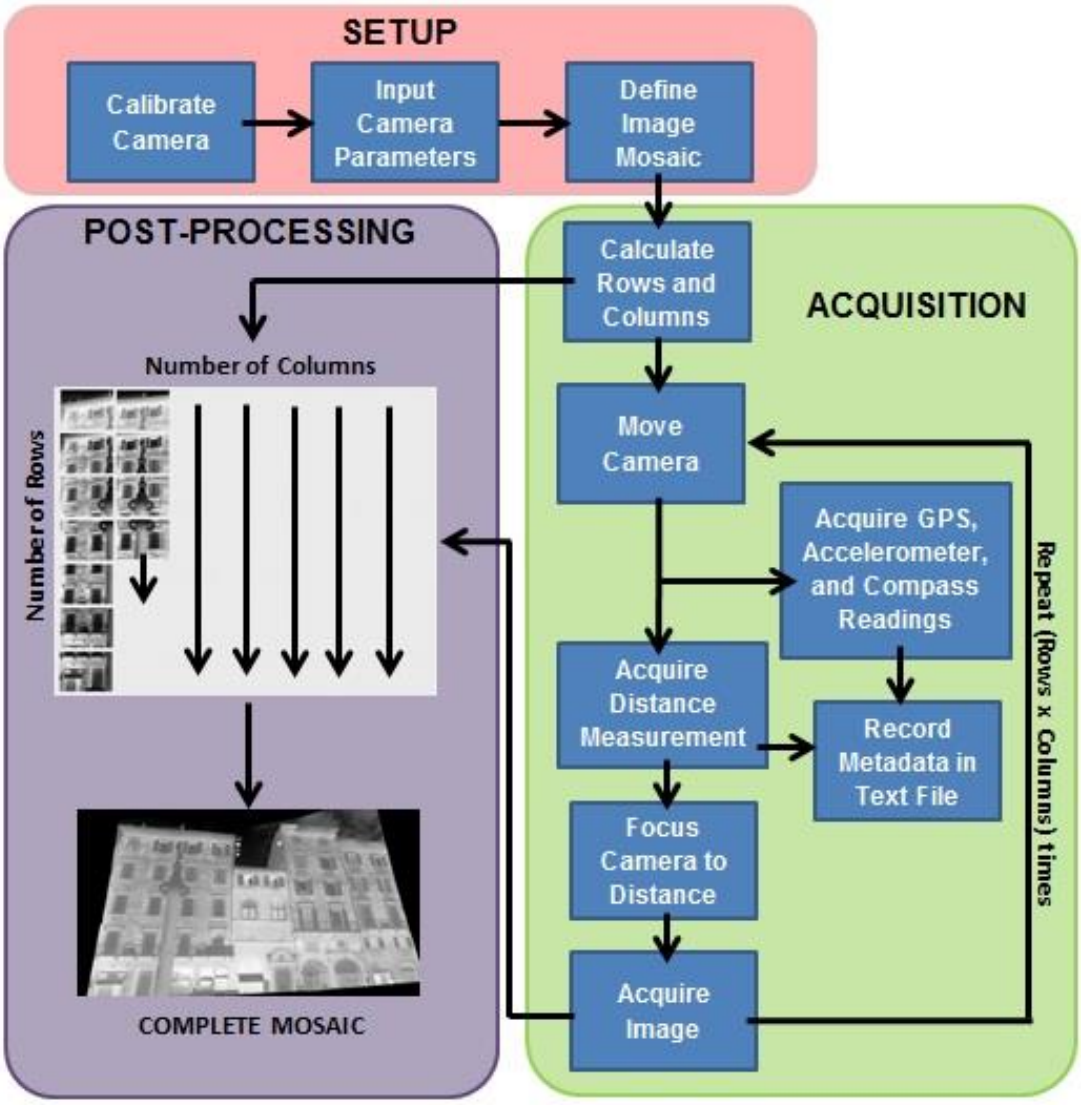

Figure 4.3 APT workflow diagram organized into setup, acquisition and post-processing.

4.2.1 Setup

In order to obtain accurate and meaningful results, multiple calibration steps are required. The most important initial step is camera calibration which establishes the camera's intrinsic parameters. The calibration provides the camera's lens distortion parameters that aid in the accurate final assembly of the image mosaic, as well as the horizontal and vertical fields of view which are utilized for the initial camera orientation and image recording, resulting in the desired image overlaps.

To establish the thermal camera's intrinsic parameters, thermal images of a reference checkerboard were acquired from different points of view while using a halogen lamp to provide reflections to help focus the camera and provide contrast in the thermal images. The camera's radial and tangential distortion models were calculated using these checkerboard calibration images (Bouguet, 2004) and the resulting distortion model, shown in

Figure **4.4**, can then be used in the post-processing to undistort all of the thermal images to yield an accurate assembly of images.

In addition to the camera calibration and setup, there is the physical setup onsite. The ASTM C1153-10 standard (ASTM, 2010) titled Standard Practice for Location of Wet Insulation in Roofing Systems Using Infrared Imaging, discussed by VanOcker et al., provides a suitable reference for recommended operating conditions for passive thermography (VanOcker, Johnson, & Marcotte, 2009). Operational specifications such as environmental considerations are helpful in determining when the conditions are best for passive thermal imaging. The operator must establish what is being imaged in order to physically place the imager in a location that will provide a view of the entire target with the desired resolution. Once the camera parameters are known and the imager is in place, the acquisition procedure can be performed.

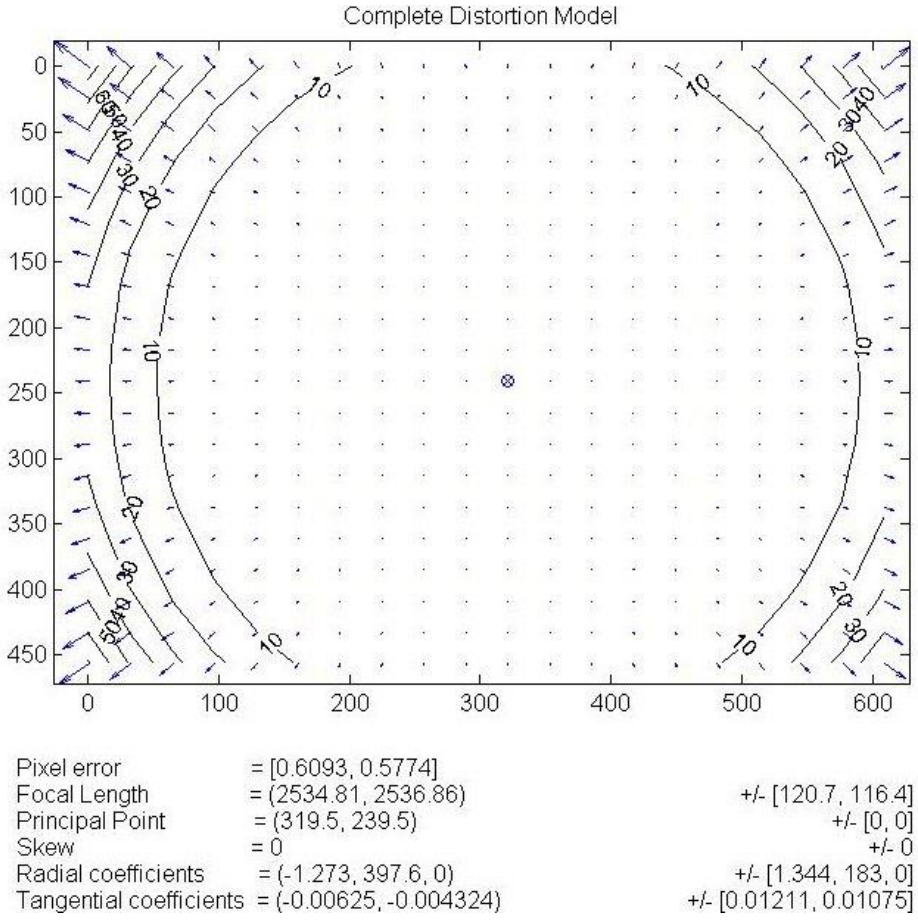

Figure 4.4 Complete distortion model calculated in MATLAB (Bouguet, 2004)**.**

In accordance with the ASTM C1153-10 guidelines (ASTM, 2010), imaging was performed in appropriate atmospheric conditions to take advantage of passive environmental thermal gradients. The thermal gradients supply contrast in the thermal images which allows for the detection of anomalies which are present. The imaging equipment was then transported around various sites and positioned in order to acquire complete mosaics of the target structures.

4.2.2 Acquisition

The first step in the acquisition process is to define the region of interest, i.e. the area to be imaged. Once the bounding area is set, the controls system calculates the number of grid positions based on both the desired overlap of the images and the camera parameters. The control system

then communicates with the motion platform and camera simultaneously in order to acquire images while the platform is stationary at each grid position. While the system is acquiring images it also records metadata and readings from the onboard sensors for subsequent use in image processing and consistent digital reporting. This information can include pan and tilt angles at every image, the distance to the target surface, etc. and can be further augmented with other sensor data. All of this information can prove to be extremely useful in the postprocessing of the images and subsequent analysis.

In the presented system, the area to be imaged is defined by the operator aiming the camera at the top left and bottom right corners of the acquisition area respectively using a graphical user interface. Once the bounding area is set, the number of grid positions is calculated based on the specified overlap of the images and the camera parameters determined in the camera calibration. In the implemented APT system, the acquisition starts at the top left corner and continues down and to the right acquiring images column by column. Based on experimentation in the lab and in the field, overlapping images 33% in the horizontal direction and 45% in the vertical was found to be effective. While the system is acquiring images it records metadata and readings from the on-board sensors for subsequent use in image processing and consistent reporting.

The overall speed of the implemented APT system is governed by two steps in the acquisition procedure. The first is the movement of the motion platform which is a function of the types of motors used and the payload weight. The prototype APT platform uses a very economical pan-tilt camera mount ($350) with servo motors which can be upgraded if faster and more precise results were necessary and if the budget were to allow it. The second time-intensive aspect of the process is the focusing of the camera. Focusing the camera is a two-step process: distance measurement to the target, followed by operating the camera's motor to refocus to that distance. The acquisition at each image location takes approximately ten seconds in the implemented design,

resulting in a panoramic mosaic in a matter of minutes. As the proposed design is small and light, it can easily be moved around a site to thermal site surveys in a short amount of time.

4.2.3 Post-Processing

After the acquisition of the images is complete, the camera parameters, relevant metadata and the raw thermal images are used to create the high-resolution thermal image mosaic. The first step in post-processing is to correct the raw images for lens distortion as determined in the setup stage. The spatial relationships recorded in the metadata can then guide the placement of the undistorted images. Specifying which images overlap and by how much saves computation time by eliminating the need to check every other image for feature correspondences and only searching for feature correspondences in overlapping areas of the images. Once features detected and matched in all overlapping images, the new composite image can be generated by placing all of the thermal images in their calculated positions and blending them into one high-resolution thermal image.

In the presented implementation, the raw temperature data is stored in 16-bit thermal images as pixel intensities measured in degrees Kelvin to one one-hundredth of a degree. A problem with the 16-bit images is the lack of feature articulation due to the narrow range of data contained in the images. Initial iterations of thermal image stitching failed due to a lack of features in the raw images. Computing a successful mosaic first required contrast enhancement, which rescales the pixel values over the whole range thus losing the raw data contained in the images. This remapping of the image data as well as the grid spacing recorded in the metadata during acquisition allows for automated detection and matching of the newly enhanced features which enables calculation of image positions and orientations (New House Internet Services B.V.). Once the enhanced images are aligned and stitched, the location and orientation of the individual images are recorded as a template and applied to the raw images to recover the raw temperature measurements in the final high-resolution mosaic.

4.3 Results

Multiple building-scale thermal surveys of historic landmarks in Florence, Italy were conducted measuring relative temperature gradients in order to study construction details and detect anomalies. As discussed earlier, it is only practical to perform passive thermography at the scale of building surveys, so only environmental heating and cooling is measured. The imaging was performed in the month of October with an average daily high of 21°C and average nightly low of 12°C. The buildings being surveyed are inhabited and therefore internally heated providing an interior heat source to contrast the cold night air. Imaging campaigns were conducted in early mornings when the air temperature was lowest to ensure sufficient thermal gradients for the image mosaics.

The thermal mosaic shown in Figure 4.5b was acquired in the heart of Florence near the famous Santa Maria del Fiore Cathedral focusing on the residential apartments that surround the historical site. The image mosaic is composed of forty-nine images organized into seven rows and seven columns, yielding a five-megapixel image. The average spatial resolution is approximately one pixel per square centimeter of the physical building surface which spans thirty-seven meters wide and six stories high. The acquisition of the forty-nine images took ten minutes, averaging twelve seconds per image. In order to capture the same building facade in one image using the same camera and a wide-angle lens, the maximum spatial resolution would be thirty square centimeters per pixel, or thirty times less resolution than the presented image mosaic.

Figure 4.5a is a visible night-time image of the buildings being surveyed and when compared alongside Figure 4.5b, differences in construction materials can be observed in the thermal image where they are not normally detectable due to the layer of plaster covering the building's surface. Different types of stone will return a different heat signature and it can be observed, especially below the windows, that stones have been replaced or added at some point in

(a) Visible image showing the entire building façade.

(b) Thermal image mosaic showing the entire building facade

(c) Single thermal image

Figure 4.5 Thermal image mosaic of apartment buildings in Florence, Italy.

the buildings' histories. Using the full resolution thermal image, individual stones under the plaster layer can be identified. Figure 4.5c shows an individual thermal image from the mosaic which is outlined in white in Figure 4.5b demonstrating how this automated approach can produce holistic surveys of large buildings while maintaining the fine detail of an individual thermal image.

4.4 Conclusion

This work outlines a new approach for automated high-resolution thermography for the non-destructive evaluation (NDE) of structures. Infrared thermography is an established technology for NDE, but an efficient workflow has yet to be established for the acquisition of thermal image mosaics for building-scale documentation. The approach presented in this Chapter incorporates a cost effective robotic platform, efficient workflow and overall methodology that together enable generation of seamless high-resolution thermal image mosaics which facilitate the detection of small features over an entire building facade. The presented methodology is formed to be repeatable regardless of the user or equipment used, and the workflow also ensures consistent post-processing of the images using the digitally recorded metadata.

The presented methodology was successfully deployed in Florence, Italy, generating a multitude of case examples demonstrating its utility. The advantages of this approach are its time efficiency during field acquisitions, post-processing and diagnostic review of the resulting data. When analyzing the thermographic data, it is advantageous to have a holistic, contextual view of the target while maintaining the level of detail required for inspection of small anomalies, instead of scanning through multiple spot surveys. Once the anomaly is observed, it is also much easier to locate and document it in the context of the whole structure instead of a single image with possibly no perspective of location.

The development of an efficient methodology for thermal surveying of large structures is essential in order to monitor the aging built infrastructure. For historic monuments especially,

multiple domain experts (structural engineers, architects, historians, restorers, etc.) will often collaborate, contributing the expertise needed to read the data. The presented work demonstrates how trusted data can be acquired to inform the decisions of these trained professionals. This work also demonstrates how automated systems can reduce the time complexity and cost of conducting high-resolution thermal surveys while also establishing consistent digital data recording regardless of the site or operator. The proposed methodology is a comprehensive strategy to increase the capabilities of existing thermal cameras for use in building scale diagnostics. With this methodology in place, it is now possible to pursue a wide range of derivative work, exploring material characterization, damage pattern detection, investigation of construction history, etc. based on the high-resolution data that can now be acquired for large surface areas.

4.5 Acknowledgements

This work was supported by the National Science Foundation under award #DGE-0966375, ‘‘Training, Research and Education in Engineering for Cultural Heritage Diagnostics,” and award #CNS-1338192, ‘‘MRI: Development of Advanced Visualization Instrumentation for the Collaborative Exploration of Big Data.” Additional support was provided by the Qualcomm Institute at UC San Diego, the Friends of CISA3, and the World Cultural Heritage Society. Dimetix FLS-C10 laser distance sensor provided courtesy of DIMETIX USA (www.dimetix-usa.com) – laser distance sensors for industry. Opinions, findings, and conclusions from this study are those of the authors and do not necessarily reflect the opinions of the research sponsors.

This chapter, in part, is a reprint of the material as it appears in the Journal of Infrared Physics & Technology. Hess, M., Vanoni, D., Petrovic, V. and Kuester, F. (2015). “High-resolution thermal imaging methodology for non-destructive evaluation of historic structures” *Infrared Physics & Technology*, 73, 219-225. The dissertation author was the primary investigator and first author of this publication.

Chapter 5 Automated Fusion of Visible and Thermal Images

Presented in this Chapter is the combination of two dissimilar, two-dimensional imaging modalities for building scale documentation. The outlined approach automatically registers thermal images to visible images by utilizing known relative camera positions. There are multiple areas of application for the fusion of visible and thermal images, but previous approaches require feature detection and matching in both visible and infrared ranges in order to register the two imaging modalities. In the application domain of structural diagnostics, it is not guaranteed that corresponding features will be present in the thermal images. The diagnostic imaging is being performed on building-scale targets which is another characteristic of this application that separates itself from prior thermal-visible registration studies. Non-destructive evaluation of structures could require the inspection of entire building facades which necessitates many thermal images to yield a desirable level of resolution and detail. As discussed in Chapter 4, the acquisition of high-resolution thermal image mosaics generates the level of detail required while also providing context for the entire target structure.

A low-cost camera mount was custom designed, and 3D printed in order to mount visible cameras around a thermal camera. Once the system is calibrated with a pair of multimodal images that contain corresponding features, every subsequent pair of images can be automatically registered. An application for this approach is presented in which the generation of a visible image mosaic in turn automatically generates a registered thermal image mosaic. The benefit of this approach is that there is no reliance on features being present in the thermal images in order to register them to the visible images.

5.1 Introduction

Registration and fusion of thermal and visible imaging modalities can enhance analysis of a scene by combining information from the visible and infrared ranges, which is useful in many application domains. Previous works require features to exist in both the visible and infrared images in order to register the two modalities. This paper considers the case where feature matching between modalities is not possible, but the accurate registration of the images is still desired. We present a methodology for automatically registering thermal images to visible images using a low-cost, 3D printed camera mount designed to securely mount visible cameras around a thermal camera. This approach does not require performing feature detection on every thermal-visible image pair, but only on an initial set of images to calibrate the system. Once the calibration of the system has been completed, all subsequent thermal images can be registered to their respective visible images.

The specific application for this technique is aimed at the non-destructive evaluation (NDE) of structures in which infrared thermography can be used to monitor energy losses, map areas of moisture, and detect delamination and cracks (Balaras & Argiriou, 2002; Grinzato, Bison, & Marinetti, 2002; Ljungberg, 1994). Thermography presents a non-destructive methodology for reading warning signs and detecting issues that may not be visible to the human eye. This strength of thermography proves to be its weakness for registration with visible images, because it can detect details that are not visible which leads to the inability to match features or the generation of false positive correspondences. A great example in the realm of building thermography that would show this weakness is imaging a plain studded wall; the thermal image will reveal the studs within the wall where the visible image will show everything that is visible on the surface of the wall. The benefit in this case is that both imaging modalities present unique information, but the weakness is that the modalities do not share corresponding features that allow for accurate co-registration. A

similar scene will be discussed later in the presented case example in which we show the benefit of our approach with an example of a stitched mosaic. In this example the visible images are stitched, which can be accomplished with a variety of available software, to create a template to guide the creation of the registered thermal image mosaic. The resulting high-resolution thermal mosaic provides a holistic survey of a large-scale built environment that can be used to perform NDE.

5.2 Brief Review of Previous Work

Registration of thermal images and visible images is applied in areas of security, military and human detection, but the previous works all have a common thread of feature matching between imaging modalities (Krotosky & Trivedi, 2007; Toet, IJspeert, Waxman, & Aguilar, 1997). Popular approaches for registering thermal images to visible images include edge based methods and mutual information. Although these approaches have produced promising results in previous work, they rely on similar features being present in both images. The mutual information and edge based approaches worked well for the previous works because most tests included humans as targets, which give great features in both the visible and infrared ranges. Krotosky et al. use mutual information for person tracking for surveillance applications (Krotosky & Trivedi, 2007). Person tracking inherently assumes that the features of humans are present for detection, which means that the clean heat signature of the person and their visible shape can be matched. Coiras and Kong both utilize edge based feature matching to register thermal and visible images (Coiras, Santamaria, & Miravet, 2000; Kong, et al., 2007). When discussing their face detection method, Kong states that their algorithm emphasizes the importance of prominent face components and one of the issues encountered in thermal face recognition is the occlusion of eyes by eyeglasses. The specificity of the applications mentioned makes the performance completely dependent on the presence of prominent features in both the thermal and visible images.

5.3 Approach

The approach presented in this section does not rely on corresponding features in the thermal images, but instead takes advantage of the fixed geometry of a custom-built camera mount in order to automatically register thermal images to their visible counterparts. The 3D printed camera mount was designed to hold three visible web cameras and attach directly to the thermal camera. The case discussed here only considers the registration of one thermal image to one of the visible images, but the process can be extended to the other two cameras as well in order to have stereo pairs and chances for increased registration accuracy. The relation of the images is considered to be an infinite homography due to the distance at which the images will be taken and the close proximity of the camera centers. For this application we will show that this method yields great results.

5.3.1 Setup

The implemented system uses a FLIR A615 uncooled thermal camera and a laser distance meter (Dimetix AG, 2015) to measure accurate distance readings in order to focus the thermal camera to the target. Figure 5.1 outlines the configuration of the instrumentation used. The visible cameras are oriented in an equilateral triangle with sides measuring 150mm. As mentioned previously, this paper will only discuss the registration of the thermal image to the visible image from one camera.

In order to test the proposed methodology, a test scene was chosen and imaged following the procedure outlined below. The scene contained visible targets such as printed checkerboard patterns, thermal targets in the form of a metal grate, and other objects which would prove to be interesting when overlaying the two imaging modalities. The scene presented challenges of variable depth with two planar surfaces stretching away from the cameras, the glass windows for which the

thermal images would reveal no information beyond the glass surface, and the flat wall for which no visible features exist, but studs can be located in the thermal images.

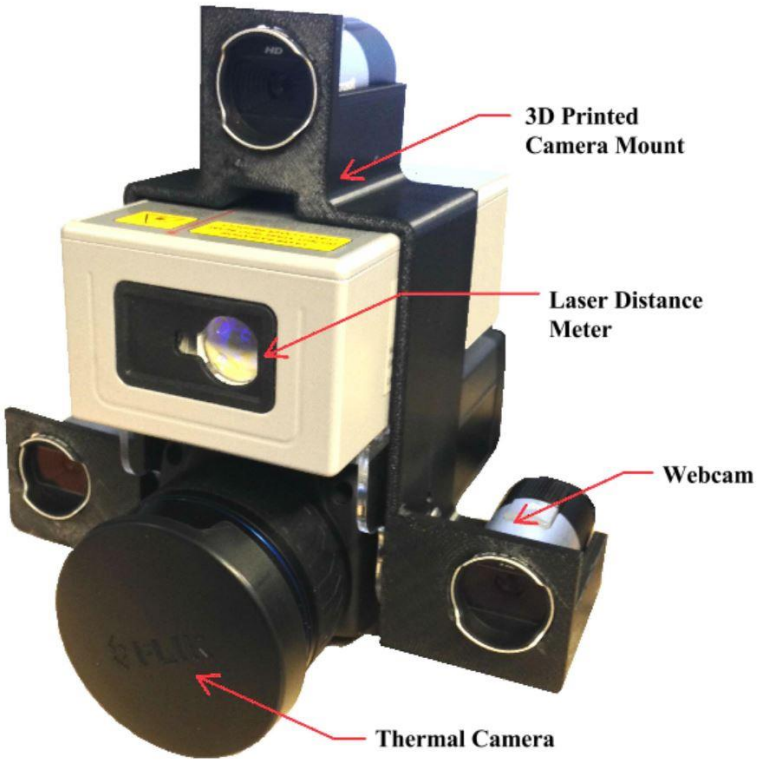

Figure 5.1 Custom camera configuration.

5.3.2 Calibration

The first step in the proposed methodology is to take a set of calibration images with the cameras, such as the ones shown in Figure 5.2. It is very important that this calibration scene has well defined features that can be deciphered in the visible and infrared ranges. First, calibration of the individual cameras must be performed to correct for radial lens distortions. Once the calibration images are corrected for distortion, they are used to calibrate the relation of the thermal camera with respect to the visible camera. At least four corresponding control points are selected or detected in one thermal-visible pair of images in order to rectify the thermal image so that it is projected into the same space as the visible image. The rectification transformation is calculated using the Direct Linear Transformation (DLT) algorithm which uses a set of 2D to 2D image

correspondences to calculate a linear solution for the transformation (Hartley & Zisserman, 2003). Knowing the rectification transformation and the fact that the cameras are fixed relative to each other, different scenes can be imaged and registration can be performed using the same transformation.

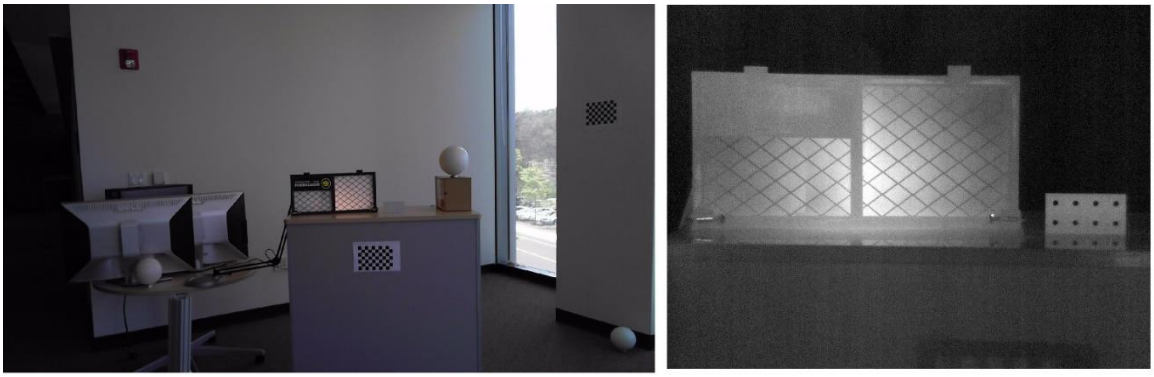

Figure 5.2 Calibration Images: Visible (Left) and Thermal (Right).

5.3.3 Acquisition

Once the cameras and the camera system have been calibrated, all subsequent image pairs can be automatically registered using the same rectification transformation. We also aim to address the acquisition of high-resolution thermal images which requires taking many images in order to generate an image mosaic because the resolution of the thermal camera is only 640x480 pixels, which is one of the highest resolutions for an uncooled thermal camera (FLIR Systems Inc., 2014). High-resolution imagery allows for better inspection of the data because detail and context can both be maintained in one image. For this test case, images were taken from a rotating tripod mount at forty-four locations yielding forty-four thermal-visible pairs to be registered. It can be seen from the calibration images in Figure 5.2 that the field of view is much larger for the visible camera than it is for the thermal camera. For this reason, the mosaic was acquired maintaining an overlap in the thermal image so as to have a seamless thermal mosaic in the end. The overlap varied between thermal images with an average of 35% horizontally and 50% vertically.

5.3.4 Creation of Registered Mosaic

The generation of a stitched image mosaic typically requires feature detection and matching. We are trying to avoid this altogether for thermal images due to lack of reliable features so a different solution must be developed. In order to work around this constraint, two aspects are leveraged: the relationship between the thermal images and visible images is known from the initial rectification, and that feature matching can be performed on the visible images. In the presented approach the visible images are stitched using their own corresponding features in order to create a template for the camera positions and orientations. Using this template, the thermal images are projected using the rectification transformation obtained during calibration using the same camera directions as the visible mosaic. In doing this, the feature detection and matching is only applied to the visible images which is a much easier task because of the existing software that is successful in doing so. This process generates a high-resolution thermal image mosaic which is registered to a stitched visible mosaic, all while avoiding feature detection in thermal images.

Figure 5.3 New calibration images: the thermal image is overlaid and fused onto the visible.

5.4 Results

Due to the visual nature of this inspection technique, the first assessment of the results was based on the visual output. Using the transformation obtained from the calibration set of images, there was a consistent offset of the thermal images that resulted in the misalignment of thermal-visible image pairs. In order to improve upon these initial results, the rectification procedure was performed on a thermal-visible pair of images from within the mosaic acquisition, as shown in Figure 5.3. The new trial still used one projective transformation for all of the other image pairs, but yielded much better results. Now with an accepted visual result, a metric for comparison had to be chosen in order to quantify the difference in results. For the analysis of how well the registration performed, the reprojection error was calculated for each registration attempt. This error metric measures the adjustment necessary to obtain a transformation (and its inverse) that maps points in either the thermal or visible image to the same point in the corresponding image. This metric assumes that there is error in the location of the feature points in both images.

For points in the two images, x_i and x_i' the error is defined as (Hartley & Zisserman, 2003):

$$\sum_i d(\boldsymbol{x_i}, \widehat{\boldsymbol{x_i}})^2 + d\left(\boldsymbol{x_i'}, \widehat{\boldsymbol{x_i}'}\right)^2 \tag{5.1}$$

where,
$$\widehat{x_i}' = \widehat{H}\widehat{x_i}' \tag{5.2}$$

and,
$$d(x_i', \widehat{\boldsymbol{x}}_i')^2 = \left(\frac{x_i'}{w_i'} - \frac{\hat{x}_i'}{\hat{w}_i'}\right)^2 + \left(\frac{y_i'}{w_i'} - \frac{\hat{y}_i'}{\hat{w}_i'}\right)^2 \tag{5.3}$$

The transformation $\widehat{H}$ represents the homography that perfectly maps points $\hat{x}_i$ and $\hat{x}_i'$ between the two images.

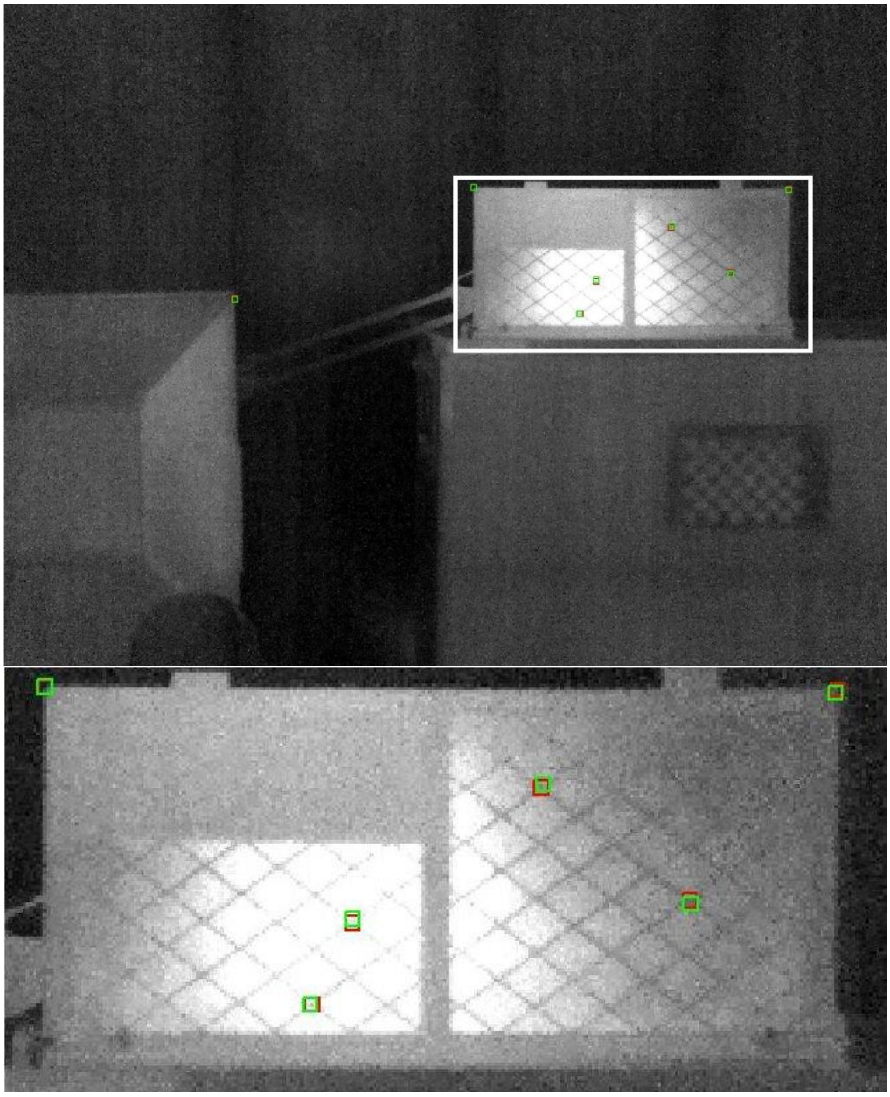

Figure 5.4 Error Shown on Thermal Image: Red squares represent initial points selected in the thermal image and green represents points projected from the visible image using the second rectification trial.

In order to quantifiably evaluate this method, correspondences were selected in ten multimodal image pairs with a total of fifty-five sets of points. Using this error metric, the original registration using the calibration images yields 80,718 where the second registration has a total error of 7,132. Now the problem is constructed such that error can be optimized because there are existing control points that have not been used other than for the calculation of error. This led to a third iteration on the registration where we used the 55 feature points and optimized the

transformation in order to minimize the reprojection error. This optimization was accomplished using a Random Sample Consensus (RANSAC) algorithm that minimizes error by eliminating outlier correspondences, and once a suitable solution is found, calculates the DLT estimate from the set of inliers. The linear DLT estimate and inlier correspondences were then used to optimize further with a nonlinear Levenberg-Marquardt (LM) algorithm to achieve an optimal transformation estimate. After optimizing over the new set of control points the registration error was reduced by almost six times to a value of 1,213. It can be difficult to understand what this error metric represents, so Figure 5.4 shows a visual representation of the initial error in one of the thermal-visible image pairs.

Once a suitable rectification transformation is calculated, the high-resolution mosaic can be assembled. Following the previously discussed procedure, we stitched the visible images in order to build a template to be used for the rectified thermal images. For this test PTGui was used to stitch the visible images and save the camera positions and orientations. Forty-four visible images were stitched in PTGui in under a minute and the template was saved. MATLAB was used to rectify all of the thermal images taking about 0.8 seconds per image, so theoretically, the stitching of the visible images and the rectification of the thermal images could be performed simultaneously and would be completed in the same amount of time. The assembly of the thermal images using the template does not take any extra processing time, it is just a matter of saving the resulting high-resolution image. Though the error measurements show that the optimized transformation contained six times less error, the visual comparison of registered mosaics shows that the optimized iteration is nearly indistinguishable from the initial registration. This is very promising because even though the optimization increased the accuracy of the registration, it required more control points from the other image pairs which is not always possible. Figure 5.5 shows the visible and thermal image mosaics separately as well as the fusion of the two which enhances the understanding of the space by combining the information from the two different modalities.

(a) Visible image mosaic

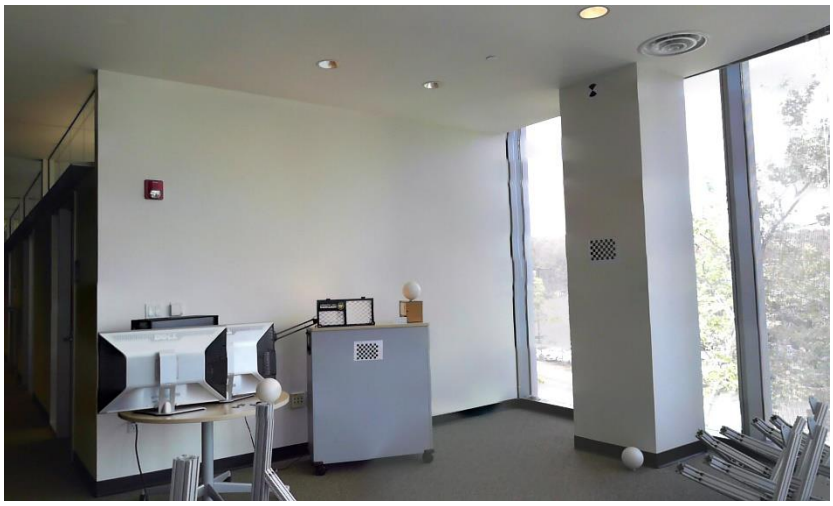

(b) Thermal image mosaic

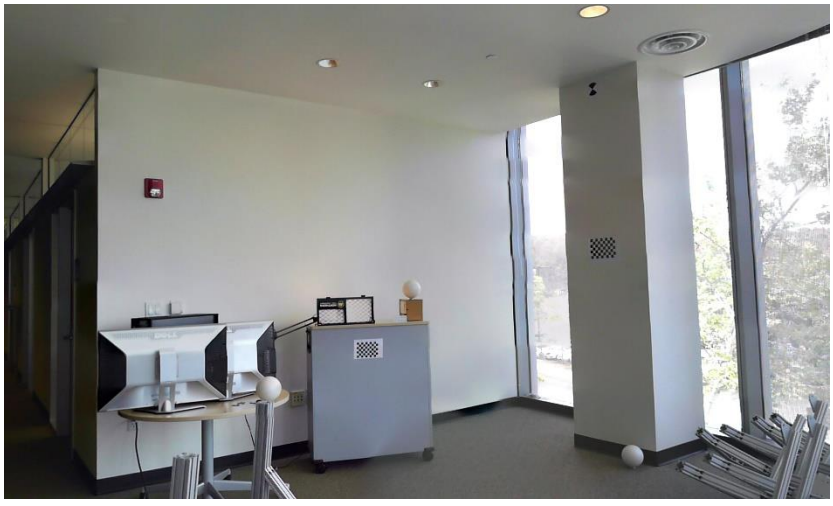

(c) Thermal-visible image fusion

Figure 5.5 Resulting high-resolution mosaics.

(a) **(b)**

Figure 5.6 Multimodal registration attempts using mutual information (a) Success with features and (b) Failure with no common features.

In addition to the reprojection error, we thought it best to demonstrate how mutual information performs due to its popularity in previous approaches for thermal-visible registration. We used a sliding window over the visible image that was the same size as the thermal image (640x480) and computed the mutual information between the thermal image and visible window at each position in order to determine where the thermal images should be overlaid. The sliding window location with the maximum mutual information would be taken as the location of the thermal image. Figure 5.6 shows the thermal images in their true locations in relation to the visible images as well as the green and red rectangles showing the mutual information estimate of the thermal image locations. As shown in Figure 5.6a, mutual information is successful in determining the proper location of the thermal image because corresponding features are present in the thermal and visible images. When faced with no features in the thermal image to match features in the visible image, such as in Figure 5.6b, mutual information could not determine the correct location of the thermal image. Results from the mutual information trials emphasize our argument for a new method for thermal-visible image registration, such as the presented methodology that doesn't require shared features in the thermal and visible ranges.

5.5 Conclusions

The methodology presented in this chapter was successful in registering forty-four thermal-visible image pairs using a single projective transformation and without performing feature detection in the thermal images. These forty-four registered pairs of images were used to generate a seamless thermal image mosaic that is registered to the visible image mosaic. The multimodal fusion of the registered mosaics reveals important information that is useful for non-destructive evaluation of structures. Layering the two modalities in a single high-resolution image allows inspection of small details in both the visible and infrared range while maintaining context of where the detail is with respect to the whole scene.

It is clear from both the visual artifacts and calculated error that the second two registrations were far superior to the first attempt. Likely, the reason for the poor performance of the initial rectification is that the images were taken too close to the target which strays from the assumption of an infinite homography. For future work, rectification should be done on a more defined target specimen that is placed at a farther distance from the camera setup, preferably a distance comparable to the real target being imaged.

The demonstration of mutual information on the test case presented here accentuates the need for a different methodology when corresponding features are not present in both the visible and infrared images. Mutual information could be applied in the initial calibration pair of images in order to automate the process of aligning the initial images to calculate the rectification transformation. Another future research objective is to utilize all three of the visible cameras in the configuration. Using the methodology presented here, the same process could be repeated for all three thermal-visible pairs at each location. The hope is that with sufficient calibration of the visible cameras a point cloud could be generated by triangulating points from the visible images. From there, the method proposed in this paper can be implemented to overlay the thermal information

onto the three-dimensional model of the space. In this way, features and anomalies in the thermal images could be given some geometric meaning and even be measured if the model is calculated to scale. Being able to measure the thermal anomalies is a very powerful tool for structural diagnostics.

5.6 Acknowledgements

This work was supported by the National Science Foundation under award #DGE-0966375, "Training, Research and Education in Engineering for Cultural Heritage Diagnostics," and award #CNS-1338192, "MRI: Development of Advanced Visualization Instrumentation for the Collaborative Exploration of Big Data." Additional support was provided by the Qualcomm Institute at UC San Diego, the Friends of CISA3, and the World Cultural Heritage Society. Dimetix FLS-C10 laser distance sensor provided courtesy of DIMETIX USA (www.dimetix-usa.com) – laser distance sensors for industry. The technical input and continuous support of Professors Falko Kuester and Mohan Trivedi are highly valued. Opinions, findings, and conclusions from this study are those of the authors and do not necessarily reflect the opinions of the research sponsors.

This chapter, in part, is a reprint of the material as it appears in the Proceedings of the 2014 IEEE International Conference on Imaging Systems and Techniques (IST). Hess, M., Kuester, F. and Trivedi, M. (2014). "Multimodal registration of high-resolution thermal image mosaics for the non-destructive evaluation of structures." In *Imaging Systems and Techniques (IST), 2014 IEEE International Conference on*, 216-221. The dissertation author was the primary investigator and first author of this publication.

Chapter 6 Fusion of Multimodal 3D Data

This Chapter outlines how understanding the capabilities and limitations of different 3D acquisition techniques can enable repeatable and accurate registration of multiple geometric datasets. By leveraging complementary strengths of techniques, the fusion of modalities can enhance understanding of a site. Geometry, appearance and context are essential aspects to capture in the digital documentation of cultural heritage sites. Geometry must be accurate and should provide a level of precision necessary for quantified diagnostics. Visual appearance should capture the "as-is" state, while site specific context is important for correlation, interpretation and analysis. TLS has established itself as the premier modality for the acquisition of trusted geometry, while photogrammetry techniques like structure from motion are used to construct visually compelling models. A common challenge of these line-of-sight techniques is that the imaging equipment must be systematically moved throughout the target environment to assure that the data captures the entire target and allows for the removal of occlusions in the final model.

By combining terrestrial and airborne imaging techniques using unmanned aerial vehicles (UAV), also frequently referred to as drones, it is possible to streamline the acquisition of the target data sets. This Chapter discusses the fusion of full resolution 3D data streams generated from laser scanning, ground based photogrammetry and drone based photogrammetry. Maintaining full resolution of the data sets allows for diagnostic analysis of very subtle deformations and defects like erosion and cracks. In a presented case study in Mexico, TLS serves as a geometric scaffold that the photogrammetry data is registered to in order to generate a holistic model of a one-hectare site containing two historic structures. The laser scanning and photogrammetry datasets (see Figure 6.1) have sufficient overlap to enable fusion, and more importantly the individual sets can supplement each other, providing geometry, photorealism and context that the other set lacks.

Figure 6.1 Aerial view of the integrated data set from the site of Ecab combining TLS, ground based SfM, and aerial SfM.

6.1 Introduction

For the most useful digital documentation of cultural heritage, geometry, visual appearance and context are vital characteristics to capture. These aspects can tell the history of artifacts and sites as well as aid in understanding how they came to look and behave as they do today. ``Documentation is a complex process that includes stages of data acquisition, interpretation, and production. It is the first and most important step before starting to conserve projects and works. A short definition of it is the recording of the existent state and surroundings of the building by reports, drawings and photographs (Yilmaz, Yakar, Gulec, & Dulgerler, 2007)." The goal of these reports, drawings and photographs is to highlight the features of artifacts and sites that are essential to understanding the current state of health. The methods of documentation should constantly evolve with technology in order to attain the most accurate records of the existing conditions.

Both laser scanning and photogrammetric techniques have been discussed in literature and are increasingly utilized in the context of cultural heritage documentation. TLS is an established

technology that acquires dense collections of points to provide accurate geometry, while photogrammetry techniques like structure from motion (SfM) are used to construct photorealistic models. Motivations and goals of using these techniques can vary, but the resulting data is complimentary, so methodologies should be established to standardize acquisition and processing of multimodal data. Both of the mentioned approaches can yield high-resolution three-dimensional representations of artifacts, structures and sites, but the techniques do not need to be exclusive. This section presents the fusion of data stemming from TLS and SfM in order to produce a more complete representation of cultural heritage sites.

TLS point clouds are discussed as geometric ``scaffolds'' to which photogrammetric data can be registered in order to preserve accurate geometry as well as photorealism. Due to time constraints and equipment limitations, it is often beneficial to survey separate areas in parallel using the two approaches while maintaining adequate overlap to connect the data sets in post processing procedures. The strengths and limitations of the different approaches are discussed in order to understand how data modalities can enhance each other.

The case study presented here is work performed at the site of Ecab located at the northeastern tip of the Yucatan peninsula in Quintana Roo, Mexico. The work was performed in collaboration with the National Institute of Anthropology and History (INAH) which is the government entity that oversees the documentation and preservation of cultural heritage sites in Mexico. INAH is working to develop a conservation plan for the site because of the structures' state of health and the site's vulnerability to hurricanes on the isolated coastline. Time on site was limited to two short days because of the two-hour boat ride required to get to and from the site. The difficulty of accessing the site serves as an example that highlights the benefit of comprehensive digital documentation records which can be used off-site in order to make preservation decisions.

Figure 6.2 Site of Ecab before vegetation was removed (Top) and at the time of the survey after the vegetation was cleared (Bottom).

The site has a rich history and contains what is believed to be the first church of Mexico which was built in the mid-16th century and serves as an important part of Mexican cultural heritage. The site also contains the church caretaker's house, also referred to as Casa Cural. Both the church and Casa Cural are in a dangerous state of decay having endured centuries of hurricanes, erosion, and encroachment of vegetation (seen in Figure 6.2) which have all contributed to structural damages. The goal of the expedition was to travel to the remote site and acquire data that will inform preservation decisions and serve as an accurate historical record of the site's current state of health.

Logistics of traveling to the site included decisions on optimizing the amount of equipment that would be needed. A FARO Focus 3D scanner was used for the terrestrial laser scanning

because of its small size and portability. The ground based photography was acquired using a Canon 5D DSLR camera and the Sony QX100 and QX1 were used for multirotor based and fixed wing based imaging respectively. Following the TLS acquisition methodology from section 3.1, the survey of the church and Casa Cural required twenty-nine separate scan positions to obtain data from enough angles to yield a complete model of the structures. The point cloud can facilitate the measurement of features like cracks, erosion, plumbness, and stone dimensions down to millimeter resolution as exemplified in Figure 6.3. Thousands of high-resolution images were acquired from the ground as well as approximately forty images acquired from the aerial platforms to provide photorealism and site context.

Figure 6.3 Section cut of the church data: Example dimensions are shown to illustrate the precision and utility of TLS.

The data were collected on-site in two short days by a multidisciplinary team, and processed off-site. The TLS scans were stitched together using FARO Scene and Agisoft Photoscan was used for the SfM processing of the aerial and terrestrial photographs. The processed TLS data resulted in two models, one of each structure, totaling 800 million three-dimensional data points.

The SfM processing also yielded a model for each structure in addition to a model of the overall site generated from the aerial images.

The lower third of the exterior walls of the church and Casa Cural have suffered a significant loss of mortar between stones due most likely to erosion and vegetation intrusion. The site has endured many hurricanes since its establishment which have accelerated the effects of water on the masonry structure. It is concerning to observe loss of structural material in the lower portions of the wall that serve as support for the rest of the structure above, so one of the conservation actions would likely be the structural reinforcement of the lower walls and foundation. Other than environmental damages, the church has unfortunately also experienced acts of looting and vandalism. It can be observed that some sort of altar piece that was fixed to the wall has been ripped out and now loose stones are all that remain.

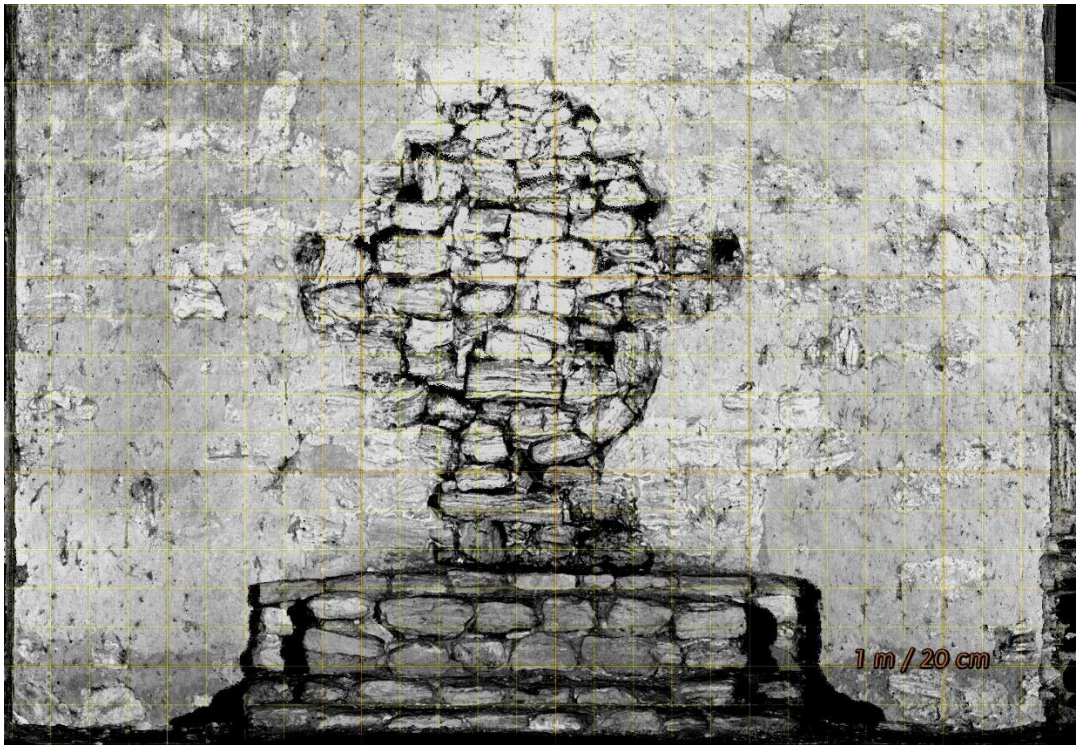

Figure 6.4 Orthogonal image from the grayscale laser scanning point cloud outlining the vandalism of the church's altar.

Using the data acquired with the laser scanner, the damaged areas can be measured in order to obtain quantitative measures of the damage as well as the qualitative determinations that can be performed using imagery. These quantities can be utilized to aid in estimates for repair material costs and to serve as building records that can be analyzed over time to see if damage is progressing. The vandalized area of the altar is shown in Figure 6.4 with a scaled grid to demonstrate how the damaged area can be measured to quantify the amount of masonry was damaged and what size stones would be required to repair the area.

6.2 Brief Review of Previous Work

In the context of cultural heritage, the main objectives are creating digital archives, performing site documentation, and monitoring artifacts and sites. In general, the most important aspects to capture are geometry and visual texture within the site context and the main sources of these data have been laser scanning and photogrammetry. Terrestrial laser scanning and photogrammetric techniques have been documented and compared to try to establish which of the two techniques is more accurate or more suitable in certain situations (Baltsavias, 1999; Guarnieri, Vettore, El-Hakim, & Gonzo, 2004; Kadobayashi, Kochi, Otani, & Furukawa, 2004; Westoby, Brasington, Glasser, Hambrey, & Reynolds, 2012; Yastikli, 2007). TLS is an extremely powerful surveying tool to capture accurate geometry, but comes with a high price tag while photogrammetry is emerging as another resource for engineers and archaeologists to digitally model sites and artifacts with a barrier to entry that is monetarily and physically more surmountable. Rather than comparing these two techniques, the different data modalities can be integrated together to yield faster acquisition times, more complete surveys, and models that provide accurate geometry, photorealism, and context.

6.2.1 Terrestrial Laser Scanning

TLS has been used for digital documentation of similar cultural heritage sites in Mexico and at other sites all over the world (Hess, et al., 2014; Hess, Petrovic, Yeager, & Kuester, 2017; Richter, Kuester, Levy, & Najjar, 2012; Bariami, Faka, Georgopoulos, Ioannides, & Skarlatos, 2012; Acosta, Pacheco, Garcia, Sifuentes, & Rodriguez, 2011; Ruggiero, et al., 2012). Having an accurate model of the existing structure can aid not only in the documentation of the site, but also in its preservation (Guidi, Russo, & Angheleddu, 3D survey and virtual reconstruction of archeological sites, 2014). Using the dense collection of 3D data captured by a laser scanner, any damages or deformations such as cracks in structures and erosion can be accurately quantified in order to assess the extent of the damages. To this point, these subtle types of damages may not be detected if the raw data were to be decimated to decrease the number of points and in turn the spatial resolution of the point clouds. It is therefore important to maintain the highest possible resolution in the data sets to allow for detailed analysis and interpretation of the existing site and artifacts. In addition to providing an accurate three-dimensional model of the existing site that can be used for quantitative analysis, the laser scanning point cloud serves as a geometric scaffold to which other types of data are registered.

6.2.2 Photogrammetry

Photogrammetry techniques like structure from motion (SfM) are being used more often due to the exponential increase in computing power and the availability of high resolution cameras. The approach processes photos taken of a target from different points-of-view in order to triangulate common features and project them into three-dimensional space. In addition to the point clouds that can result from dense feature matching in the images, the images contain the photorealistic texture that produce a visually compelling representation of the target. SfM techniques are often unsuccessful when attempting to reconstruct an interior space like a room,

therefore building surveys cannot be completed solely with photogrammetry. The resulting SfM point cloud on its own is also not a reliable source of absolute measurements unless a reference scale is specified to transform the points into accurate world coordinates.

The field of cultural heritage documentation has greatly benefited from advances in SfM processing and there is still room for growth in application of the resulting data. Photogrammetry techniques can be used in a wide range of cultural heritage applications like topographic site mapping (Fonstad, Dietrich, Courville, Jensen, & Carbonneau, 2013; Westoby, Brasington, Glasser, Hambrey, & Reynolds, 2012) three-dimensional digitization (Grun, Remondino, & Zhang, 2004; Pavlidis, Koutsoudis, Arnaoutoglou, Tsioukas, & Chamzas, 2007) and for analyzing heritage structures (Arias, Herraez, Lorenzo, & Ordonez, 2005; Yilmaz, Yakar, Gulec, & Dulgerler, 2007). One of the reasons for the adoption of SfM methodologies in cultural heritage contexts is the speed at which the surveys can be conducted. The processing time can range from hours to weeks depending on the number of images and available computing power, but time on-site can be limited and fit within common constraints of cultural heritage site access.

6.2.3 Data Fusion

Previous works have strived to integrate both laser scanning and photogrammetric techniques to achieve all of the documentation objectives mentioned in this paper. In most cases, photogrammetric techniques are solely implemented for photorealistic texturing by projecting the colors from the digital images to the 3D points rather than being used to generate three-dimensional models (Guidi, et al., 2009; Ikeuchi, Nakazawa, Hasegawa, & Ohishi, 2003; Rönnholm, Honkavaara, Litkey, Hyyppä, & Hyyppä, 2007) succeeded in presenting a methodology for integrated data from laser scanning, aerial images and terrestrial images to achieve a multimodal, multi-resolution digital model, but was not able to realize the full potential because significant amounts of data had to be discarded to limit the size of the integrated model.

Presented in this Chapter is an application of multimodal data integration that maintains full resolution of each entire data set, and instead of using each modality solely for its strengths, the modalities are utilized to supplement each other in areas where data is missing from one methodology or the other. The goal of this Chapter is to highlight the benefits of using full resolution laser scanning and photogrammetry data together for surveying cultural heritage sites. The data acquired using these methodologies should not simply serve as visual aids, but should be used to their fullest extent for collaborative analysis among a multidisciplinary team.

6.3 Integration Methodology

Digital heritage documentation aims to acquire data that depict a site at a known location and time and digitally place the data in an overall context. The goal of the presented approach is to allow all available data modalities to be incorporated into one dynamic digital model that is able to evolve. As new data become available, they can be incorporated into the same digital space, or information model, and existing data can also be reprocessed or altered all within a flexible framework.

Once the data are acquired and processed, decisions need to be made about what types of integration should be done in order to produce the most comprehensive and accurate digital representation heritage site. In this case, Casa Cural was documented after the church and due to time limitations could not be laser scanned in its entirety. This would have been extremely disappointing for the comprehensive site documentation because essential geometric data was missing from the model of Casa Cural. It was decided that the SfM data should be integrated with the TLS data of Casa Cural because the completed photogrammetric model contained data that would supplement the gaps of the laser scan.

In the process of using the photogrammetry to supplement missing data, the TLS data serves as a geometric scaffold which is used to accurately scale the photogrammetry data. Mutual

control points can be selected in each data set in order to calculate a transformation to register the photogrammetric models to the laser scanning point clouds. Fine registration of the data was performed using an Iterative Closest Point (ICP) algorithm, the results of which are shown in Appendix A. Once the necessary transformation was calculated the SfM data was integrated to realize a complete 3D model of the structure. Figure 6.5 shows the final integrated data set of Casa Cural where the SfM points are highlighted in orange. Neither the TLS nor the SfM model depicts the entire structure. The TLS model captured the interior rooms of the house which could not be captured by SfM and the SfM data captured an exterior room and exterior walls that the team did not have time to scan with TLS. Only through a combination of the data could the structure be digitally documented in its entirety.

(a) Section Cut

(b) Perspective View

Figure 6.5 Casa Cural integrated data set: SfM points are shown in orange.

Geometry is one aspect of digital documentation, but it is not the only feature that must be recorded. Capturing the photorealistic condition of the sites and artifacts can be beneficial in establishing conservation plans. Some TLS equipment have a camera onboard to capture images that assign color to the data points, but the cameras are normally not very high quality resulting in coloring of the models that does not look realistic. With an established geometry as a reference, photogrammetry can be used to provide this photorealistic appearance. In the previously mentioned case of Casa Cural, the SfM points and color were used to supplement missing TLS data. However,

if there is already sufficient geometry, the decision can be made to use the SfM images solely to texture or project the photorealistic color onto the accurate geometry of the TLS points. In the presented case study, this decision was made concerning the church.

Extra time was spent scanning the church with the laser scanner to assure accurate geometry of the complete exterior as well as the interior rooms. These scans did acquire color values for the points, but the color captured in the SfM images better encapsulates the existing appearance of the structure. The same alignment calculations were performed in order to register the photogrammetric reconstruction to the TLS geometry. Instead of using the three-dimensional data from the SfM reconstruction, the camera poses (location and orientation) were used to project the colors from the images only to the TLS points. Figure 6.6a shows the laser scanning data and outlines in orange an example where the texture of one image is projected onto the points, while in Figure 6.6b, the image's true color is used to texture the geometric points. Using custom developed point cloud visualization software (Petrovic, et al., 2011; Petrovic, Vanoni, Richter, Levy, & Kuester, 2014), it is possible to interactively select which images to use for the photorealistic texturing therefore leaving the overall framework flexible to changes.

(a) **(b)**

Figure 6.6 TLS points of the church used as a scaffold for aligned SfM images draped over in orange (a) and in photorealistic colors (b).

The third essential characteristic that should be embodied in digital documentation is context. There are different types of context, like the context in which archaeological remains are found or geographic context. Overall site context was the final problem to address in the presented case study where the relationship between the two structures was not captured in the TLS data because the structures were separated by fifty meters of jungle. The two models of the structures existed in their own digital space and required additional context in order to place them together in accurate world coordinates. The SfM reconstruction of the site derived from the fixed wing aerial imaging campaign was able to provide the required context and enable the calculations to find the transformation to take the digital structures from their own digital space to one overall model where the geometric relationships of the entire site could be studied. The final model, as seen in Figure 6.7, is the result of integrating five different data sets into one digital representation that contains accurate geometry, photorealism and context of the site of Ecab. The final model contains a total of one billion points which are all visualized in real-time using the previously mentioned visualization software.

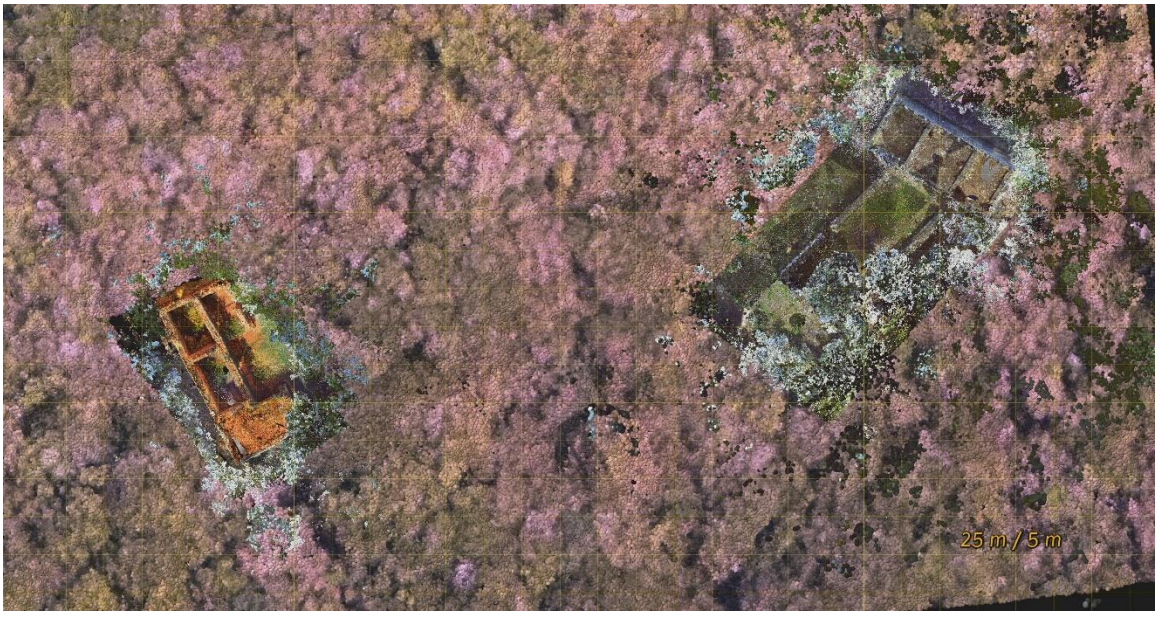

Figure 6.7 Plan view of the integrated data set with Casa Cural (left) and the church (right): Aerial SfM is shown in purple and ground-based SfM in orange.

6.4 Benefits of Data Fusion

The goal of this section is to highlight the benefits of using TLS and photogrammetry data sets in tandem for surveying cultural heritage sites. The methodologies for acquisition and processing of the modalities are very different, but once processed, the 3D data can be combined to provide additional context to each other. As mentioned previously, TLS serves as a dense scaffold of 3D coordinates which provides geometric context for the photogrammetric point clouds and images. Depending on the scale of the individual models, one modality can put others in the context of the overall heritage site. For example, in the case study, photogrammetry from aerial photographs served as a way to orient separate laser scanning data sets and provide overall site context. Context can also be provided at the object scale where photogrammetric modeling results provide accurate representations of small artifacts found on-site. The artifacts could then be digitally referenced to the TLS point cloud to depict the context in which they originally existed on the site. It is extremely important to maintain this degree of contextual resolution for archaeological analysis and interpretation.

One's ability to accurately interpret archaeological deposits or sites is greatly enhanced by the ability to view and evaluate the spatial contextual relationships between objects or features – be they cultural or natural. The ability to embed spatially referenced models of objects and features within a digital site is both novel and powerful. Multimodal and multi-scalar reality capture and presentation tools can facilitate the analytical framing and reframing of objects or features within the larger coordinate system. The result is a bridge between intellectual and technological toolkits both essential to interpretation.

One of the most important benefits in combining modalities is the savings in acquisition times. Often time on site and available equipment are limited, so the teams acquiring the data must use all of their tools to gather as much information as possible in a small amount of time. In the

case of TLS and photogrammetry, the two can be performed in parallel by multiple users or even by the same user if planned accordingly; the laser scanner can be started in one survey position and photos can be acquired while the scanner is running. In the presented case study, photogrammetry played a vital role in both filling in gaps in the TLS data set and providing site context and photorealism. Laser scanning and photogrammetric techniques have been proven useful on their own for a variety of objectives, but when combined they can prove even more valuable to preservation and restoration planning and decision making.

6.5 Conclusions

The goal of this Chapter is to highlight the benefits of combining full resolution TLS and photogrammetry data sets in order to achieve comprehensive surveys of cultural heritage sites. The different data modalities can be useful on their own, but as seen in the presented case study, the integration of the data sets enhances the digital record. For accurate interpretation and analysis, the digital documentation must capture the existing geometry, visual appearance, and the overall context of the site and the artifacts within it.

3D data streams generated from TLS, ground based SfM and drone-based SfM were fused to generate a holistic model of the significant cultural heritage site of Ecab. The individual data sets have sufficient overlap to enable fusion, and most importantly the individual sets supplement each other, providing geometry, photorealism and context that another set may lack. Full resolution of all data sets was maintained which is extremely important for diagnostic analysis of deformations and defects and for future preservation planning. Maintaining all of the data in a flexible framework where data can be added and altered at any time is important for future work. If the same methodology were repeated in the future, the data can be compared with the earlier records to track changes to the site. Utilizing the presented integration methodology, an accurate record of the site of Ecab was generated with the hope that this dense set of data will allow local officials and

government entities to make preservation decisions based on the accurate measurements, appearances and context of the site as it currently exists.

6.6 Acknowledgements

This work was supported by the National Science Foundation under award #DGE-0966375, ``Training, Research and Education in Engineering for Cultural Heritage Diagnostics," and award #CNS-1338192, ``MRI: Development of Advanced Visualization Instrumentation for the Collaborative Exploration of Big Data." Additional support was provided by the Qualcomm Institute at UC San Diego, the Friends of CISA3, and the World Cultural Heritage Society. Opinions, findings, and conclusions from this study are those of the authors and do not necessarily reflect the opinions of the research sponsors. Huge thanks to Centro INAH Quintana Roo, Adriana Velazquez Morlet, Luis Leira Guillermo, Enrique Terrones, Sandra Elizalde, Vid Petrovic, Dominique Meyer, Aliya Hoff, Alexandra Hubenko, Vanessa Pool, Fabio Esteban Amador, Jeffrey Glover, Andrew Vaughn, Roberto Echeverria, Manuel Joya, Reymundo Joya, Carlos Basto, and Marcia Kirby. The continuous support of this project and guidance of Dominique Rissolo and Professor Falko Kuester is greatly valued.

This chapter, in part, is a reprint of the material as it appears in Digital Heritage, 2015. Vol. 2. Hess, M., Petrovic, V., Meyer, D., Rissolo, D. and Kuester, F. (2015). “Fusion of multimodal three-dimensional data for comprehensive digital documentation of cultural heritage sites.” In *Digital Heritage, 2015,* vol. 2, 595-602. The dissertation author was the primary investigator and first author of this publication.

Chapter 7 Integrating N-D Data: As-built Information Models for Structural Health Assessment

In traditional BIM applications for new construction, the intention is for the initial model to serve as a guide and a scaffold for future updates and maintenance planning. The same is true for the proposed as-built information model. The difference is that there is no initial scaffold to update or add to, so there is an additional first step which is to create the first records of a structure. A dense 3D geometric record of a structure can serve as a diagnostic tool on its own, as in Section 3.1.1.3, but more importantly, it can serve as the digital scaffold that houses all past, current and future data. This is the ultimate goal of the as-built information model. This Chapter explores how to extend the geometric model to include data layers from other modalities in a way that supports the integrated use of the high-dimensional information model for structural health assessment.

7.1 Introduction

The hypothesis of this dissertation research is that multimodal as-built information models will facilitate full scale structural health assessment (SHA) of existing structures, especially those with no previous records. The previous chapters have stepped through different aspects of non-destructive imaging data collection and how each data asset is useful. Also presented in the previous chapters is the notion that these data assets can be combined into an overall holistic model in order to extract additional assessments through a combination of modalities. This chapter highlights ways in which the resulting as-built information model can be used to yield valuable structural assessments.

The previous chapters have shown how each technology or data type can contribute towards the understanding of an existing structure. Concluded here is how the combination of all these data into one holistic as-built information model provides new insights as well as more

accurate analyses and diagnoses. The success of this approach should not only be measured by the number of assessments made; a more important initial measure of success is the degree of understanding about an existing structure that is gained. If emphasis is placed on the accurate characterization, documentation, and cataloging of existing structures, more accurate assessments will be made from the comprehensive representations. The as-built information model is a more effective methodology for diagnosing patients, which in this case are historical structures. Accurate diagnoses based on empirical evidence contributed through information models will in turn yield better maintenance, preservation, and restoration of all existing structures.

The utility of the presented as-built information modeling approach is exemplified here through two case studies: The Baptistery of San Giovanni and Palazzo Vecchio, which are both located in Florence, Italy. These two examples together tell a compelling story in which the impact of accurate existing information at the surface, subsurface and volumetric levels is abundantly clear. The combination of geometry, appearance and context enable analyses and assessments that could not otherwise be performed. The most influential conclusions for structural engineering insights will be provided using the information model data to guide numerical modeling and simulation.

The presented results show that generic assumptions are not only useless but can also be dangerous for structural assessments. Using an assumed ideal model to study either Palazzo Vecchio or the Baptistery would yield results that are misleading and overestimate the capacity of the existing structures. They would not tell you about the actual damage patterns or how the structure is functioning under the given loading scenarios. Any preservation judgments made using these generic models could lead to ineffective restoration efforts, at best, or lead to catastrophic consequences. Historic structures are complex and heterogeneous structures which function discontinuously due to disparities in the material properties. If one is looking for an understanding as to how a structure came to be in a certain state or what the possible load capacity is under current

circumstances, then capturing the true nature of the existing geometry, appearance, context and materials is crucial.

7.2 Background

Palazzo Vecchio, which has been the center of Florentine government power since the 14th century, still serves as the city hall in Florence and is also partially open to the public in the form of a museum. At the turn of the 14th century, Arnolfo di Cambio constructed the initial incarnation of Palazzo Vecchio which over time would see changes and additions completed by others including Giorgio Vasari and Marco del Tasso. What is now the front facade of Palazzo Vecchio constructed in 1298 is predated by medieval buildings which were once separate, but then joined over time to create the Southeast corner of the Palazzo. The Salone dei Cinquencento ("Hall of the Five Hundred") was initially built in 1495, but then restructured during the Renaissance by Giorgio Vasari. The main area of interest in this Chapter is the Southeast corner of the building and its additions and restructuring over time.

One room in particular, Sala degli Elementi (or "Room of the Elements"), has been studied to try to diagnose the potential causes of observed damages in the form of settlement and cracking. Palazzo Vecchio is an extremely complicated complex that was formed over many years through the assemblage of existing structures into one larger building. Through this combination process, there were obviously many different connection points, materials and workmanship utilized in each case. This chapter only touches on the details of the areas adjacent to the Room of the Elements.

To study the Room of the Elements, a thorough TLS campaign was conducted in the room of concern as well as the surrounding rooms, staircase, balcony and exterior walls. In addition to the geometric data acquisition, high resolution visible and thermal image mosaics were also acquired to provide supplementary surface and subsurface information. The concerns for the integrity of the structure stem from extensive cracks throughout the room that are clearly visible at

the surface, as seen in Figure 7.1. Cracks like this can be observed throughout the room with the majority of the damage observed in the walls that run North to South.

As early as 1558 there were concerns with the integrity of the Southeast corner of Palazzo Vecchio, as was indicated by an invoice directed to Giorgio Vasari for steel reinforcing bars - later detected using metal detection equipment (Alessandri, Cappelli, Leggeri, Muccini, & Tralli, 1970). The building's complex construction through the connections between other existing buildings has therefore obviously been a topic of concern since the times when the connections were being made. Vasari was an artist, historian and designer well known for initiating architectural modifications. Being a self-proclaimed historian, he was also one to write about the events of the day, so we have some historical records of the constructions and alterations of the time.

Figure 7.1 Image showing an example of the observed cracking in the Room of the Elements.

Previous authors have studied some of the observed damages in Palazzo Vecchio and attempted to reason why they may have occurred. The Southeast corner in particular has been of

great interest which happens to be the region in which the Room of the Elements is located on the top floor. Driven by a damaged pillar on the ground level in the Southeast corner, overall deformation of the Southern exterior wall was measured over thirty months displaying that the floors of the structure do not provide sufficient horizontal resistance (Alessandri, Cappelli, Leggeri, Muccini, & Tralli, 1970). This observed out of plane deformation in the South wall was also demonstrated through numerical modeling, though simplified geometry and material properties were used (Barba & Fiori, 1970).

The cracking patterns in Sala degli Elementi have been mapped previously using laser scanning and visible imagery in order to understand the potential causes (Wood, Hutchinson, Wittich, & Kuester, 2012). This work acknowledged the complications that accompany studying historical structures without detailed understanding of the construction details, material properties and alterations to the structure throughout a building's lifetime.

The background of the Baptistery's construction has been discussed in Chapter 3. Previous works have looked at portions of the building's history and construction details. For example, tomographic techniques were used on the vault of the "Scarsella," situated on the West side of the Baptistery, to study its internal structure. This work, which used a combination of electrical resistivity tomography (ERT), seismic transmission tomography, and GPR, concluded that between the inner brick vault structure and the roof of the vault construction is composed of unconsolidated, assorted fill materials (Cardarelli, et al., 2002). Previous works have also used passive sensing techniques to measure the structure's response to ambient vibrations. Using two types of equipment, seismometers and a microwave interferometer, the first modal frequency was measured at 2.67 Hz and 2.65 Hz respectively (Lacanna, Ripepe, Marchetti, Coli, & Garzonio, 2016; Fratini, Pieraccini, Atzeni, Betti, & Bartoli, 2011). These measurements will become extremely valuable when validating numerical models of the structure.

7.3 Approach

Preceding chapters have detailed non-destructive imaging data collection and how each data asset is useful. These data assets are also complementary and can be combined into a holistic digital model to generate additional assessments through a combination of modalities. This chapter highlights ways in which the resulting as-built information model can be used to yield valuable structural assessments and how the combination of data modalities decreases the entropy of the structural system. Without any knowledge of the structure, there are infinite geometric configurations as well as an infinite number of possible construction materials. Each empirical observation made about the structure decreases the amount of uncertainty as to the configuration of the system, therefore decreasing the overall entropy.

This idea of decreasing entropy can be extended to be modeled after the Dempster-Shafer Theory (DST), or evidence theory. DST is a great framework for modeling systems that have extreme levels of uncertainty. For historical structures, DST can be a very powerful tool to quantify the utility of acquired data, because there are so many unknowns as to material properties, construction methods and modifications to the structure over time. DST is also capable of resolving instances where multiple experts have differing diagnoses of a given scenario. Bao demonstrated through DST that combining multivariate data streams can lead to improved damage diagnosis of a structural system (Bao, Li, An, & Ou, 2012). The goal of this chapter is to show tangible examples of how an increased amount of information, and therefore less entropy, will lead to more accurate and meaningful assessments.

7.3.1 Data Acquisition and Integration

The laser scanning campaign at the Baptistery of San Giovanni was already discussed in detail in Chapter 3. A similar comprehensive scanning effort was undertaken at Palazzo Vecchio to capture geometry of the entire exterior as well as the interconnected rooms adjacent to the Room

of the Elements. Presented in this section are the other imaging techniques that were used in the multi-modal documentation effort of both structures. In addition to the high-resolution geometric record obtained through TLS, other methods including thermal imaging, photogrammetry and ground penetrating radar (GPR) were used to acquire complementary data at the subsurface and volumetric levels of the structures.

In Chapter 4 and Chapter 5 the creation of building scale thermal image mosaics was presented, but ideally these image mosaics should be placed in their context. To address the integration of thermal image mosaics into the information model, recall section 6.3, specifically Figure 6.6. The photogrammetric concepts from SfM can be extended to apply towards adding a thermal layer, or any other image layer, to the geometric data. The first step towards integration is the estimation of the camera position. In this case, the camera position represents where the APT instrumentation was placed to acquire the high-resolution thermal image mosaics. Recalling Chapter 5, it is possible to automatically fuse visible and thermal images through a calibrated transformation. This approach in many cases is the most useful because, as discussed in Chapter 5, there are typically very few mutual features shared in the thermal and visible images. The integration, therefore, is transitive wherein the thermal images are registered to the visible images which are in turn registered to the geometry -- being generated through either photogrammetry or laser scanning techniques.

For the registration of image data to 3D geometry, the key variables are the camera's location and orientation in the geometric coordinate system as well as the camera's internal parameters. The registration of visible images to a geometric model created through photogrammetry straightforward because the process is inherently performed in the SfM algorithm. In order to triangulate the geometry from 2D image sources, SfM must precisely estimate the

positions of each camera. After the 3D model is generated, the computed camera positions and orientations can be saved in order to locate the raw images in the 3D coordinate space.

If the images being aligned have not been used in SfM operations, then the alignment can be enabled by the 3D model. First, the user can navigate within the 3D model to the approximate position and orientation of the given camera within the geometric coordinate space. The parameters of this virtual image can then be extracted to record the position, orientation, and projection of the virtual camera. The image to be layered can then be aligned with the virtual camera image using feature detection and matching techniques in order to compute a homography which encapsulates the translation and rotation of the image in relation to the virtual image. Using this homography, the image to be layered is transformed into the coordinate space of the virtual image. Finally, the parameters that were extracted in the creation of the virtual image are used to reprojection the new image layer onto the 3D geometry. Examples of these parameters are shown in Appendix A, where the 3D model and a subsequent virtual image were used to align a thermal image mosaic layer to the South exterior wall of the Palazzo Vecchio model.

This approach was used for the Baptistery as well as Palazzo Vecchio. Thermal image mosaics were acquired for all eight exterior façades of the Baptistery, registered to the high-resolution visible image layers and then layered onto the geometric data acquired with TLS (see Figure 7.2). As for Palazzo Vecchio, thermal mosaics were collected inside the Room of the Elements in addition to the exterior walls of the room from the outside (see Figure 7.3).

Using the same approach utilized with the Baptistery, the thermal mosaics for the Room of the Elements were registered to their high-resolution visible counterparts and subsequently layered onto the TLS data. With a newly achieved geometric context, the high-resolution thermal data can now be viewed, annotated, and measured in an interactive 3D environment. The thermal data does not overwrite the data it has been registered to, but acts as an additional layer that can be toggled

on and off (refer to Figure 7.8). Another way to think about it is as an additional attribute (color, temperature, coordinate, etc.) associated with each data point in the geometric model. In this sense, pointwise calculations and operations can be performed using all available point attributes.

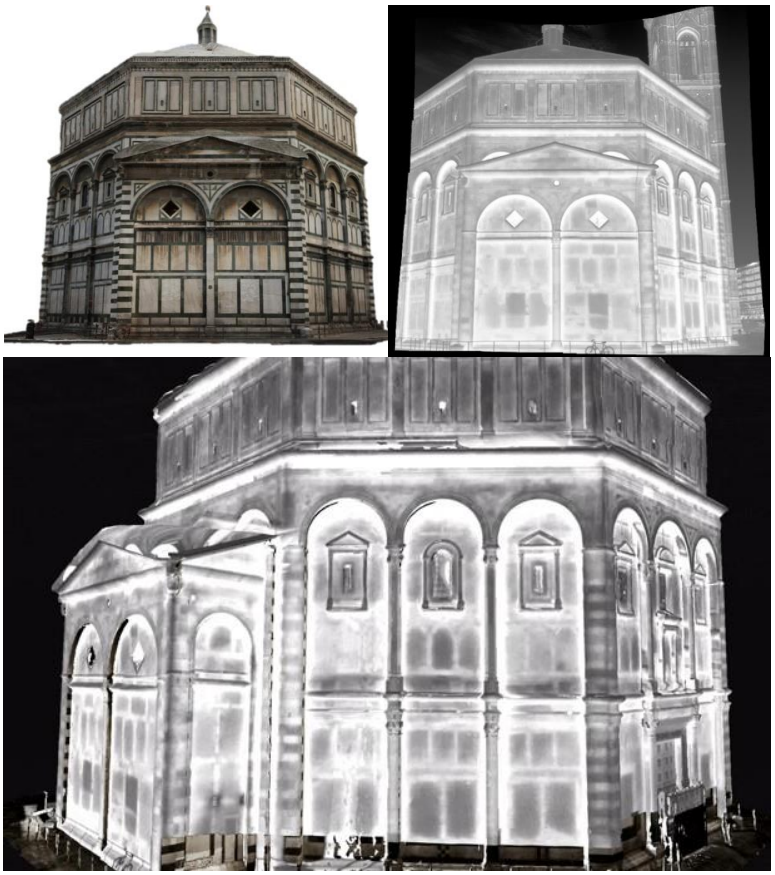

Figure 7.2 Visible layer (top-left), Thermal mosaic (top-right), and thermal added as a layer (bottom) to the holistic information model of the Baptistery.

This layering concept can also be extended to other multi-dimensional modalities. The requirement for integration is some knowledge of geometric context in the target scene's coordinate system. The context can be represented as image coordinates, GPS coordinates of a local coordinate system within the overall coordinate system of the information model or as a single point (e.g. the location where a material sample has been collected). For 2D and 3D data, there must be a minimum of three mutual features between the integrated datasets and the 3D information model. At the

Baptistery, GPR data was also collected to survey a portion of the floor inside the building (shown in Figure 7.4) and also a small sample on one of the marble covered walls at the ground floor level.

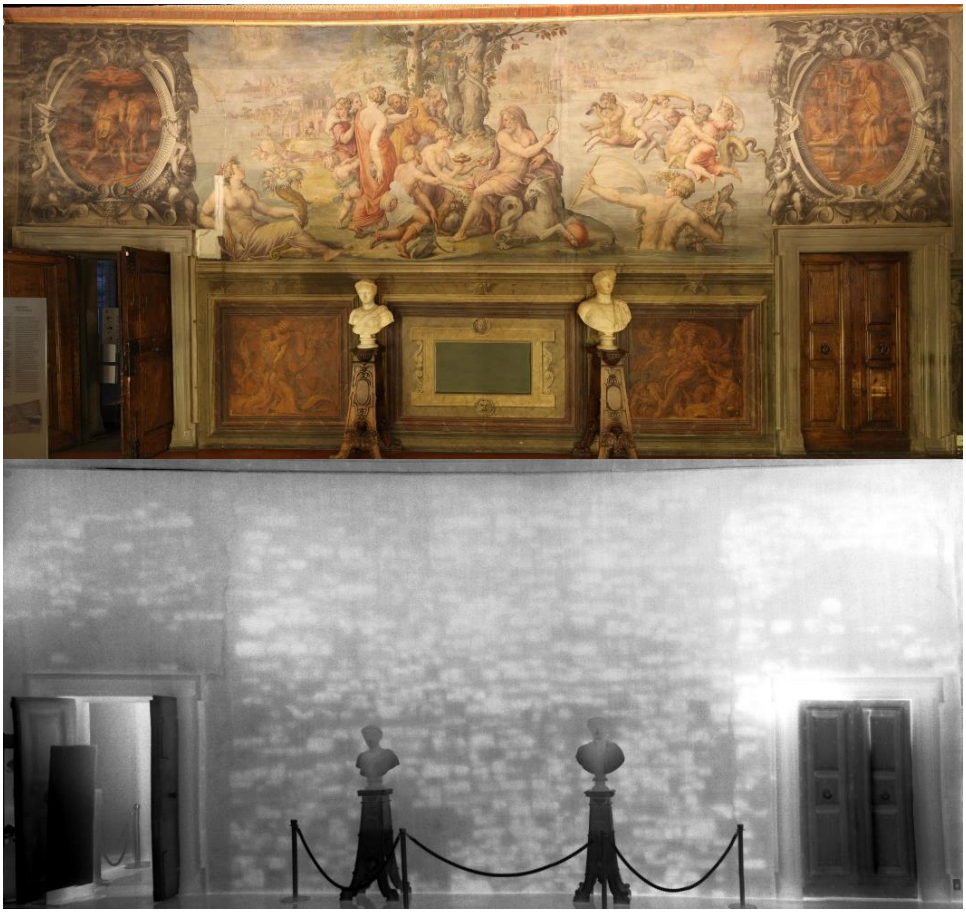

Figure 7.3 High-resolution thermal and visible layers of the Room of the Elements' West wall.

Figure 7.4 Area of the Baptistery floor that was imaged using GPR.

The GPR data was acquired and assembled according to a GPS coordinate system that was set up for the task. Using these coordinates, the individual slices of radar data were aligned with each other and the overall GPR dataset was incorporated into the holistic information model of the Baptistery (as seen in Figure 7.5). The GPR system used was an IDS stream-x equipped with an array of 600 MHz antennas allowing for the simultaneous acquisition of 11 parallel radargrams in a single pass. The floor dataset is composed of 187 radargrams, totaling about 2310 meters of GPR profiles. The raw data was then processed using multiple types of signal analysis and filtering. With the individual GPR profiles aligned, 3D volumes and surfaces were successfully rendered for further understanding of the data.

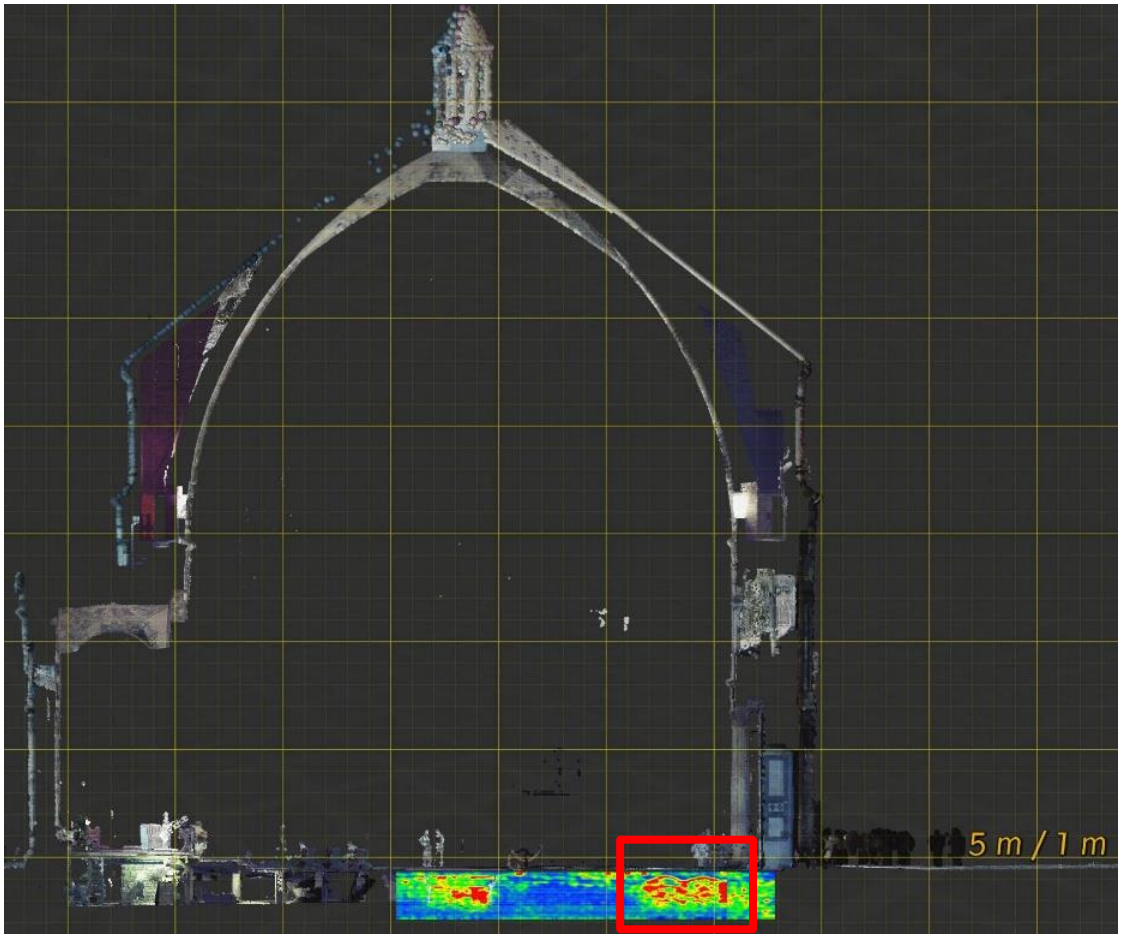

Figure 7.5 Section of the as-built information model showing the GPR data integrated with the TLS geometry – the location of the discovered vaults is highlighted in red.

7.4 Assessments

This section will ultimately demonstrate the benefits that can be gained from the combination of data records in one common information model. The combined data are not only from varying imaging techniques, but also layers corresponding to derivative data generated through analyses. One of the most important enhancements gained through the layered information model is the aspect of context. Seeing different data streams and analysis results in their context can provide much more meaningful interpretations. For 2D data assets, geometric context is also added so that measurements can be taken from data that before did not have accurate reference of

scale. As stated earlier, the most tangible gains, especially for the field of structural engineering, can be seen through numerical modeling and simulation of these masonry structures. Numerical simulation in these cases can help to predict future building performance and also provide feedback for any intended intervention or restoration.

7.4.1 Baptistery of San Giovanni

Beginning with the addition of context, TLS can be immensely useful for providing measurements and perspectives that were not before possible. The following examples demonstrate how the Baptistery is an excellent example of how TLS can supplement contextual information that would otherwise not be possible. The first example shows how taking a thin slice of the one and a half billion-point integrated TLS data reveals dimensions of the inner and outer dome constructions. Without the combined TLS data from the interior, exterior and space between the dome shells these measurements could not be made. The second example refers back to the damaged foundation wall discussed in Chapter 3. Without the TLS data of the excavated area beneath the Baptistery the damaged wall would not have been documented. Additionally, when these data are integrated with the scans of the interior of the Baptistery, contextual information is added to show a structural column resting directly above the damaged area.

As discussed in Chapter 3, the TLS data alone can also be used to compute and visualize deformation patterns. For the Baptistery, this was done for the dome and the floor in order to obtain any deviations from a previous geometric state. In this case, the previous state was assumed to be idealized, or perfectly constructed, but the next time the structure is scanned the two time-varying datasets can be compared as well. As previously mentioned, one of the most powerful impacts of the as-built information model is the ability to layer derivative data, such as the floor settlement analysis, back into its context. In the case of the Baptistery, seeing the floor settlement pattern in

combination with the excavated area, as was seen in Figure 3.8, generated new hypotheses as to whether the reinforced slab above the excavation may have caused differential settlement.

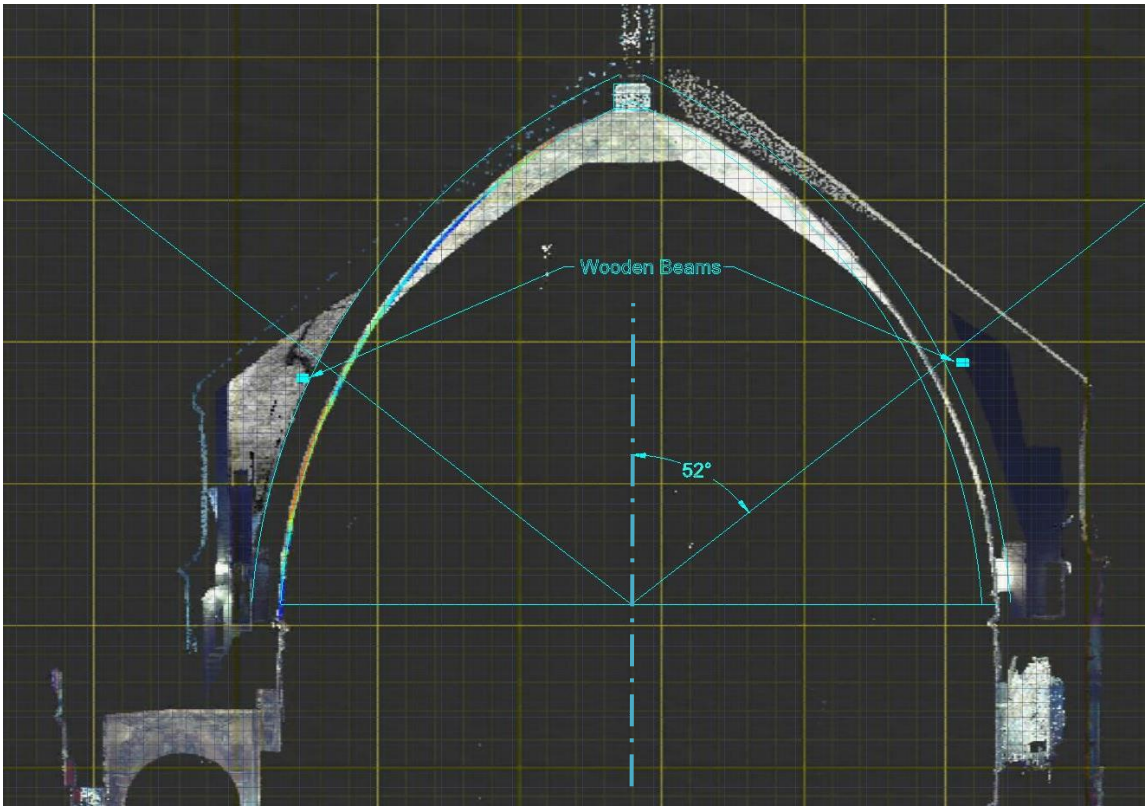

Figure 7.6 Section cut of the Dome highlighting the location of the wooden beams located approximately 52 degrees from vertical.

The similar example of the dome deformation presented in Chapter 3 also provides interesting derivative insights when layered back into its context. In this case, the area of interest is the wooden beam that encircles the inner dome to provide reinforcing. The wooden beam was inserted about halfway up the dome, as seen in Figure 7.6. The curious aspect is that the location of the wooden beam is near where a dome typically transitions from compression to tension, therefore not providing any benefits of resistance. The location that makes the most sense is where the dome is experiencing the most tension. Ottoni describes this issue of insufficient reinforcing and references the installation of an iron reinforcing ring added around 1514 (Ottoni, Blasi, Betti,

& Bartoli, 2016). This iron ring is located near the dome's base to provide more efficient tensile resistance to the dome's natural tendency to bulge outwards.

These reinforcing rings are incredibly important aspects that must be taken into account when conducting numerical simulations on the Baptistery. Also important is the historical information associated with each ring. The wooden beam was studied to determine its species and age using radiocarbon dating and dendrochronological analysis. Two time periods were identified: one for the chestnut beam structure dating to the 11th-12th century and the second corresponding to the silver fir elements which dated to 1268 (Bernabei, Bontadi, Quarta, Calcagnile, & Diodato, 2016). Each of these date ranges can now correspond to additional attributes which can be associated with the wooden beams in the as-built information model. The iron ties would then have a similar attribute which highlights its addition around 1514. These date attributes, that can now be associated with the information model, represent another layer of historical context concerning the construction history of the structure and show that some of the observed damage may preexist the iron reinforcing. Taking historical context into account can become extremely powerful when diagnosing complex ancient structures.

Thermal imaging and GPR can be added as additional layers to expand on the topic of revealing construction history. The wooden reinforcing ring and iron ties are both details that can be visually identified and studied, but thermal and GPR data can provide information beyond what is visible to the human eye. The GPR collected at the Baptistery helped study the internal wall structure as well as an area below the Baptistery which had not been excavated. Using the integrated radar data, two vaulted spaces were discovered beneath the Baptistery in an area that was not previously excavated. The two vaults, seen in Figure 7.7, can now be located in the overall context of the Baptistry once integrated into the information model. As seen in Figure 7.5, when the GPR data is incorporated into the geometric information model, the vaulted spaces can be located both

in the floorplan of the structure and in their depth to show that the vaults are at a depth consistent with the constructions excavated beneath the Western portion of the Baptistery.

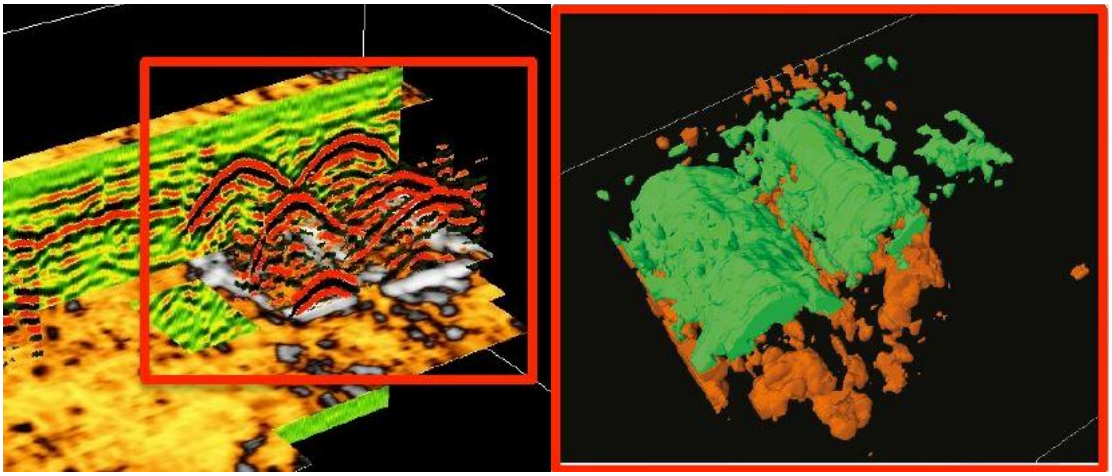

Figure 7.7 The vaults shown in a depth slice of the GPR data (left) and a surface rendering (right).

The GPR data collected on the wall surface of the structure is an example which adds information pertinent to structural engineers and historians alike. The GPR data on the wall enables the measurement of the decorative marble slabs which adorn the interior and exterior of the structure. With these new data, the structural wall can now be modeled more accurately to represent its real thickness when subtracting the thickness of the marble panels. The numerical modeling implications of this added measurement is explored later.

As previously mentioned, high-resolution thermal image mosaics were acquired for each facade of the Baptistery using the methods presented in Chapter 4. With the thermal data added as a layer to the information model, assessments can now be made using a combination of geometric, visual and thermal data of the exterior marble facades. Figure 7.8 shows the thermal layer added to the model and there are indications of marble slabs that have been replaced (darker in thermal layer), as well as areas that are cracked and likely moisture penetration.

Figure 7.8 Information model of the Baptistery showing the toggling of the thermal layer.

Even though the captured electromagnetic spectrum range is the same, SfM can, in some cases, add details to the geometric model formed with TLS. For the Baptistery, this is the case for the dome of the structure. High-resolution images were acquired and used to reconstruct the geometry of the dome using photogrammetry. Due to the enhanced color fidelity as well as smaller distance between data points, the SfM dataset of the dome was crucial when mapping the cracks that are visible on the surface of the dome (Figure 7.9). Not only are the new 3D points now available as a layer in the information model, but the raw images are also accessible from their point of view in the context of the Baptistery's coordinate system. In many cases, the raw images will be more useful for making visual assessments at a small scale. These raw image pixels can be toggled on and projected onto the dome geometry as in Figure 6.6 to visualize the photorealistic texture from each image at their point of view.

Figure 7.9 High-resolution SfM point cloud used to map the cracks in the dome through interactive annotation which highlights the cracked areas in red.

An additional attribute that SfM data can provide, which can prove to be useful for surface morphology analysis and lighting, is a surface normal at each point on the structure. Inherently in the photogrammetry process is the determination of the surface normal for each point in the resulting 3D point cloud. This is because the camera positions and orientations are very accurately calculated, and each pixel therefore has a direction traveling away from the camera. Through the triangulation of many images that see the same pixel or feature, an accurate surface normal is generated. Recall the point cloud classification example in Section 3.2.3, and how the mortar could be located using a combination of color attributes and surface normal attributes for every point. The use of surface normals enhances one's ability to detect cracks and small-scale surface deformations.

7.4.2 The Room of the Elements

The complexity of Palazzo Vecchio's construction and history makes it a very difficult patient to diagnose. As discussed earlier, the primary focus is the Room of the Elements, located

on the top floor of Palazzo Vecchio in the Southeast corner of the building. The observed damages have been a cause for concern for some time beginning as early as 1558 and are still being studied today. The Room of the Elements exemplifies one of the largest difficulties when attempting to remedy damages in historical constructions; the structure is the art and the art is the structure. All four walls of the room are decorated in frescoes. Frescoes, which are prevalent throughout Italy, are paintings created by applying pigment to wet plaster to yield a decorative wall covering when dried. These artworks are bonded to the structure and any intervention to one affects the other. This accentuates the need for accurate diagnosis so effective interventions can be made as minimally as possible. The work at Palazzo Vecchio was performed in collaboration with the City Architect to determine an effective preservation plan that accounts for the supporting structure as well as the art that adorns it.

TLS was used to form a comprehensive geometric record of the Room of the Elements as well as the surrounding interior rooms and the exterior of Palazzo Vecchio. As in the Baptistery project, the TLS data alone can be used to study aspects of the structure such as floor deformation, as seen in Figure 7.10. The raw point cloud data was also used to study the planarity of the individual walls. Each of these derivative datasets are now incorporated as layers in the information model (example shown in Figure 7.11).

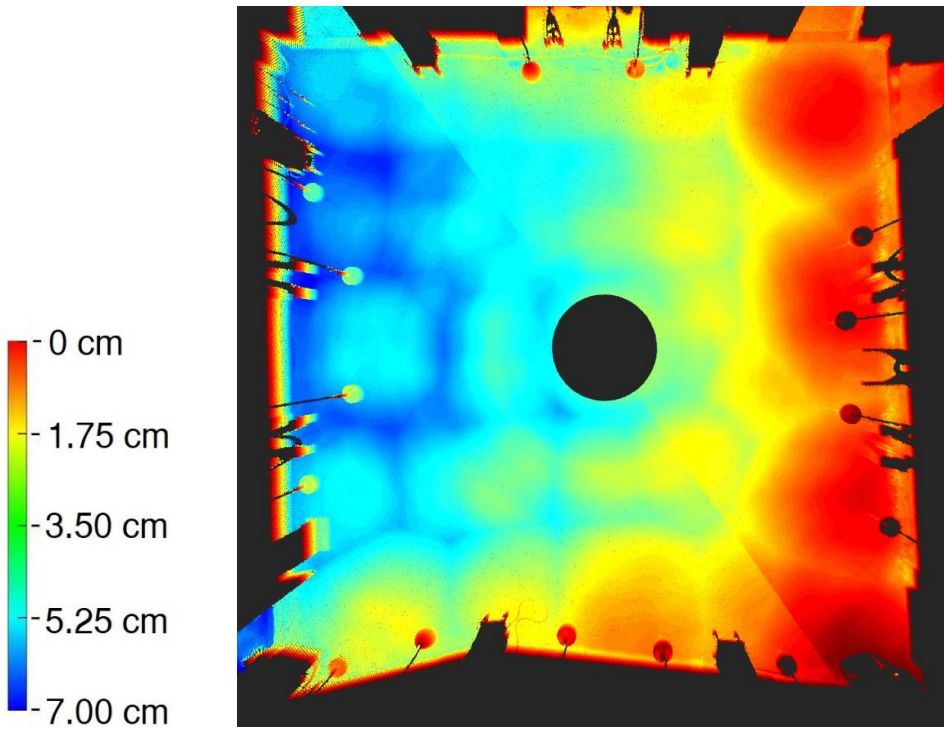

Figure 7.10 Vertical displacement map of the floor in the Room of the Elements.

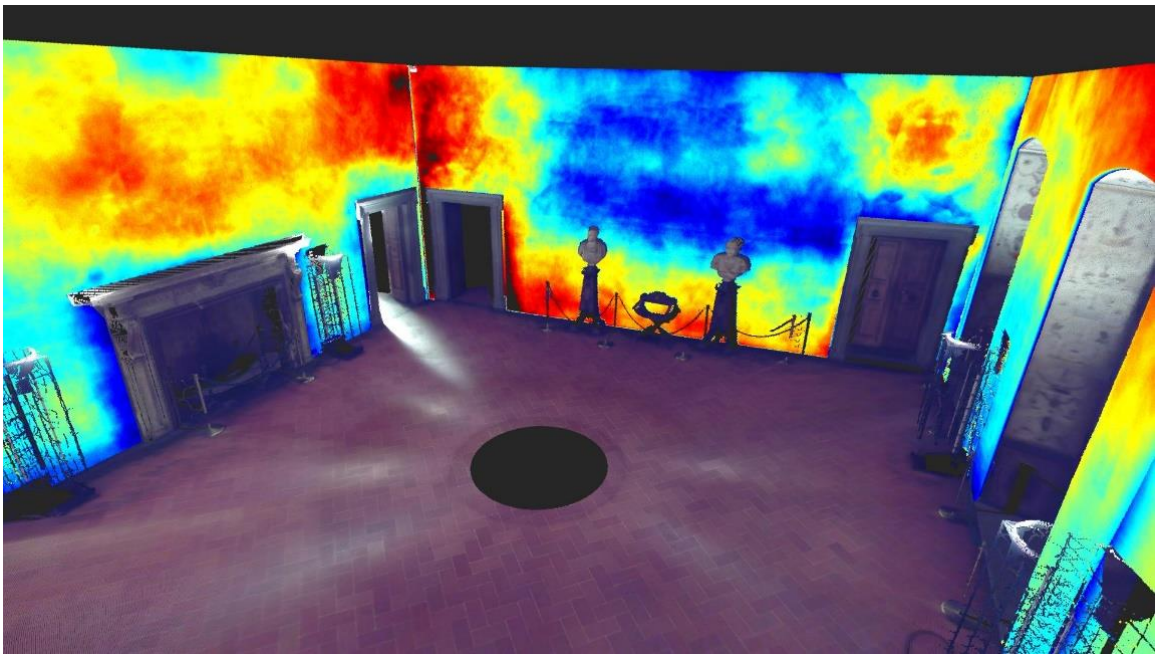

Figure 7.11 Displacement maps of each wall integrated back into the holistic model as layers.

High-resolution photographs were also acquired to document the network of cracks in the frescoes. The photorealistic appearance contributed by the photographs greatly enhances the assessment of the cracks because many of the smaller cracks in the fresco surface cannot be captured by TLS. High-resolution thermal image mosaics were also acquired for every interior wall of the room in addition to the exterior of the South wall. Using photogrammetric principles, the visible and thermal image data were then draped onto the geometric model formed by TLS as additional layers of the information model of the structure.

All three layers of the information model (geometry, visual and thermal) are crucial to understanding the health of the building. However, these are not the only sources of information; there are many sources for historical information on Palazzo Vecchio that prove to be vital to the overall understanding of the structural dynamics. This refers again to the notion of historical context and associating each piece of empirical evidence with its place in the construction history of the structure.

Studying the history of Palazzo Vecchio's construction, the Manieri building complex (see Figure 7.12) was purchased by Town Hall in 1335 and incorporated into the building (Pecchioli, Corrado, & Bardi, 1970). The Manieri complex integration into Palazzo Vecchio is a crucial piece of information for the Room of the Elements because of the different construction phases and discontinuities as can be seen in Figure 7.12. Interestingly, in the thermal images, there are possible hints of these original exterior walls shown by the filled-in arches above the doors on the East and West walls. Comparing the size and shape of these outlined arches with the existing exterior windows on the South wall shows that the East and West doors were likely the same size originally and functioned as exterior windows.

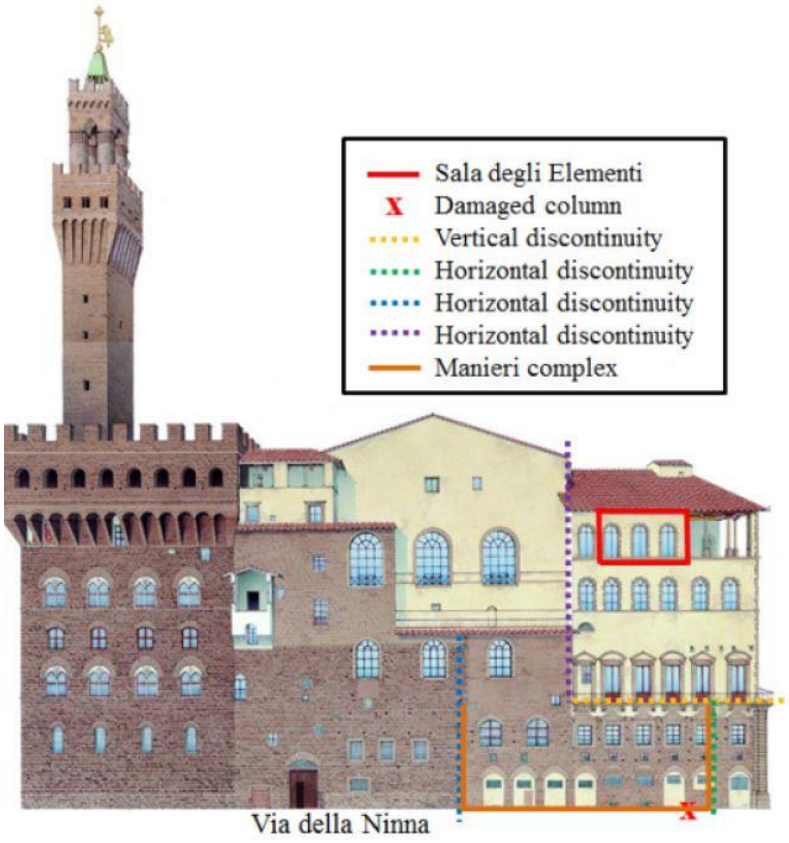

Figure 7.12 Schematic of Palazzo Vecchio's South Façade (Wood, Hutchinson, Wittich, & Kuester, 2012).

Figure 7.13 Visible and thermal layers of the South wall revealing construction details below the plaster on higher floors.

Others have highlighted some of the discontinuities in the construction of the South exterior wall of Palazzo Vecchio (Figure 7.12). The discontinuity on the far right of the wall between the first two windows (green dashed line) is an example where two walls - likely from different time periods - were joined without proper toothing. Previous researchers have acknowledged this visual discontinuity, but highlighted that it was unclear if it continued up through the higher floors because of the plastered walls (Pecchioli, Corrado, & Bardi, 1970; Wood, Hutchinson, Wittich, & Kuester, 2012). The thermal image mosaic that was acquired facing this exact wall, shown in Figure 7.13, shows evidence of the wall seam continuing on the higher floors. Here, the insights gained from the as-built information model is clearly demonstrated. Without the thermal imaging data in addition to the visual observations and historical context, the understanding of the construction sequence was not fully known.

Previous studies have also highlighted the damaged "pillar" on the first floor below the Room of the Elements and explained the steel reinforcing that has been added to resist further cracking on the exterior structure. Further understanding is also gained from studying interventions made around 1975 where an internal wall, also on the first floor below the Room of the Elements, was erroneously removed likely contributing to the observed damages (Pecchioli, Corrado, & Bardi, 1970; Wood, Hutchinson, Wittich, & Kuester, 2012).

These previous studies and interventions must also be incorporated into the information model to accurately model the interactions of all structural members from its foundations up to the wooden ceiling of the room. Each piece of historical evidence adds more insight and understanding to the initiation and propagation of the damages that exist today.

7.5 Numerical Modeling and Simulation

The most compelling and influential results are generated through advanced numerical simulations of the surveyed structures. This section specifically highlights the risks associated with

ignoring existing damages and imperfections when performing numerical simulations. These dangers are demonstrated through examples which compare different geometric configurations and loading scenarios.

To start with a relatively straight forward example, a comparison of column loading is explored at the Baptistery. Using the laser scanning model, a 3D solid model of one of the Baptistery walls was created. The lower portion of the Southwest wall was selected in order to study the foundation wall below it (recall Figure 3.12), and the numerical modeling strategy is described in 3.1.1.3. If one were to assume that the Baptistery's walls were constructed entirely of structural material, the gross dimensions of the wall would be used in the numerical model. However, it can be clearly observed that the exterior and interior surfaces of the walls are decorated with marble slabs. If the decorative marble slabs are not considered part of the supporting structure, then the resultant load carried by the columns will not be the same as if the entire wall were structural. The GPR data acquired on a sample of the wall, and subsequently integrated into the as-built information model, provides data concerning the thickness of the marble slabs and the supporting wall hidden beneath them.

Updating the numerical model to a version in which the decorative marble slabs do not carry structural loads nearly doubles the magnitude of the reaction at the base of the columns, though, in reality, the correct column loading is likely somewhere in the middle of the two scenarios. This result is extremely significant especially when the column load is then transferred to the foundation wall beneath it. This exemplifies how additional information from other modalities can alter structural analysis and assessment.

These types of assumptions can lead to misleading and false results. Historical buildings are complex and heterogeneous structures which function discontinuously due to disparities in the material properties. If one is looking for an understanding as to how a structure came to be in a

certain state of health or what the possible load capacity is under current circumstances, then including the true nature of the geometry and materials is crucial. Communicating these assessments to stakeholders and other professionals can be disastrous if the varying scenarios can yield a discrepancy of 100%.

Figure 7.14 View of the foundation wall in its context with the information model (left) and an image from the excavated area showing a view of the cracked wall.

To build on this example, a more detailed analysis of the foundation wall beneath the columns has been conducted. Recall, the foundation wall was being studied to assess the observed cracking damage with the goal of diagnosing the potential causes - the cracked mortar joints are show in Figure 7.14. In this analysis, a combination of Finite element (FE) and Distinct Element (DE) methods were used to study the effects of varying column load as well as differing geometry and settling patterns. Again, the existing geometry was extracted from the TLS data acquired in the excavated area of the Baptistery. First, using finite element methods (FEM), the foundation wall was simulated under the two loading scenarios. The material properties used in the simulations are

the same as were presented in 3.1.1.3. The results, seen in Figure 7.15, show that areas of increased strain propagate more extensively in the mortar under double the load. Also, the path of these increased strain areas is also where the observed cracks are found.

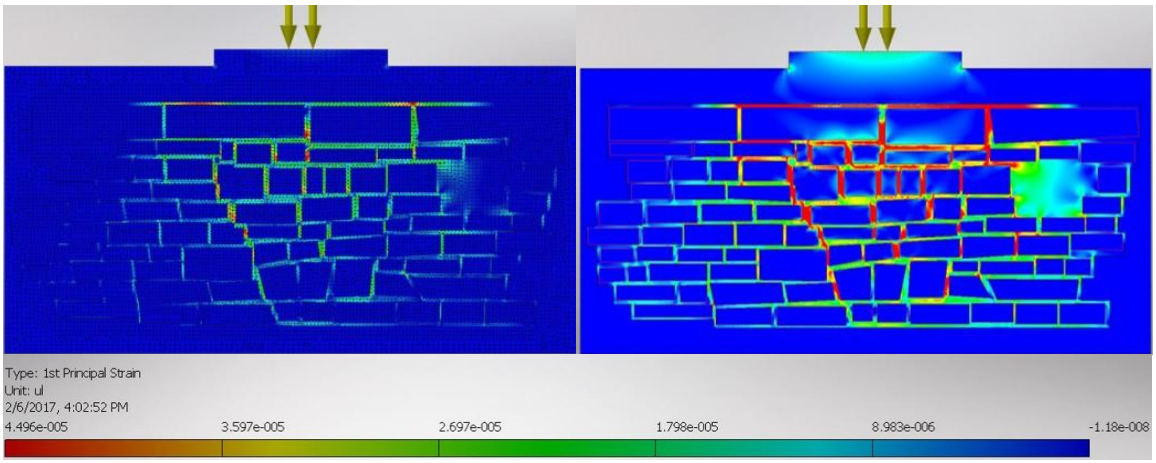

Figure 7.15 Initial FEM simulations to see the effects of doubling the column load on the foundation wall.

For a more accurate representation of masonry mechanics, discrete element modeling (DEM) was also used to simulate the foundation wall. Using a detailed micro-modeling approach, different geometric configurations were simulated to test the dangers associated with inadequate representation of masonry stones layout. In each geometric configuration, three conditions were simulated: 1) column load only, 2) column load and 0.05 meters of settling on the left half of the wall and 3) column load and 0.05 meters of settling on the right half of the wall. First, the existing geometry was modeled, which is the same input geometry used in the FEM example. In these simulations, the wall is considered as if it is undamaged to try and replicate the observed damage patterns.

The DEM simulations were executed in Itasca Consulting Group's commercial program 3DEC. The approach taken in 3DEC was mixed numerical approach, FDEM, where the stones are modeled as distinct, rigid elements and the mortar is incorporated as a continuous deformable body

(Napolitano, Hess, Coe-Scarff, & Glisic, 2018). Through the simulation results for the existing geometry, it can be shown in Figure 7.16 that neither of the settling conditions would likely lead to a damage pattern that closely mirrors what is observed at the Baptistery. Though, the dead load alone does cause a continuous line of tension that follows the path of the observed cracks. Whether or not these magnitude tensile stresses (>0.4 MPa) would cause failure in the mortar cannot be definitively determined without characterizing the exact materials used in the Baptistery foundation wall. The concentrated areas of tensile stresses do however closely mimic the existing damage pattern.

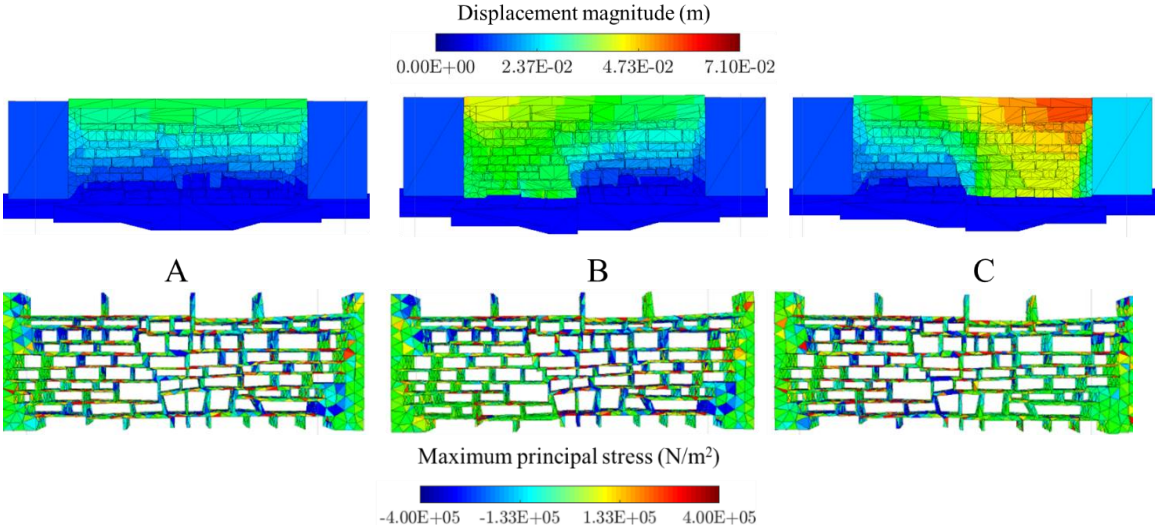

Figure 7.16 Combined FDEM simulations of the existing geometry for each of the three settlement cases: A) No settlement, B) Left side settled 0.05 meters, C) Right side settled 0.05.

The next test utilized a homogenized masonry pattern assembled with the average stone and mortar sizes measured in the foundation wall (seen in Figure 7.17c). The purpose of this experiment was to evaluate the potential effects of inaccurate modeling of the existing masonry layout in a relatively simple wall. The results were rather conclusive in that the stress distribution bears no resemblance to what was seen in the existing geometric layout, as can be seen in Figure 7.18. Most of the stress is dissipated through the first few courses of stones, and there is no distinct

pattern or indication of where a crack would propagate. Again, more accurate results could be generated with physical characterization of the material on-site.

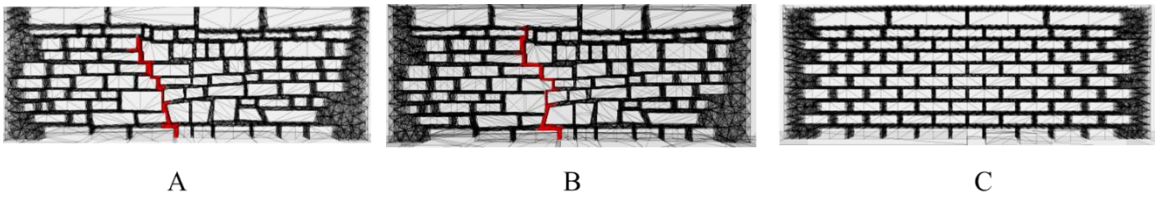

Figure 7.17 The three input geometries for the foundation wall: A) Existing pattern of stones and mortar, B) Wall with small alterations in the pattern of the stones and mortar along the red joint, and C) Isodomic patterning of averaged stone and mortar sizes.

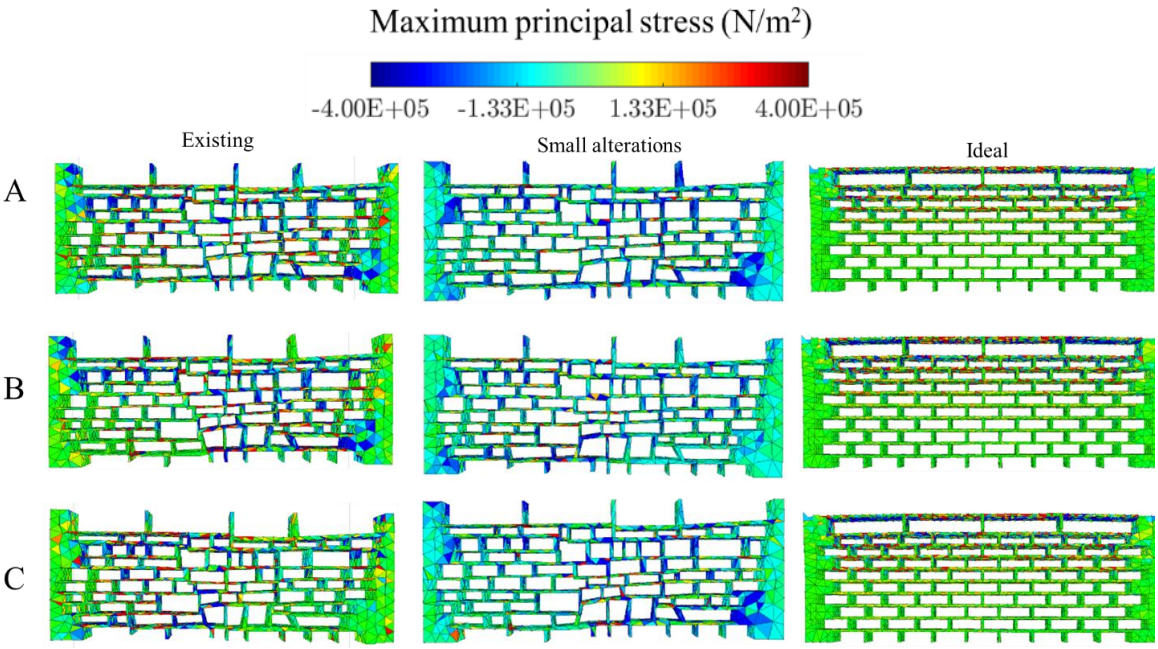

Figure 7.18 Simulated maximum principal stress for the each of the geometries and each of loading scenario A) No settlement, B) Left settled 0.05 meters, C) Right settled 0.05 meters.

Lastly, a test was conducted to evaluate the sensitivity of detailed micro-modeling in this case study. As seen in Figure 7.17a, the vertical joints in the existing configuration provide a path of least resistance for the crack to propagate. Figure 7.17b shows the final configuration in which there are subtle adjustments to the joint locations aimed at breaking the propagation path of the cracking. Again, this configuration was simulated through the three loading scenarios. Figure 7.18

shows that the stress is more distributed throughout the wall removing a principal direction for crack propagation. It is extremely interesting that such minor alterations to the masonry's configuration can completely alter the way in which the stress in the wall is distributed. More on the FDEM modeling strategy and results can be found in (Napolitano, Hess, Coe-Scarff, & Glisic, 2018).

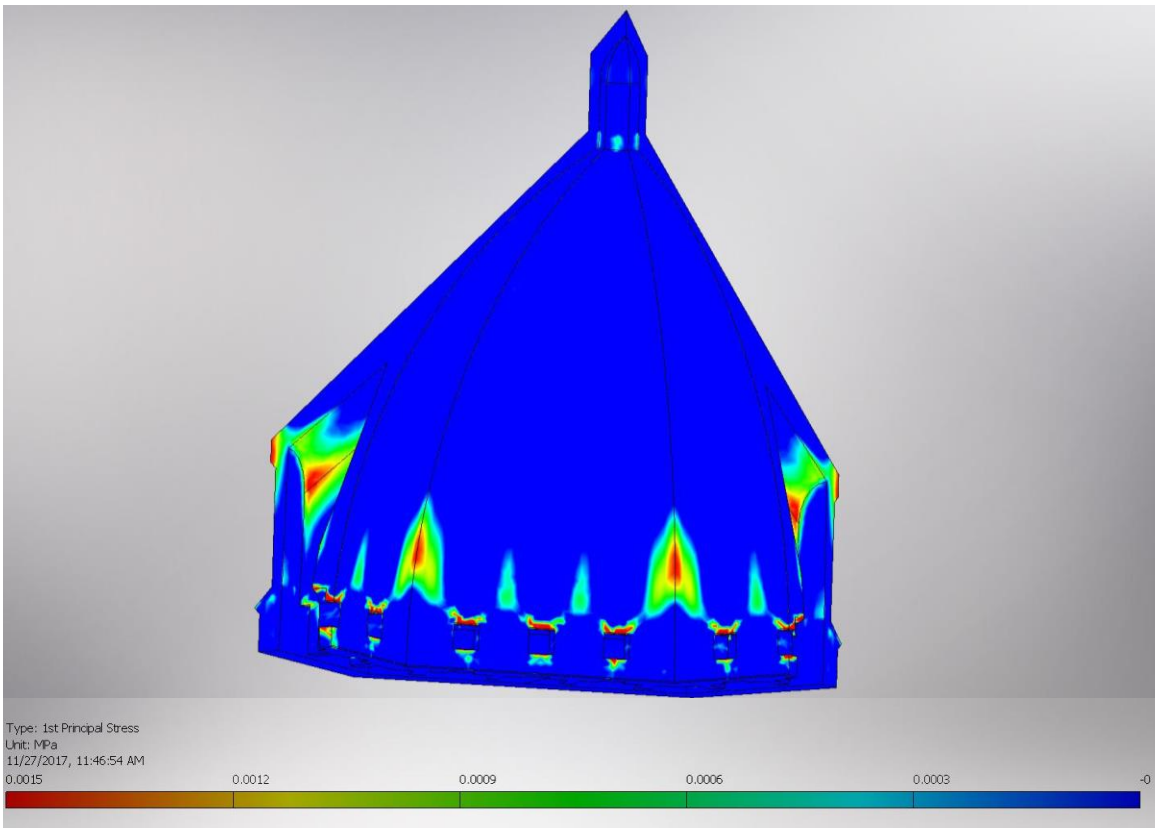

Figure 7.19 One quarter of the FEM simulation for the idealized undamaged dome.

Additional insight was also gained in FEM of the Baptistery dome structure. Using TLS data as a guide, an idealized solid dome model was constructed using CAD software. The complicated spaces between the inner and outer dome shells was also captured in order to gather understanding about the cracks that exist and were mapped through the SfM point cloud (Figure 7.9). Many of the cracks can be found in the corner seams of the dome where the eight sides intersect each other. Using FEM, the dome structure alone was simulated under gravitational

loading to visualize the stress distribution in the dome structure. Figure 7.19 visualizes the results of the FE analysis in which it can be seen that the stress is highly concentrated in the seams where the cracks are observed at the surface.

At Palazzo Vecchio in the Room of the Elements, a similar study was conducted. The utility of the combined data in the as-built information model is highlighted in this scenario because there are no records or indications as to the masonry configuration. The walls are completely covered in painted plaster, so the locations of the stones are only hypothesized through the evidence provided in the thermal imaging data. Though it was not completed, if GPR were performed on the walls in the room, it could also help detail the size and locations of the stones beneath the plaster once incorporated into the holistic information model (Colla, Fernàndez, Garanzini, & Marelli, 2010).

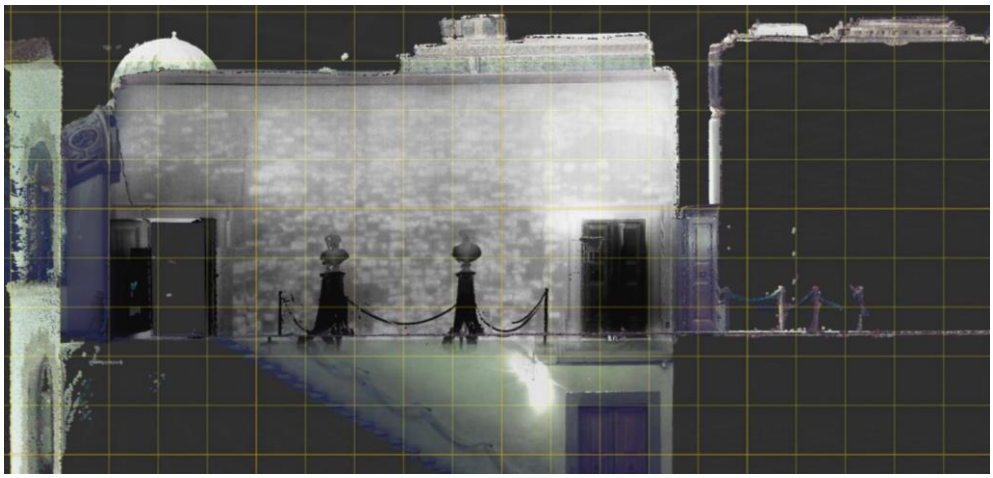

Figure 7.20 Information model of the Room of the Elements with thermal layer set on.

Using the ground truth geometry of the TLS model and the apparent stone locations from the thermal image mosaics (Figure 7.20), a 3D solid model of the West wall was created. The simulation strategy and material properties used are the same as described in 3.1.1.3. Similar to the Baptistery study, two other versions of the same wall were created to study the differences between existing geometry and idealized masonry patterns. Both other models are homogenized masonry patterns; the first utilizes stone and mortar dimensions consistent with the exterior of Palazzo

Vecchio and the second is the same ratio of mortar and stone seen in the thermal image but organized into a homogeneous pattern.

Initial modal analysis was conducted using FEM to evaluate the different mode shapes and frequency responses of the three models. Figure 7.21 shows the results of the experiment detailing the frequency of the first mode for the three cases. The completely idealized version of the wall is considerably stiffer than the other two models with a first mode frequency that is one and a half times that of the existing geometry. This is due to the higher percentage of stone material which is much stiffer than the more deformable mortar material. Especially in earthquake design and preparedness, the frequency response of a structure is one of the key drivers. It is therefore very important to accurately characterize the frequency response of existing structures, especially for masonry structures which are vulnerable to the lateral accelerations of earthquakes.

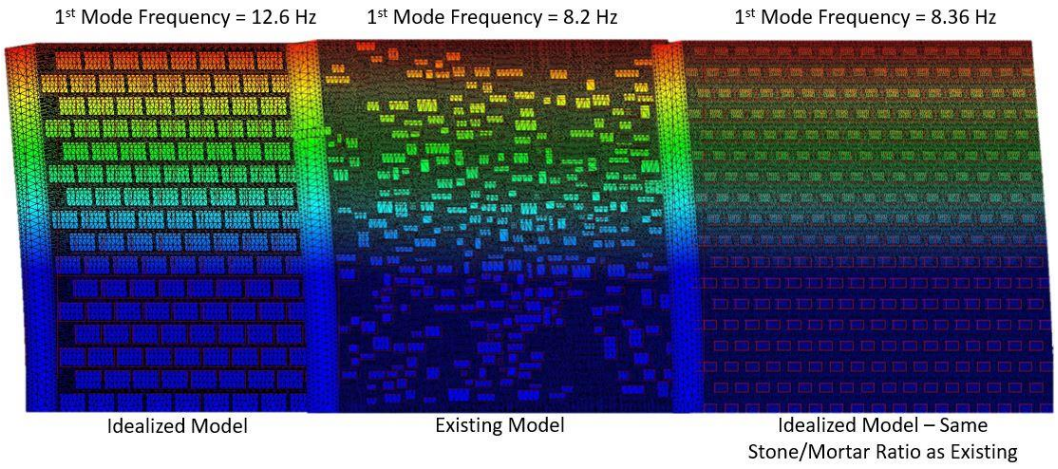

Figure 7.21 FEM simulations of the three input geometries to calculate natural frequencies.

Next, DEM was utilized, as in the Baptistery foundation example, to study the observed cracking patterns and begin to hypothesize the potential causes. As in the Baptistery, the wall models were simulated as if they were undamaged with the goal of recreating the damage patterns that can be seen today. Once the models are calibrated and validated, the damaged models could

then be simulated to predict future performance of the structure and identify which interventions, if any, would best preserve the structure's integrity.

The initial FDEM results (Figure 7.22) from the three configurations again demonstrate the importance of accurate modeling of existing geometric patterns in masonry construction. The displacements experienced in the existing configuration are an order of magnitude greater than the displacements calculated in the fully idealized model. Again, recall that the walls are covered in plaster, so the arrangement of stones could not have been known or accurately modeled without the integration of thermal imaging data.

One final analysis was conducted to again sample the sensitivity of the model to existing geometry perturbations. There are areas in the thermal data that appear homogeneous. In the previous analysis, these areas were considered to be a homogenous concrete-like material. However, from domain expert input and previous experience with historical structures, it is hypothesized that these areas are likely infilled with brick and mortar. The thermal properties of brick and mortar are much more similar than those of stone and mortar (Avdelidis & Moropoulou, 2004) so the bricks cannot be differentiated through thermal imaging alone. This is an example of where GPR data could compliment the thermal data by helping discriminate masonry patterns in these areas.

For the final analysis, instead of the concrete-like material that was used previously, those areas were filled with a masonry pattern as in Figure 7.23. As in the Baptistery, these seemingly minor changes to the masonry configuration make a large impact on the simulated response. Comparing Figure 7.22a and Figure 7.22d, the displacement magnitudes of the concrete infilled model are thrice that of the altered model with brick and mortar infill. The assessments gained from the Room of the Elements simulations are not entirely conclusive, but the workflow for data acquisition, integration and use for numerical modeling was successful.

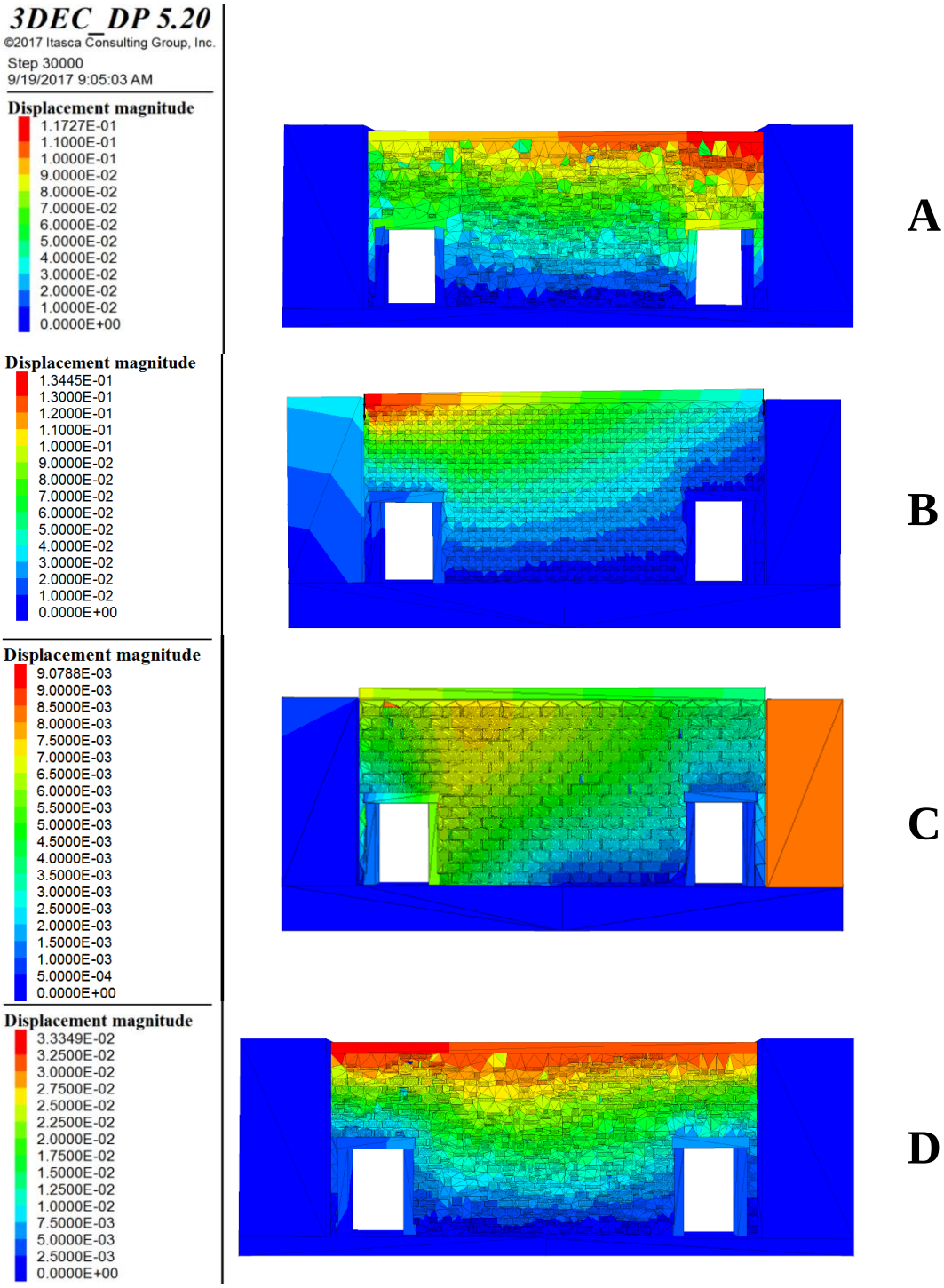

Figure 7.22 DEM results for the West wall of in the Room of the Elements: A) Existing geometry will infill B) Homogeneous pattern with same existing mortar/stone ratio C) Idealized model D) Existing geometry with a masonry pattern instead of infill.

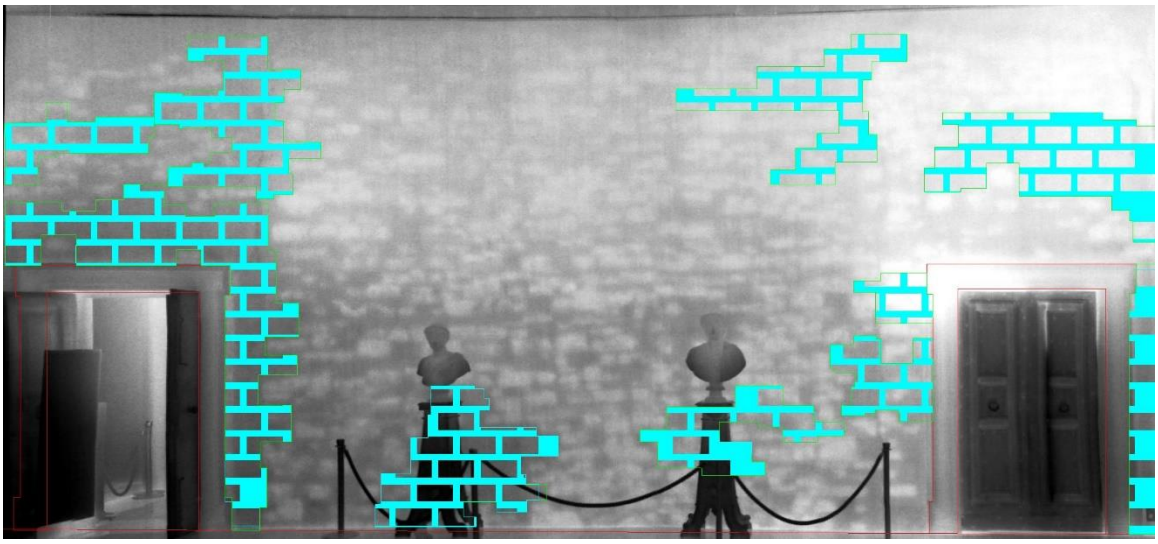

Figure 7.23 Infill of homogeneous thermal data with stone and mortar.

These initial numerical results are just the tip of the iceberg, but they demonstrate how as-built information modeling can inform the creation of these numerical models. The goal of this methodological pipeline is that the as-built information model will inform the numerical modeling which in turn will update the information model. Ultimately, the use of information modeling for collaborative analysis and domain expert assessments will enable better life cycle management of all existing structures.

7.6 Conclusions

The desire for more effective methodologies for documentation and analysis of historical structures has been highlighted by previous authors (Decanini, et al., 2004; Barazzetti L. , et al., 2015; Volk, Stengel, & Schultmann, 2014; Tang, Huber, Akinci, Lipman, & Lytle, 2010; Megahed, 2015; Wood, Hutchinson, Wittich, & Kuester, 2012), but is best summed up by Valluzzi: “The very specific peculiarities of historical masonry structures make systematic study according to generalized rules difficult, as regards both analysis and choice of intervention. A cautious,

multidisciplinary approach is essential, based on preliminary knowledge by accurate survey (Valluzzi, 2007)."

This chapter is a culmination of those preceding it in which the multi-modal, building-scale data are effectively combined into holistic as-built information models of two complex historical structures. The multidimensional data both supplement and complement each other while working to inform better hypotheses, analysis, assessments and ultimately life-cycle management of existing structures. These information models should serve as data repositories for both past and future datasets to be incorporated into. The key to the presented approach for information modeling is that the input data types are not prescribed but remain flexible to old and new technologies enabling greater collaboration and understanding of complex systems and interactions.

The goal of this chapter, and the dissertation as a whole, is to prove that the documentation of existing structures as well as numerical model formation can be performed accurately, and that these methodologies are ready for when computational capacities catch up. Instead of waiting until the computations are possible, the focus must remain on characterizing existing structures as accurately as possible through data integration strategies. The presented as-built information model is one way to address the ever-growing data avalanche caused by the development and use of new sensor technologies for multidisciplinary engineering projects.

As computational power and capacity are increasing as such a rapid pace, complexity and high-computational requirements should not limit how masonry structures are modeled and simulated. The presented approach demonstrates that the existing conditions of a structure can be documented, characterized and transformed into a numerical model for simulation. The goal should be to accurately characterize the performance and failure mechanisms, not to quickly simulate a model that will not represent reality.

7.7 Acknowledgements

This work was supported by the National Science Foundation under award #DGE-0966375, ‘‘Training, Research and Education in Engineering for Cultural Heritage Diagnostics,” and award #CNS-1338192, ‘‘MRI: Development of Advanced Visualization Instrumentation for the Collaborative Exploration of Big Data.” Additional support was provided by the Kinsella Fund, the Qualcomm Institute at UC San Diego, the Friends of CISA3, and the World Cultural Heritage Society. Opinions, findings, and conclusions from this study are those of the authors and do not necessarily reflect the opinions of the research sponsors.

Chapter 8 Conclusions and Recommendations

8.1 Motivation and Scope

In the field of healthcare, the idea of regularly updated health records is well established and accepted as a vital contributor towards preventative care. This dissertation evaluates the potential of digital health records for enhanced understanding, protection and management of existing infrastructure. Much of the built infrastructure that exists today has outlived its intended life and the unknown health of these structures pose safety and life-time maintenance concerns. The lack of reliable understanding as to a structure's current state of health, oftentimes results in the expensive demolition and replacement of entire structures. If professionals were instead equipped with a comprehensive structural health assessment that provides actionable data describing an existing structure, they could then make more informed decisions with potential for less consequential and expensive remedies.

Presented here is an integrative methodology that leverages the acquisition of multiple data streams that are then used as inputs for processing, analysis, and dissemination pipelines. Diagnostic imaging techniques, including light detection and ranging (LiDAR), photogrammetry and photography, combined with thermography and tomographic techniques, can be the initial steps in digital surrogate creation, providing accurate surface and sub-surface information needed for the creation of a baseline model. Once in place this initial information model enables a broad range of inquiries and analyses for existing structures at any scale.

Historical structures have been chosen as the target application of this research because replacement is not an option due to their economic, social and cultural impacts. The field of cultural heritage is in dire need of better engineering solutions for diagnosis and management of a wide range of cultural assets from sites to artifacts. Though the initial scope highlights applications with

historical structures, the developed methods for assessment and analysis can be extended to any existing structure at any scale

The presented acquisition techniques contribute information at the surface, sub-surface and volumetric levels with the goal of digitally documenting and reconstructing all existing components in the structure in a single holistic, digital representation. Additional techniques not presented here could also be added to the workflow if supplementary details about the structure are needed, but the overall methodology for acquisition, processing, analysis and dissemination will be the same.

Specific emphases are placed on the acquisition methodologies to be repeatable, comprehensive, and accurate. For the purposes of structural health assessment and monitoring, any methodology that does not meet these three criteria will not withstand the test of time and will be rendered unusable for scientific investigation. If a methodology is repeatable, it can be performed in subsequent documentation campaigns and used to monitor changes over time. Additionally, repeatability is important in respects to utility of emerging technologies; this is to say that a methodology should not be limited to technology that exists today, but open to welcome new technology by focusing on the output information. A methodology must be comprehensive to guarantee stakeholders and future users of the data, that any damages, deficiencies and changes have been captured. Finally, accuracy is paramount to the success of surveying existing structures to ensure an overall reliability of the generated data.

Many of the acquisition techniques have been proven effective individually for different aspects of structural health assessment, but the diagnostic value of the data can be increased if combined into a multi-dimensional layered model. The layered nature of this digital as-built information model enhances interpretation and understanding by correlating results from different modalities in time and space. Professionals and stakeholders can make more informed decisions if equipped with an accurate digital documentation record that captures flaws and damages both at

the surface and internally. This digital model can serve as the core hub for processing, analysis, dissemination and decision-making processes.

The initial measure of success for this approach is the degree of understanding about an existing structure that is gained. If emphasis is placed on the accurate characterization, documentation, and cataloging of existing structures, more accurate assessments will be made from the comprehensive representations. The overall goal is to reduce the amount of uncertainty in the digital model to enable numerical modeling and simulations which will generate more accurate predictions for a given structure's response to both past and future loading scenarios. The as-built information model is a more effective methodology for diagnosing patients, which in this case are historical structures. Accurate diagnoses based on empirical evidence contributed through information models will in turn yield better maintenance, preservation, restoration or demolition of all existing structures.

The ability to generate these models efficiently can greatly improve the investigation and maintenance of built infrastructure all over the world. In the United States specifically, there is a dire need to address problems with crumbling civil infrastructure and all over the world there are common problems associated with the life-time maintenance and stewardship of historical structures. The culmination of this dissertation is a repeatable methodology for the creation of as-built information models that serve to inform professionals and stakeholders about a given structure's state of health. The creation of these information models must be repeatable in order to gather vital temporal changes. Benefits of building information modeling (BIM) has been documented and quantified for new construction, but an approach to generate these records from existing structures has not been created.

This dissertation aims to address three primary research objectives with the ultimate goal of attaining a better understanding and approach towards the structural assessment of existing

structures. The first objective is to identify data acquisition modalities aimed at measuring and analyzing surface, subsurface and volumetric information at building scale. The second objective is to develop a methodology for the integration of these data into one holistic as-built information model. The final objective of this dissertation is to utilize these as-built information models to make more informed structural health assessments and decisions.

This chapter offers a concise summary of the above dissertation. The key results and conclusions of the three main research objectives are presented in the following sections. Following the key results is a summary of the impact of this research on the study of existing infrastructure, especially historical structures. Finally, this Chapter concludes with recommended topics for further study that build would upon the research presented in this dissertation.

8.2 Key Results

8.2.1 Repeatable Non-Destructive Imaging at Building Scale

This portion of the research focused on establishing, testing and validating repeatable methodologies to gather non-destructive imaging data. The mission of these methodologies being to measure an existing structure's geometry at the surface, sub-surface and volumetric levels as well as capturing both appearance and context. The primary imaging techniques presented here are TLS, photogrammetry, thermal imaging and GPR. The main contributions in this phase of research include:

- Geometric data acquisition methodologies using laser scanning and photogrammetric techniques were developed and tested in real documentation projects in the field. The acquisition, visualization and analysis of these geometric data were utilized for historical documentation, structural health assessment, disaster response and classification of construction materials.

- A methodology for high-resolution thermal imaging is presented. Through the presented approach, passive thermography can be conducted at building scale achieving superior resolution in the imaging data enabling detailed documentation and analysis. The thermal imaging methodology is designed to be repeatable as well as adaptable to future sensor technology innovations.

8.2.2 Data Integration for As-Built Information Modeling

This phase of the dissertation aims to take all the previous data modalities and integrate them into a holistic as-built information model. Here an as-built information model represents a digital surrogate of an existing structure that serves as a comprehensive repository for diagnostic data. This information model should capture, as accurately and completely as possible, the existing state of a structure at the surface, subsurface, and volumetric levels. For the greatest diagnostic potential, the data contained in the information model should maintain their raw, full resolution and not be subsampled, simplified or approximated. These as-built information models can then be used to augment or update an existing BIM as well as generate a new BIM for a structure with no previous records. The main contributions in this phase of research include:

- A methodology for automatic registration of thermal and visible images for the creation of high-resolution, multimodal image mosaics. The presented approach to image registration and alignment does not rely on mutual features between the thermal and visible images because in the real-world application of these techniques, mutual information is not always guaranteed. Some of the most important information revealed through thermal imaging is because it contains exclusive information not visibly represented at the surface.
- Combination of 3D imaging data for comprehensive documentation of existing structures in the field. Combining data generated through TLS and SfM methodologies can provide time and cost savings in the field and improve the results of the documentation campaign.

The data modalities can be used to supplement and complement one another, therefore enhancing the diagnostic and preservation potential of the resulting information model.

- Integration of multi-resolution, multimodal imaging data into an interactive as-built information model. Using repeatable imaging methodologies that maintain context within some mutual coordinate system enables the combination of the data assets into a more comprehensive and useful information model. The as-built information model is flexible to include different data types with varying resolutions and dimensionalities from past and future sensing technologies.
- Two examples from Florence, Italy are presented where as-built information models were created for two monumental structures: The Baptistery of San Giovanni and Palazzo Vecchio. Both of the structures were documented using varying imaging technologies including TLS, photography, SfM, thermal imaging and GPR.

8.2.3 As-Built Information Models for Structural Health Assessment

The last phase of this dissertation demonstrates how as-built information models can be used to make more accurate and meaningful assessments of existing structures. Through the combination of non-destructive imaging data, assumptions concerning a building's construction can be avoided which in turn can prevent misinforming professionals and stakeholders. Future management of existing infrastructure will rely on interactive, predictive models in combination with a decision-making framework, enabling day-to-day life-cycle management and rapid assessment and response following extreme events. The as-built information model approach presented here is adaptable to the injection of newly emerging data and can be used for rapid creation of actionable information. The as-built information model presented here is a larger vision of as-built structural health assessment that pushes toward a BIM logic approach of creating

comprehensive models that dynamically integrate data and can be used for decision making and analysis. The main contributions in the final phase of research include:

- Utilizing as-built information models for hypothesis generation, analysis, assessment and future planning. Through the creation of a multi-layered as-built information model, more accurate and impactful insights can be gained.
- The two as-built information models from the Baptistery of San Giovanni and Palazzo Vecchio are utilized for more detailed structural analysis and health assessment. The information model enabled a better understanding of the structures' construction histories as well as more informed diagnosis of observed damage conditions. Numerical models were created through a combination of modalities contained in the information models and simulated using FEM and FDEM to observe the effects of varying existing geometric assumptions.
- The results from the numerical simulations demonstrate the dangers associated with inaccurate representation of existing conditions as it pertains to geometric imperfections and observed damages.

8.3 Research Impact

This dissertation addresses three primary research objectives all aimed to attain better structural health assessment of existing structures. The main contributions are: 1) specification and validation of repeatable data acquisition methodologies to measure and analyze surface, subsurface and volumetric information at building scale, 2) integration of these multi-dimensional, multi-resolution and multi-model data into one holistic as-built information model, and finally 3) the utilization of these as-built information models to make more informed structural health assessments and decisions.

The methodologies presented in this dissertation can be used by professionals and researchers to better study and understand existing structures, specifically historical structures. The methodologies are not instrument or software specific, but procedurally outlined in order to repeatably integrate datasets from any input sensor in the most effective way. As in the medical practice, a holistic diagnosis of an existing structure's state of health cannot be rendered without a multidisciplinary effort which assembles historical, qualitative, and quantitative evidence.

8.4 Recommendations for Future Work

Recommended future research areas include:

- More development of numerical methods for modeling and simulation of complex masonry structures likely in the realm of discrete element modeling (DEM).
- Generate and evaluate predictive models with the above mentioned numerical methods applied to as-built structures taking into account all of the existing damages and imperfections
- Experimental testing of more complex masonry constructions like vaults and domes to aid in the validation of numerical results.
- The areas of potential information gain and improvements to current methods of assessing historical structures have been presented. Future work is encouraged using probabilistic or evidence based techniques such as DST to quantify the benefits of utilizing layered as-built information modeling for structural diagnostics.

References

Acosta, A., Pacheco, J., Garcia, E. J., Sifuentes, M., & Rodriguez, J. M. (2011). St. Nicholas of Tolentino monastery and church in Actopan, Hidalgo: preservation, surveying and reuse of a heritage building in Mexico. *Structural Studies, Repairs and Maintenance of Heritage Architecture XII, 12*.

Alani, A. M., Aboutalebi, M., & Kilic, G. (2013). Applications of ground penetrating radar (GPR) in bridge deck monitoring and assessment. *Journal of Applied Geophysics, 97*, 45-54.

Alani, A. M., Aboutalebi, M., & Kilic, G. (2014). Integrated health assessment strategy using NDT for reinforced concrete bridges. *Ndt \& E International, 61*, 80-94.

Alessandri, C., Cappelli, E., Leggeri, B., Muccini, U., & Tralli, A. (1970). Critical discussion about some measurements on a damaged corner of Palazzo Vecchio. *WIT Transactions on The Built Environment, 16*.

Arias, P., Herraez, J., Lorenzo, H., & Ordonez, C. (2005). Control of structural problems in cultural heritage monuments using close-range photogrammetry and computer methods. *Computers \& Structures, 83*, 1754-1766.

Arletti, R., Conte, S., Vandini, M., Fiori, C., Bracci, S., Bacci, M., & Porcinai, S. (2011). Florence baptistery: chemical and mineralogical investigation of glass mosaic tesserae. *Journal of Archaeological Science, 38*, 79-88.

ASTM. (2010). ASTM C1153-10 Standard Practice for Location of Wet Insulation in Roofing Systems Using Infrared Imaging. ASTM International. doi:10.1520/c1153-10

Avdelidis, N. P., & Moropoulou, A. (2004). Applications of infrared thermography for the investigation of historic structures. *Journal of Cultural Heritage, 5*, 119-127.

Balaras, C. A., & Argiriou, A. A. (2002). Infrared thermography for building diagnostics. *Energy and buildings, 34*, 171-183.

Baltsavias, E. P. (1999). A comparison between photogrammetry and laser scanning. *ISPRS Journal of photogrammetry and Remote Sensing, 54*, 83-94.

Banfi, F. (2016). Building Information Modelling--A Novel Parametric Modeling Approach Based on 3D Surveys of Historic Architecture. *Euro-Mediterranean Conference*, (pp. 116-127).

Bao, Y., Li, H., An, Y., & Ou, J. (2012). Dempster--Shafer evidence theory approach to structural damage detection. *Structural Health Monitoring, 11*, 13-26.

Barazzetti, L., Banfi, F., Brumana, R., Gusmeroli, G., Oreni, D., Previtali, M., . . . Schiantarelli, G. (2015). BIM from laser clouds and finite element analysis: combining structural analysis and geometric complexity. *The International Archives of Photogrammetry, Remote Sensing and Spatial Information Sciences, 40*, 345.

Barazzetti, L., Banfi, F., Brumana, R., Gusmeroli, G., Previtali, M., & Schiantarelli, G. (2015). Cloud-to-BIM-to-FEM: Structural simulation with accurate historic BIM from laser scans. *Simulation Modelling Practice and Theory, 57*, 71-87.

Barba, S., & Fiori, F. (1970). Portion of the south front of Palazzo Vecchio: numerical modeling and stressing state. *WIT Transactions on The Built Environment, 29*.

Bariami, G., Faka, M., Georgopoulos, A., Ioannides, M., & Skarlatos, D. (2012). Documenting a UNESCO WH Site in Cyprus with Complementary Techniques. *International Journal of Heritage in the Digital Era, 1*, 27-32.

Barlish, K., & Sullivan, K. (2012). How to measure the benefits of BIM—A case study approach. *Automation in construction, 24*, 149-159.

Benjemaa, R., & Schmitt, F. (1998). A solution for the registration of multiple 3D point sets using unit quaternions. *European Conference on Computer Vision*, (pp. 34-50).

Bernabei, M., Bontadi, J., Quarta, G., Calcagnile, L., & Diodato, M. (2016). The Baptistry of Saint John in Florence: The Scientific Dating of the Timber Structure of the Dome. *International Journal of Architectural Heritage, 10*, 704-713.

Bernardini, F., & Rushmeier, H. (2002). The 3D model acquisition pipeline. *Computer graphics forum, 21*, pp. 149-172.

Betti, M., & Vignoli, A. (2011). Numerical assessment of the static and seismic behaviour of the basilica of Santa Maria all'Impruneta (Italy). *Construction and Building Materials, 25*, 4308-4324.

Bianchini, C., Ippolito, A., & Bartolomei, C. (2015). The Surveying and Representation Process Applied to Architecture: Non-Contact Methods for the. *Handbook of Research on Emerging Digital Tools for Architectural Surveying, Modeling, and Representation*, 44.

Bolles, R. C., Baker, H. H., & Marimont, D. H. (1987). Epipolar-plane image analysis: An approach to determining structure from motion. *International Journal of Computer Vision, 1*, 7-55.

Boscardin, M. D., & Cording, E. J. (1989). Building response to excavation-induced settlement. *Journal of Geotechnical Engineering, 115*, 1-21.

Bosche, F., Ahmed, M., Turkan, Y., Haas, C. T., & Haas, R. (2015). The value of integrating Scan-to-BIM and Scan-vs-BIM techniques for construction monitoring using laser scanning and BIM: The case of cylindrical MEP components. *Automation in Construction, 49*, 201-213.

Bosiljkov, V., Uranjek, M., Žarnić, R., & Bokan-Bosiljkov, V. (2010). An integrated diagnostic approach for the assessment of historic masonry structures. *Journal of Cultural Heritage, 11*, 239-249.

Bouguet, J.-Y. (2004). Camera calibration toolbox for matlab.

Bourke, P. (2014). Automatic 3D reconstruction: An exploration of the state of the art. *GSTF Journal on Computing (JoC), 2*.

Brumana, R., Oreni, D., Raimondi, A., Georgopoulos, A., & Bregianni, A. (2013). From survey to HBIM for documentation, dissemination and management of built heritage: The case study of St. Maria in Scaria d'Intelvi. *Digital Heritage International Congress (DigitalHeritage), 2013, 1*, pp. 497-504.

Brunetaud, X., Luca, L. D., Janvier-Badosa, S., Beck, K., & Al-Mukhtar, M. (2012). Application of digital techniques in monument preservation. *European Journal of Environmental and Civil Engineering, 16*, 543-556.

Cardarelli, E., Godio, A., Morelli, G., Sambuelli, L., Santarato, G., & Socco, L. V. (2002). Integrated geophysical surveys to investigate the Scarsella vault of St. John's baptistery in Florence. *The Leading Edge, 21*, 467-470.

Carpinteri, A., & Lacidogna, G. (2006). Damage monitoring of an historical masonry building by the acoustic emission technique. *Materials and Structures, 39*, 161-167.

Coiras, E., Santamaria, J., & Miravet, C. (2000). A segment-based registration technique for visual-IR images. *Optical Engineering, 39*, 282-289.

Colla, C., Fernàndez, A. J., Garanzini, S., & Marelli, M. (2010). Diagnostic by imaging: 3D GPR investigation of brick masonry and post-tensioned concrete. *Ground Penetrating Radar (GPR), 2010 13th International Conference on*, (pp. 1-7).

Cosentino, P. L., Capizzi, P., Martorana, R., Messina, P., & Schiavone, S. (2011). From geophysics to microgeophysics for engineering and cultural heritage. *International journal of Geophysics, 2011*.

Davis, J. L., & Annan, A. P. (1989). Ground-penetrating radar for high-resolution mapping of soil and rock stratigraphy. *Geophysical prospecting, 37*, 531-551.

Decanini, L., De Sortis, A., Goretti, A., Langenbach, R., Mollaioli, F., & Rasulo, A. (2004). Performance of masonry buildings during the 2002 Molise, Italy, earthquake. *Earthquake Spectra, 20*, S191--S220.

DeFanti, T. A., Dawe, G., Sandin, D. J., Schulze, J. P., Otto, P., Girado, J., . . . Rao, R. (2009). The StarCAVE, a third-generation CAVE and virtual reality OptIPortal. *Future Generation Computer Systems, 25*, 169-178.

Dimetix AG. (2015, 3). Dimetix Products: FLS Laser Distance Sensor. Retrieved from http://www.dimetix.com

Facconi, L., Plizzari, G., & Vecchio, F. (2013). Disturbed stress field model for unreinforced masonry. *Journal of Structural Engineering, 140*, 04013085.

FARO. (2017). Laser Scanner FARO Focus3D - Overview - 3D Surveying.

Flint, R. C., Jackson, P. D., & McCann, D. M. (1999). Geophysical imaging inside masonry structures. *NDT \& E International, 32*, 469-479.

FLIR Systems Inc. (2014, 7). Automation Applications Infrared Camera: FLIR A315 / A615. Retrieved from http://www.flir.com/automation/display/?id=41330

FLIR Systems Inc. (2014, 7). FLIR SC8000 HD Series. Retrieved from http://www.flir.com/thermography/

Flügge, W. (2013). *Stresses in shells.* Springer Science & Business Media.

Fonstad, M. A., Dietrich, J. T., Courville, B. C., Jensen, J. L., & Carbonneau, P. E. (2013). Topographic structure from motion: a new development in photogrammetric measurement. *Earth Surface Processes and Landforms, 38*, 421-430.

Fox, T. (2013). New WAVE Display Technology Rises at UC San Diego.

Francis, A. J., Horman, C. B., & Jerrems, L. E. (1971). The effect of joint thickness and other factors on the compressive strength of brickwork. *Proceedings of 2nd international brick masonry conference, Stoke-on-Trent*, (pp. 31-37).

Fratini, M., Pieraccini, M., Atzeni, C., Betti, M., & Bartoli, G. (2011). Assessment of vibration reduction on the Baptistery of San Giovanni in Florence (Italy) after vehicular traffic block. *Journal of Cultural Heritage, 12*, 323-328.

Ganz, H. R., & Thürlimann, B. (1984). Tests on masonry walls under normal and shear loading. *Rep. No. 7502, 4*.

Ghiassi, B., Soltani, M., & Tasnimi, A. A. (2012). A simplified model for analysis of unreinforced masonry shear walls under combined axial, shear and flexural loading. *Engineering Structures, 42*, 396-409.

GigaPan Systems. (2015, 3). Share, Play and Zoom in on the World through High–resolution Images. Retrieved from http://www.gigapan.com

Giordano, A., Mele, E., & De Luca, A. (2002). Modelling of historical masonry structures: comparison of different approaches through a case study. *Engineering Structures, 24*, 1057-1069.

Giusti, A. (2000). *The Baptistery of San Giovanni in Florence.* La Mandragora s.r.l.

Grinzato, E., Bison, P. G., & Marinetti, S. (2002). Monitoring of ancient buildings by the thermal method. *Journal of Cultural Heritage, 3*, 21-29.

Grun, A., Remondino, F., & Zhang, L. (2004). Photogrammetric reconstruction of the great Buddha of Bamiyan, Afghanistan. *The Photogrammetric Record, 19*, 177-199.

Guarnieri, A., Vettore, A., El-Hakim, S., & Gonzo, L. (2004). Digital photogrammetry and laser scanning in cultural heritage survey. *The International Archives of the Photogrammetry, Remote Sensing and Spatial Information Sciences, 35*, B5.

Guidi, G., Remondino, F., Russo, M., Menna, F., Rizzi, A., & Ercoli, S. (2009). A multi-resolution methodology for the 3D modeling of large and complex archeological areas. *International Journal of Architectural Computing, 7*, 39-55.

Guidi, G., Russo, M., & Angheleddu, D. (2014). 3D survey and virtual reconstruction of archeological sites. *Digital Applications in Archaeology and Cultural Heritage, 1*, 55-69.

Haddad, N. (2007). Towards creating a dialogue between the specialized technician and non technician users of the 3D laser scanner. *The International Archives of the Photogrammetry, Remote Sensing and Spatial Information Sciences, 36*, C53.

Hartley, R., & Zisserman, A. (2003). *Multiple view geometry in computer vision.* Cambridge university press.

Hess, M., Meyer, D., Hoff, A., Rissolo, D., Guillermo, L. L., & Kuester, F. (2014). Informing Historical Preservation with the Use of Non-destructive Diagnostic Techniques: A Case Study at Ecab, Quintana Roo, Mexico. In *Digital Heritage. Progress in Cultural Heritage: Documentation, Preservation, and Protection* (pp. 659-668). Springer.

Hess, M., Petrovic, V., Yeager, M., & Kuester, F. (2017). Terrestrial laser scanning for the comprehensive structural health assessment of the Baptistery di San Giovanni in Florence, Italy: an integrative methodology for repeatable data acquisition, visualization and analysis. *Structure and Infrastructure Engineering*, 1-17.

Hoehler, M. S., Smith, C. M., Hutchinson, T. C., Wang, X., Meacham, B. J., & Kamath, P. (2017). Behavior of steel-sheathed shear walls subjected to seismic and fire loads. *Fire Safety Journal*.

Huber, D. F., & Hebert, M. (2003). Fully automatic registration of multiple 3D data sets. *Image and Vision Computing, 21*, 637-650.

Huber, D., Akinci, B., Oliver, A. A., Anil, E., Okorn, B. E., & Xiong, X. (2011). Methods for automatically modeling and representing as-built building information models. *Proceedings of the NSF CMMI Research Innovation Conference.*

Ikeuchi, K., Nakazawa, A., Hasegawa, K., & Ohishi, T. (2003). The great Buddha project: Modeling cultural heritage for VR systems through observation. *Proceedings of the 2nd IEEE/ACM International Symposium on Mixed and Augmented Reality*, (p. 7).

Imposa, S. (2010). Infrared thermography and georadar techniques applied to the "Sala delle Nicchie"(Niches Hall) of Palazzo Pitti, Florence (Italy). *Journal of Cultural Heritage, 11*, 259-264.

Kadobayashi, R., Kochi, N., Otani, H., & Furukawa, R. (2004). Comparison and evaluation of laser scanning and photogrammetry and their combined use for digital recording of cultural heritage. *International Archives of the Photogrammetry, Remote Sensing and Spatial Information Sciences, 35*, 401-406.

Kilic, G. (2015). Using advanced NDT for historic buildings: Towards an integrated multidisciplinary health assessment strategy. *Journal of Cultural Heritage, 16*, 526-535.

Kim, C., Kim, H., Park, T., & Kim, M. K. (2010). Applicability of 4D CAD in civil engineering construction: case study of a cable-stayed bridge project. *Journal of Computing in Civil Engineering, 25*, 98-107.

Kong, S. G., Heo, J., Boughorbel, F., Zheng, Y., Abidi, B. R., Koschan, A., . . . Abidi, M. A. (2007). Multiscale fusion of visible and thermal IR images for illumination-invariant face recognition. *International Journal of Computer Vision, 71*, 215-233.

Krotosky, S. J., & Trivedi, M. M. (2007). Mutual information based registration of multimodal stereo videos for person tracking. *Computer Vision and Image Understanding, 106*, 270-287.

Lacanna, G., Ripepe, M., Marchetti, E., Coli, M., & Garzonio, C. A. (2016). Dynamic response of the baptistery of San Giovanni in Florence, Italy, based on ambient vibration test. *Journal of Cultural Heritage, 20*, 632-640.

Laefer, D. F., Truong-Hong, L., Carr, H., & Singh, M. (2014). Crack detection limits in unit based masonry with terrestrial laser scanning. *NDT \& E International, 62*, 66-76.

Leite, F., Akcamete, A., Akinci, B., Atasoy, G., & Kiziltas, S. (2011). Analysis of modeling effort and impact of different levels of detail in building information models. *Automation in Construction, 20*, 601-609.

Lemmens, M. (2011). Terrestrial laser scanning. In *Geo-information* (pp. 101-121). Springer.

Ljungberg, S. A. (1994). Infrared techniques in buildings and structures: operation and maintenance. *Infrared methodology and technology*, 211-252.

Lourenço, P. B., Krakowiak, K. J., Fernandes, F. M., & Ramos, L. F. (2007). Failure analysis of Monastery of Jerónimos, Lisbon: How to learn from sophisticated numerical models. *Engineering Failure Analysis, 14*, 280-300.

Lualdi, M., & Zanzi, L. (2002). GPR investigations to reconstruct the geometry of the wooden structures in historical buildings. *Ninth International Conference on Ground Penetrating Radar, 4758*, pp. 63-68.

Maierhofer, C. (2003). Nondestructive evaluation of concrete infrastructure with ground penetrating radar. *Journal of Materials in Civil Engineering, 15*, 287-297.

Maser, K. R. (1996). Condition assessment of transportation infrastructure using ground-penetrating radar. *Journal of infrastructure systems, 2*, 94-101.

Megahed, N. (2015). Towards a theoretical framework for HBIM approach in historic preservation and management. *International Journal of Architectural Research: ArchNet-IJAR, 9*, 130-147.

Napolitano, R., Hess, M., Coe-Scarff, R., & Glisic, B. (2018). Numerical modeling of crack propagation in masonry structures. *SAHC2018-10th International Conference on Structural Analysis of Historical Constructions.* Cusco, Peru. Preprint.

New House Internet Services B.V. (n.d.). Photo Stitching Software 360 Degree Panorama Image Software: PTGui. Retrieved from http://www.ptgui.com

Olsen, M. J., Kuester, F., Chang, B. J., & Hutchinson, T. C. (2009). Terrestrial laser scanning-based structural damage assessment. *Journal of Computing in Civil Engineering, 24*, 264-272.

Oreni, D., Brumana, R., & Cuca, B. (2012). Towards a methodology for 3D content models: The reconstruction of ancient vaults for maintenance and structural behaviour in the logic of BIM management. *Virtual Systems and Multimedia (VSMM), 2012 18th International Conference on*, (pp. 475-482).

Oreni, D., Brumana, R., Banfi, F., Bertola, L., Barazzetti, L., Cuca, B., . . . Roncoroni, F. (2014). Beyond Crude 3D Models: From Point Clouds to Historical Building Information Modeling via NURBS. *EuroMed*, (pp. 166-175).

Oreni, D., Brumana, R., Della Torre, S., Banfi, F., & Previtali, M. (2014). Survey turned into HBIM: the restoration and the work involved concerning the Basilica di Collemaggio after the earthquake (L'Aquila). *ISPRS Annals of the Photogrammetry, Remote Sensing and Spatial Information Sciences, 2*, 267.

Orlando, L., & Slob, E. (2009). Using multicomponent GPR to monitor cracks in a historical building. *Journal of Applied Geophysics, 67*, 327-334.

Ottoni, F., Blasi, C., Betti, M., & Bartoli, G. (2016). The effectiveness of ancient “hidden” tie rods in masonry dome preservation: San Giovanni in Florence.

Ottoni, F., Coïsson, E., & Blasi, C. (2010). The Crack Pattern in Brunelleschi's Dome in Florence: Damage Evolution from Historical to Modern Monitoring System Analysis. *Advanced Materials Research*, *133*, pp. 53-64.

Pavlidis, G., Koutsoudis, A., Arnaoutoglou, F., Tsioukas, V., & Chamzas, C. (2007). Methods for 3D digitization of cultural heritage. *Journal of cultural heritage, 8*, 93-98.

Pecchioli, M., Corrado, A., & Bardi, L. (1970). *An'insula'In The Third Court Of Palazzo Vecchio In Florence: Identification Of Medieval Pre-existing Structures* (Vol. 16). WIT Press.

Petrovic, V., Gidding, A., Wypych, T., Kuester, F., DeFanti, T. A., & Levy, T. E. (2011). Dealing with archaeology's data avalanche. *Computer*, 56-60.

Petrovic, V., Vanoni, D. J., Richter, A. M., Levy, T. E., & Kuester, F. (2014). Visualizing high resolution three-dimensional and two-dimensional data of cultural heritage sites. *Mediterranean Archaeology and Archaeometry, 14*, 93-100.

Quattrini, R., Malinverni, E. S., Clini, P., Nespeca, R., & Orlietti, E. (2015). From TLS to HBIM. High quality semantically-aware 3D modeling of complex architecture. *The International Archives of Photogrammetry, Remote Sensing and Spatial Information Sciences, 40*, 367.

Reddy, B. V., Lal, R., & Rao, K. S. (2009). Influence of joint thickness and mortar-block elastic properties on the strength and stresses developed in soil-cement block masonry. *Journal of Materials in Civil Engineering, 21*, 535-542.

Richter, A. M., Kuester, F., Levy, T. E., & Najjar, M. (2012). Terrestrial laser scanning (LiDAR) as a means of digital documentation in rescue archaeology: Two examples from the Faynan of Jordan. *Virtual Systems and Multimedia (VSMM), 2012 18th International Conference on*, (pp. 521-524).

Rönnholm, P., Honkavaara, E., Litkey, P., Hyyppä, H., & Hyyppä, J. (2007). Integration of laser scanning and photogrammetry. *International Archives of the Photogrammetry, Remote Sensing and Spatial Information Sciences, 39*, 355-362.

Ruggiero, C., Gallo, A., Lio, A., Zappani, A., Fortunato, G., & Muzzupappa, M. (2012). An Integrated Methodology for the Digitization, Survey and Visualization of Santa Maria Patirion's Church. *International Journal of Heritage in the Digital Era, 1*, 21-26.

Sander, K. A., Olhoeft, G. R., & Lucius, J. E. (1992). Surface and borehole radar monitoring of a DNAPL spill in 3D versus frequency, look angle and time. *Symposium on the Application of Geophysics to Engineering and Environmental Problems 1992*, (pp. 455-469).

Scaioni, M. (2005). Direct georeferencing of TLS in surveying of complex sites. *Proceedings of the ISPRS Working Group, 4*, 22-24.

Shull, P. J. (2002). *Nondestructive evaluation: theory, techniques, and applications.* CRC press.

Solla, M., González-Jorge, H., Álvarez, M. X., & Arias, P. (2012). Application of non-destructive geomatic techniques and FDTD modeling to metrical analysis of stone blocks in a masonry wall. *Construction and Building Materials, 36*, 14-19.

Son, M., & Cording, E. J. (2005). Estimation of building damage due to excavation-induced ground movements. *Journal of Geotechnical and Geoenvironmental Engineering, 131*, 162-177.

Stang, A. H., Parsons, D. E., & McBurney, J. W. (1929). Compressive strength of clay brick walls. *Bureau of Standards Journal of Research, 3*, 507-71.

Tang, P., Huber, D., Akinci, B., Lipman, R., & Lytle, A. (2010). Automatic reconstruction of as-built building information models from laser-scanned point clouds: A review of related techniques. *Automation in Construction, 19*, 829-843.

Titman, D. J. (2001). Applications of thermography in non-destructive testing of structures. *NDT \& E International, 34*, 149-154.

Toet, A., IJspeert, J. K., Waxman, A. M., & Aguilar, M. (1997). Fusion of visible and thermal imagery improves situational awareness. *Displays, 18*, 85-95.

US, G. S. (2009). Gsa Bim Guide for 3D Imaging. *Washington, DC: US General Services Administration. http://www. gsa. gov/graphics/pbs/GSA_BIM_Guide_Series_03. pdf*.

Valero, E., Bosché, F., Forster, A., Wilson, L., & Leslie, A. (2017). . Evaluation of Historic Masonry: Towards Greater Objectivity & Efficiency. In *Heritage building information modelling* (pp. 75-101). Taylor and Francis London.

Valluzzi, M. R. (2007). On the vulnerability of historical masonry structures: analysis and mitigation. *Materials and structures, 40*, 723-743.

VanOcker, D. A., Johnson, E. M., & Marcotte, T. D. (2009, 1). The Identification of Corrosion-Related Damage from Cramp Anchors in a Limestone-Clad Building Façade Using NDE Techniques. In *Repair, Retrofit and Inspection of Building Exterior Wall Systems* (pp. 35--35--12). ASTM International. doi:10.1520/stp47763s

Volk, R., Stengel, J., & Schultmann, F. (2014). Building Information Modeling (BIM) for existing buildings—Literature review and future needs. *Automation in construction, 38*, 109-127.

Vollmer, M., & Mollmann, K.-P. (2010). *Infrared thermal imaging: fundamentals, research and applications.* John Wiley & Sons.

Wang, X., Hutchinson, T. C., Hegemier, G., Gunisetty, S., Kamath, P., & Meacham, B. (2016). Earthquake and fire performance of a mid-rise cold-formed steel framed building--test program and test results: rapid release (preliminary) report (SSRP-2016/07). *San Diego, CA*.

Westoby, M. J., Brasington, J., Glasser, N. F., Hambrey, M. J., & Reynolds, J. M. (2012). 'Structure-from-Motion'photogrammetry: A low-cost, effective tool for geoscience applications. *Geomorphology, 179*, 300-314.

Williams, K. (1994). The sacred cut revisited: the pavement of the Baptistery of San Giovanni, Florence. *The Mathematical Intelligencer, 16*, 18-24.

Wittich, C. E., Hutchinson, T. C., Lo, E., Meyer, D., & Kuester, F. (2014). The South Napa Earthquake of August 24, 2014: drone-based aerial and ground-based LiDAR imaging survey. *Structural Systems Research Project Report: SSRP, 9*.

Woo, J., Wilsmann, J., & Kang, D. (2010). Use of as-built building information modeling. *Construction Research Congress 2010: Innovation for Reshaping Construction Practice*, (pp. 538-548).

Wood, R. L., Hutchinson, T. C., Wittich, C. E., & Kuester, F. (2012). Characterizing Cracks in the Frescoes of Sala degli Elementi within Florence's Palazzo Vecchio. *Euro-Mediterranean Conference*, (pp. 776-783).

Yamaoka, S., Doerr, K.-U., & Kuester, F. (2011). Visualization of high-resolution image collections on large tiled display walls. *Future Generation Computer Systems, 27*, 498-505.

Yastikli, N. (2007). Documentation of cultural heritage using digital photogrammetry and laser scanning. *Journal of Cultural Heritage, 8*, 423-427.

Yilmaz, H. M., Yakar, M., Gulec, S. A., & Dulgerler, O. N. (2007). Importance of digital close-range photogrammetry in documentation of cultural heritage. *Journal of Cultural Heritage, 8*, 428-433.

Zavalis, R., Jonaitis, B., & Lourenço, P. B. (2014). Analysis of bed joint influence on masonry modulus of elasticity. *9th International Masonry Conference*, (pp. 1-11).

Appendix A

This appendix includes details as to the exact creation of the presented data fusion. Included here are:

- JavaScript code for the point cloud classification “smart brush”
- Example metadata file for thermal image mosaics
- Template parameters for thermal to visible mosaic fusion
- Alignment transformations and error calculations for 3D data fusion
- Example workflow of aligning 2D and 3D data using the information model

A.1 JavaScript code for “smart brush function

```
function wmon(a)
{
 jsend("wmon", a);
}

function go_expansion()
{
 var opt = [30, 3, 0.75];
 var onames = ["ccount", "sdmul", "nthresh"];

 function upcfg(x)
 {
  if(!x || !x.m || !x.m.data) return;
  opt = x.m.data[0];
  print("\nex_op: " + jstring(opt));
 }

 function init()
 {
  var c = [];
  for(var i in onames)
  {
   c.push({n:onames[i], numeric: '0[.]00', edit:true});
  }
  jbind("exbru", upcfg);
  jsend("spread", {op: "new", name: "ex_op", onchange: "exbru", cols: c, data: [opt]});
 }
 init();
```

```
 jsend("spread", {op: "new", name:"mike", cols: ["text",{n:"mean", numeric: '0[.]00'}
,{n:"sd", numeric: '0[.]000'} ]});
 jsend("spread", {op: "new", name:"mike2", cols: [{n:"red", numeric: '0[.]00'} ]});
 jsend('jsplots',{op:'new', name:'mike_plot'});
 function line(p1,p2,w,c) {jsend('mike_plot',{op:'line', data: {p1: p1, p2: p2, w: w, c:
c}});}

 var bins = new Float32Array(32);
 var my=this;
 var nom = new Float64Array(3);
 var ns = new Float64Array(3);

function brush_b(nf, jk)
 {
  print("\n(comb op " + jk.op + ")\n");
  if(jk.length<5) return;
  var psgn = 0;
  if(jk.op==-2) psgn = -1;  // mark
  else if(jk.op==-3) psgn = 1;  // unmark
  var stag = parseFloat(liveVars.get('labeltag').get()); // the selected tag (number in
bubble)
  if(stag<0) return;
  jk.seek(1);
  hh.init(jk);
  hh.state_push(); // undoer history push

  var pp = jk.p; // raw position (untransformed)
  var pt = jk.pos;
  var cc = jk.c;
  var nn = jk.n;
  var aa = jk.a; // can use as per-point scratch space (aux);
  var tt = jk.tag;
  var sz = jk.length;

  var sum = 0;
  var sum2 = 0;
  var sumg = 0;
  var sum2g = 0;
  var sumb = 0;
  var sum2b = 0;
  var sumBW = 0;
  var sum2BW = 0;
  var Dmax = 0;
  var sumD=0;
  var sum2D=0;
  var dist;
  var s = 0;
  var t = 0;
  var u = 0;
```

```
    var BW = 0;
    var i, r, g, b, ri, gi, bi, bwi, grayscale;

    var sumnx = 0;
    var sum2nx = 0;
    var sumny = 0;
    var sum2ny = 0;
    var sumnz = 0;
    var sum2nz = 0;
    var nx, ny, nz, nxs, nys, nzs, distn, distsdn;
    var sz2 = Math.min(opt[0],sz);

////////////////Loop to sum variables in brush/////////////////////////////////////////
    for(i=0; i<sz2; ++i)
    {
     jk.seek(i);
     if(i===0)
     {
       ri= (cc[0]);
       gi = (cc[1]);
       bi = (cc[2]);
     }
     s = (cc[0]);
     sum += s;
     sum2 += s*s;

     t = (cc[1]);
     sumg += t;
     sum2g += t*t;

     u = (cc[2]);
     sumb += u;
     sum2b += u*u;

     BW = (s + t + u) / 3;
     sumBW += BW;
     sum2BW += BW*BW;

     ////////// NORMALS ////////////////////
     nx = nn[0];
     sumnx += nx;
     sum2nx += nx*nx;

     ny = nn[1];
     sumny += ny;
     sum2ny += ny*ny;
     nz = nn[2];
     sumnz += nz;
     sum2nz += nz*nz;
```

```
    }
////////////////End Loop to sum variables in brush//////////////////////////////////////
    var ic = 1/sz2;
    var meanr = sum*ic;
    var sdr = sum2*ic - meanr*meanr;
    sdr = Math.sqrt(sdr);

    var meang = sumg*ic;
    var sdg = sum2g*ic - meang*meang;
    sdg = Math.sqrt(sdg);

    var meanb = sumb*ic;
    var sdb = sum2b*ic - meanb*meanb;
    sdb = Math.sqrt(sdb);

    var meanBW = sumBW*ic;
    var sdBW = sum2BW*ic - meanBW*meanBW;
    sdBW = Math.sqrt(sdBW);

    bwi=(ri + gi + bi) / 3;

////////////////Finding average normals//////////////////////////////////////
    var meannx = sumnx*ic;
    var sdnx = sum2nx*ic - meannx*meannx;
    sdnx = Math.sqrt(sdnx);

    var meanny = sumny*ic;
    var sdny = sum2ny*ic - meanny*meanny;
    sdny = Math.sqrt(sdny);

    var meannz = sumnz*ic;
    var sdnz = sum2nz*ic - meannz*meannz;
    sdnz = Math.sqrt(sdnz);

    distsdn=Math.sqrt((meannx-sdnx)*(meannx-sdnx)+(meanny-sdny)*(meanny-
sdny)+(meannz-                    sdnz)*(meannz-sdnz));

    /** /
    var                                meannL                                =
Math.sqrt((meannx)*(meannx)+(meanny)*(meanny)+(meannz)*(meannz));
    meannx=meannx/meannL;
    meanny=meanny/meannL;
    meannz=meannz/meannL;
    /**/
    nom[0] = meannx;
    nom[1] = meanny;
    nom[2] = meannz;
    NN.normalize(nom);
```

```
////////////////End Finding average normals/////////////////////////////////////////
   if(true)
   {
     ic = 1/sz;
    ////////////////Measuring Distances/////////////////////////////////////////
    for(i=0; i<sz; ++i)
    {
      jk.seek(i);
      r = Math.abs(cc[0]);
      g = Math.abs(cc[1]);
      b = Math.abs(cc[2]);
      dist=Math.sqrt((meanr-r)*(meanr-r)+(meang-g)*(meang-g)+(meanb-b)*(meanb-b));
      sumD += dist;
      sum2D += dist*dist;
      if(Dmax<dist) Dmax=dist;
    }
   }
   var meanD = sumD*ic;
   var sdD = sum2D*ic - meanD*meanD;

   sdD = Math.sqrt(sdD);

   ////////////////////End Meausring Distances/////////////////////////////////////////
   var disti;
   var Ndot=0;
   var nL;
   var thr = meanr + sdr;
   var thr2 = 220;
   var thrmult =1.5;
   var bs = bins.length/(15*sdr);
   var bsm = 0.5*bins.length;

   jsend("spread", {op: "clear", name:"mike2"});

   for(i=0; i<sz; ++i)
   {
    jk.seek(i);
    r = (cc[0]); // red? |pp[3]| i size
    g = (cc[1]);
    b = (cc[2]);
    grayscale = (r + g + b) / 3;

    dist=Math.sqrt((meanr-r)*(meanr-r)+(meang-g)*(meang-g)+(meanb-b)*(meanb-b));

    ns[0] = nn[0];
    ns[1] = nn[1];
    ns[2] = nn[2];
    NN.normalize(ns);
```

```
    /** /
    meannL = Math.sqrt((nxs)*(nxs)+(nys)*(nys)+(nzs)*(nzs));
    nxs=nxs/meannL;
    nys=nys/meannL;
    nzs=nzs/meannL;

    distn=Math.sqrt((meannx-nxs)*(meannx-nxs)+(meanny-nys)*(meanny-
nys)+(meannz-nzs)*(meannz-nzs));
    Ndot=meannx*nxs+meanny*nys+meannz*nzs;
    /**/

    Ndot = nom[0]*ns[0] + nom[1]*ns[1] + nom[2]*ns[2];

    if(dist<opt[1]*sdD && Ndot > opt[2]) hh.set_tag(jk, pp, tt, psgn, stag);
    else break;
    bins[Math.floor((s-meanr)*bs + bsm)] += 1;
   }

   jsend('mike_plot',{op:'clear'});

   var dx = 2/bins.length;
   var dy = 1/sz;
   var xx = -1, y4=-0.5, yy=-0.5, y2=0;

   for(i in bins)
   {
    //if(bins[i] !== 0)
    {
     y2 = -0.5+dy*bins[i];
     line([xx-dx,yy,-1],[xx,y2,-1], 0.003, [0.8,1,0,0.5]);
     yy = y2;
    }
    xx += dx;
    bins[i] = 0;
   }
   xx = -1 + dx * (sdr*bs+bsm);
   line([xx,-0.55,-1],[xx,0.5,-1], 0.002, [0.8,0.5,0,0.25]);

   jsend("spread", {op: "push", name:"mike", row:[jk.file, meanr, sdr]});
   wmon("\n(mean red: " + meanr + ") ");
   jsend('mike_plot',{op:'draw'});
  }
  brush.add('mikeexp', brush_b, 'mikeexp', 'expand\\ brush');
}
go_expansion();
```

A.2 Example metadata file for thermal image mosaics

Below is an example of a metadata file that is generated when the thermal image mosaics are acquired. The first line is the file base name, followed by the acquisition direction and how many rows and columns are needed to span the defined acquisition area. Finally, for each image is listed its image number, distance to the surface of the surveyed structure, pan and tilt angles of the robotic platform.

```
Elem_Int_W1
LtoR
8 Columns and 8 Rows
Img#  DIST(m)   PAN   TILT
   1 7.642300    120    114
   2 10.633100    120    120
   3 11.957800    120    126
   4 11.755700    120    132
   5 11.586300    120    138
   6 11.522600    120    144
   7 11.405600    120    150
   8 7.775000    120    156
   9 9.473000    110    114
  10 10.721100    110    120
  11 11.179700    110    126
  12 10.953700    110    132
  13 10.727400    110    138
  14 10.291200    110    144
  15 10.386200    110    150
  16 7.809600    110    156
  17 9.918200    100    114
  18 9.683900    100    120
  19 10.134000    100    126
  20 9.914500    100    132
  21 9.783200    100    138
  22 9.756200    100    144
  23 9.829500    100    150
  24 7.902300    100    156
  25 9.354300     90    114
  26 9.094500     90    120
  27 9.502900     90    126
  28 9.309500     90    132
  29 9.180500     90    138
  30 9.156200     90    144
  31 9.218900     90    150
  32 7.999800     90    156
```

```
33 9.054300     80    114
34 9.110100     80    120
35 9.230400     80    126
36 9.052700     80    132
37 8.927000     80    138
38 8.645600     80    144
39 8.950500     80    150
40 8.112200     80    156
41 9.031400     70    114
42 9.096100     70    120
43 9.296500     70    126
44 9.105200     70    132
45 8.973700     70    138
46 8.947100     70    144
47 9.012000     70    150
48 8.193200     70    156
49 9.083300     60    114
50 9.182200     60    120
51 9.680200     60    126
52 9.483900     60    132
53 9.346500     60    138
54 9.436200     60    144
55 9.506400     60    150
56 8.175200     60    156
57 7.495300     50    114
58 8.064400     50    120
59 7.731900     50    126
60 7.576200     50    132
61 7.452000     50    138
62 7.393700     50    144
63 7.416200     50    150
64 7.501800     50    156
```

A.3 Template parameters for thermal to visible mosaic fusion

#-imgfile 1920 1080 "..\SFM\Left01_01.jpg"

#-metadata -1 -1 -1 0000-00-00T00:00:00 3*8 0 -1 -1 -1 * * * curve -1 * M

#-viewpoint 0 0 0 0 0

#-exposureparams 0 0 0 0

o f0 y-23.11509696738952 r1.726534581251968 p12.05188091681319 v=0 a=0 b=0 c=0 d=0 e=0 g=0 t=0

#-imgfile 1920 1080 "..\SFM\Left02_02.jpg"

#-metadata -1 -1 -1 0000-00-00T00:00:00 3*8 0 -1 -1 -1 * * * curve -1 * M

#-viewpoint 0 0 0 0 0

#-exposureparams 0 0 0 0

o f0 y-23.03745774232408 r1.782272713875386 p9.714518221782157 v=0 a=0 b=0 c=0 d=0 e=0 g=0 t=0

#-imgfile 1920 1080 "..\SFM\Left03_01.jpg"

#-metadata -1 -1 -1 0000-00-00T00:00:00 3*8 0 -1 -1 -1 * * * curve -1 * M

#-viewpoint 0 0 0 0 0

#-exposureparams 0 0 0 0

o f0 y-22.94231353210375 r1.84744806812688 p5.208061295231261 v=0 a=0 b=0 c=0 d=0 e=0 g=0 t=0

#-imgfile 1920 1080 "..\SFM\Left04_03.jpg"

#-metadata -1 -1 -1 0000-00-00T00:00:00 3*8 0 -1 -1 -1 * * * curve -1 * M

#-viewpoint 0 0 0 0 0

#-exposureparams 0 0 0 0

o f0 y-22.80406736958881 r1.895683701507153 p-1.849598190391504 v=0 a=0 b=0 c=0 d=0 e=0 g=0 t=0

#-imgfile 1920 1080 "..\SFM\Left05_01.jpg"

#-metadata -1 -1 -1 0000-00-00T00:00:00 3*8 0 -1 -1 -1 * * * curve -1 * M

#-viewpoint 0 0 0 0 0

#-exposureparams 0 0 0 0

o f0 y-22.64756767667737 r1.949040720641364 p-10.5154805627505 v=0 a=0 b=0 c=0 d=0 e=0 g=0 t=0

#-imgfile 1920 1080 "..\SFM\Left06_03.jpg"

#-metadata -1 -1 -1 0000-00-00T00:00:00 3*8 0 -1 -1 -1 * * * curve -1 * M

#-viewpoint 0 0 0 0 0

#-exposureparams 0 0 0 0

o f0 y-22.64685932894741 r1.938011313128158 p-10.51223044560697 v=0 a=0 b=0 c=0 d=0 e=0 g=0 t=0

#-imgfile 1920 1080 "..\SFM\Left07_01.jpg"

#-metadata -1 -1 -1 0000-00-00T00:00:00 3*8 0 -1 -1 -1 * * * curve -1 * M

#-viewpoint 0 0 0 0 0

#-exposureparams 0 0 0 0

o f0 y-22.5372283434161 r1.988570169325044 p-16.12617377749552 v=0 a=0 b=0 c=0 d=0 e=0 g=0 t=0

#-imgfile 1920 1080 "..\SFM\Left08_03.jpg"

#-metadata -1 -1 -1 0000-00-00T00:00:00 3*8 0 -1 -1 -1 * * * curve -1 * M

#-viewpoint 0 0 0 0 0

#-exposureparams 0 0 0 0

o f0 y-9.968697678210788 r0.9796227854768063 p-15.81834337737749 v=0 a=0 b=0 c=0 d=0 e=0 g=0 t=0

#-imgfile 1920 1080 "..\SFM\Left09_01.jpg"

#-metadata -1 -1 -1 0000-00-00T00:00:00 3*8 0 -1 -1 -1 * * * curve -1 * M

#-viewpoint 0 0 0 0 0

#-exposureparams 0 0 0 0

o f0 y-9.9601265490071 r0.9796415260109086 p-15.82223008987401 v=0 a=0 b=0 c=0 d=0 e=0 g=0 t=0

#-imgfile 1920 1080 "..\SFM\Left10_03.jpg"

#-metadata -1 -1 -1 0000-00-00T00:00:00 3*8 0 -1 -1 -1 * * * curve -1 * M

#-viewpoint 0 0 0 0 0

#-exposureparams 0 0 0 0

o f0 y-10.17517230446876 r0.9463855099165244 p-10.49635952068599 v=0 a=0 b=0 c=0 d=0 e=0 g=0 t=0

#-imgfile 1920 1080 "..\SFM\Left11_01.jpg"

#-metadata -1 -1 -1 0000-00-00T00:00:00 3*8 0 -1 -1 -1 * * * curve -1 * M

#-viewpoint 0 0 0 0 0

#-exposureparams 0 0 0 0

o f0 y-10.30147772605704 r0.9903146632209996 p-6.84109609258357 v=0 a=0 b=0 c=0 d=0 e=0 g=0 t=0

#-imgfile 1920 1080 "..\SFM\Left13_01.jpg"

#-metadata -1 -1 -1 0000-00-00T00:00:00 3*8 0 -1 -1 -1 * * * curve -1 * M

#-viewpoint 0 0 0 0 0

#-exposureparams 0 0 0 0

o f0 y-10.66263532062837 r0.9696681937770677 p2.770428804893669 v=0 a=0 b=0 c=0 d=0 e=0 g=0 t=0

#-imgfile 1920 1080 "..\SFM\Left14_03.jpg"

#-metadata -1 -1 -1 0000-00-00T00:00:00 3*8 0 -1 -1 -1 * * * curve -1 * M

#-viewpoint 0 0 0 0 0

#-exposureparams 0 0 0 0

o f0 y-10.83632849280539 r0.931253686591873 p7.454499460470657 v=0 a=0 b=0 c=0 d=0 e=0 g=0 t=0

#-imgfile 1920 1080 "..\SFM\Left15_01.jpg"

#-metadata -1 -1 -1 0000-00-00T00:00:00 3*8 0 -1 -1 -1 * * * curve -1 * M

#-viewpoint 0 0 0 0 0

#-exposureparams 0 0 0 0

o f0 y-10.99992383631434 r0.8712468679748611 p12.17780805168343 v=0 a=0 b=0 c=0 d=0 e=0 g=0 t=0

#-imgfile 1920 1080 "..\SFM\Left16_03.jpg"

#-metadata -1 -1 -1 0000-00-00T00:00:00 3*8 0 -1 -1 -1 * * * curve -1 * M

#-viewpoint 0 0 0 0 0

#-exposureparams 0 0 0 0

o f0 y-0.6249952635842533 r0.2942236659039565 p12.71210935947588 v=0 a=0 b=0 c=0 d=0 e=0 g=0 t=0

#-imgfile 1920 1080 "..\SFM\Left17_01.jpg"

#-metadata -1 -1 -1 0000-00-00T00:00:00 3*8 0 -1 -1 -1 * * * curve -1 * M

#-viewpoint 0 0 0 0 0

#-exposureparams 0 0 0 0

o f0 y-0.3874486358118929 r0.295095398377299 p8.460054542238282 v=0 a=0 b=0 c=0 d=0 e=0 g=0 t=0

#-imgfile 1920 1080 "..\SFM\Left18_03.jpg"

#-metadata -1 -1 -1 0000-00-00T00:00:00 3*8 0 -1 -1 -1 * * * curve -1 * M

#-viewpoint 0 0 0 0 0

#-exposureparams 0 0 0 0

o f0 y-0.2163870526184724 r0.3353627466681814 p5.030495754038668 v=0 a=0 b=0 c=0 d=0 e=0 g=0 t=0

#-imgfile 1920 1080 "..\SFM\Left19_01.jpg"

#-metadata -1 -1 -1 0000-00-00T00:00:00 3*8 0 -1 -1 -1 * * * curve -1 * M

#-viewpoint 0 0 0 0 0

#-exposureparams 0 0 0 0

o f0 y0.04309810307466933 r0.3138745175145346 p-0.1304201702419618 v=0 a=0 b=0 c=0 d=0 e=0 g=0 t=0

#-imgfile 1920 1080 "..\SFM\Left20_03.jpg"

#-metadata -1 -1 -1 0000-00-00T00:00:00 3*8 0 -1 -1 -1 * * * curve -1 * M

#-viewpoint 0 0 0 0 0

#-exposureparams 0 0 0 0

o f0 y0.3278990717392105 r0.2954232133637049 p-5.570702841446632 v=0 a=0 b=0 c=0 d=0 e=0 g=0 t=0

#-imgfile 1920 1080 "..\SFM\Left21_01.jpg"

#-metadata -1 -1 -1 0000-00-00T00:00:00 3*8 0 -1 -1 -1 * * * curve -1 * M

#-viewpoint 0 0 0 0 0

#-exposureparams 0 0 0 0

o f0 y0.5811859280325962 r0.2644895874393853 p-10.32547194105993 v=0 a=0 b=0 c=0 d=0 e=0 g=0 t=0

#-imgfile 1920 1080 "..\SFM\Left22_03.jpg"

#-metadata -1 -1 -1 0000-00-00T00:00:00 3*8 0 -1 -1 -1 * * * curve -1 * M

#-viewpoint 0 0 0 0 0

#-exposureparams 0 0 0 0

o f0 y0.8155689203335896 r0.2189037503636371 p-14.92595138350822 v=0 a=0 b=0 c=0 d=0 e=0 g=0 t=0

#-imgfile 1920 1080 "..\SFM\Left23_01.jpg"

#-metadata -1 -1 -1 0000-00-00T00:00:00 3*8 0 -1 -1 -1 * * * curve -1 * M

#-viewpoint 0 0 0 0 0

#-exposureparams 0 0 0 0

o f0 y8.949726922923247 r-0.2018025770816507 p-14.46204091983609 v=0 a=0 b=0 c=0 d=0 e=0 g=0 t=0

#-imgfile 1920 1080 "..\SFM\Left24_03.jpg"

#-metadata -1 -1 -1 0000-00-00T00:00:00 3*8 0 -1 -1 -1 * * * curve -1 * M

#-viewpoint 0 0 0 0 0

#-exposureparams 0 0 0 0

o f0 y8.745780890800972 r-0.1426626580490904 p-11.27200134974171 v=0 a=0 b=0 c=0 d=0 e=0 g=0 t=0

#-imgfile 1920 1080 "..\SFM\Left25_01.jpg"

#-metadata -1 -1 -1 0000-00-00T00:00:00 3*8 0 -1 -1 -1 * * * curve -1 * M

#-viewpoint 0 0 0 0 0

#-exposureparams 0 0 0 0

o f0 y8.529597062823541 r-0.1144402588467699 p-7.660252440899456 v=0 a=0 b=0 c=0 d=0 e=0 g=0 t=0

#-imgfile 1920 1080 "..\SFM\Left26_03.jpg"

#-metadata -1 -1 -1 0000-00-00T00:00:00 3*8 0 -1 -1 -1 * * * curve -1 * M

#-viewpoint 0 0 0 0 0

#-exposureparams 0 0 0 0

o f0 y8.350494125623158 r-0.1046651594944308 p-4.826282840437585 v=0 a=0 b=0 c=0 d=0 e=0 g=0 t=0

#-imgfile 1920 1080 "..\SFM\Left27_01.jpg"

#-metadata -1 -1 -1 0000-00-00T00:00:00 3*8 0 -1 -1 -1 * * * curve -1 * M

#-viewpoint 0 0 0 0 0

#-exposureparams 0 0 0 0

o f0 y8.092051890660315 r-0.06168393668332328 p-0.569124278740702 v=0 a=0 b=0 c=0 d=0 e=0 g=0 t=0

#-imgfile 1920 1080 "..\SFM\Left28_03.jpg"

#-metadata -1 -1 -1 0000-00-00T00:00:00 3*8 0 -1 -1 -1 * * * curve -1 * M

#-viewpoint 0 0 0 0 0

#-exposureparams 0 0 0 0

o f0 y7.854378884610213 r-0.03079992034614065 p3.468640744239053 v=0 a=0 b=0 c=0 d=0 e=0 g=0 t=0

#-imgfile 1920 1080 "..\SFM\Left29_01.jpg"

#-metadata -1 -1 -1 0000-00-00T00:00:00 3*8 0 -1 -1 -1 * * * curve -1 * M

#-viewpoint 0 0 0 0 0

#-exposureparams 0 0 0 0

o f0 y7.444917048557556 r-0.0872646617274313 p10.57977269009456 v=0 a=0 b=0 c=0 d=0 e=0 g=0 t=0

#-imgfile 1920 1080 "..\SFM\Left30_03.jpg"

#-metadata -1 -1 -1 0000-00-00T00:00:00 3*8 0 -1 -1 -1 * * * curve -1 * M

#-viewpoint 0 0 0 0 0

#-exposureparams 0 0 0 0

o f0 y15.33626272160157 r-0.4984958517306666 p13.20268739638843 v=0 a=0 b=0 c=0 d=0 e=0 g=0 t=0

#-imgfile 1920 1080 "..\SFM\Left31_01.jpg"

#-metadata -1 -1 -1 0000-00-00T00:00:00 3*8 0 -1 -1 -1 * * * curve -1 * M

#-viewpoint 0 0 0 0 0

#-exposureparams 0 0 0 0

o f0 y15.60303019363644 r-0.477256353067844 p8.599442487534731 v=0 a=0 b=0 c=0 d=0 e=0 g=0 t=0

#-imgfile 1920 1080 "..\SFM\Left32_02.jpg"

#-metadata -1 -1 -1 0000-00-00T00:00:00 3*8 0 -1 -1 -1 * * * curve -1 * M

#-viewpoint 0 0 0 0 0

#-exposureparams 0 0 0 0

o f0 y15.87545443879534 r-0.4615036547714624 p4.429835959213676 v=0 a=0 b=0 c=0 d=0 e=0 g=0 t=0

#-imgfile 1920 1080 "..\SFM\Left33_01.jpg"

#-metadata -1 -1 -1 0000-00-00T00:00:00 3*8 0 -1 -1 -1 * * * curve -1 * M

#-viewpoint 0 0 0 0 0

#-exposureparams 0 0 0 0

o f0 y16.15386328093737 r-0.4877700935120117 p0.2689881563366328 v=0 a=0 b=0 c=0 d=0 e=0 g=0 t=0

#-imgfile 1920 1080 "..\SFM\Left34_03.jpg"

#-metadata -1 -1 -1 0000-00-00T00:00:00 3*8 0 -1 -1 -1 * * * curve -1 * M

#-viewpoint 0 0 0 0 0

#-exposureparams 0 0 0 0

o f0 y16.53369125381607 r-0.5168746236421384 p-5.24350925605745 v=0 a=0 b=0 c=0 d=0 e=0 g=0 t=0

#-imgfile 1920 1080 "..\SFM\Left35_01.jpg"

#-metadata -1 -1 -1 0000-00-00T00:00:00 3*8 0 -1 -1 -1 * * * curve -1 * M

#-viewpoint 0 0 0 0 0

#-exposureparams 0 0 0 0

o f0 y16.88980198626197 r-0.5422771949207572 p-10.44840765604783 v=0 a=0 b=0 c=0 d=0 e=0 g=0 t=0

#-imgfile 1920 1080 "..\SFM\Left36_03.jpg"

#-metadata -1 -1 -1 0000-00-00T00:00:00 3*8 0 -1 -1 -1 * * * curve -1 * M

#-viewpoint 0 0 0 0 0

#-exposureparams 0 0 0 0

o f0 y17.17948908160014 r-0.6277042070708774 p-14.51923877217138 v=0 a=0 b=0 c=0 d=0 e=0 g=0 t=0

#-imgfile 1920 1080 "..\SFM\Left37_01.jpg"

#-metadata -1 -1 -1 0000-00-00T00:00:00 3*8 0 -1 -1 -1 * * * curve -1 * M

#-viewpoint 0 0 0 0 0

#-exposureparams 0 0 0 0

o f0 y17.36751775906583 r-0.6703479491154383 p-17.25310538563144 v=0 a=0 b=0 c=0 d=0 e=0 g=0 t=0

#-imgfile 1920 1080 "..\SFM\Left38_03.jpg"

#-metadata -1 -1 -1 0000-00-00T00:00:00 3*8 0 -1 -1 -1 * * * curve -1 * M

#-viewpoint 0 0 0 0 0

#-exposureparams 0 0 0 0

o f0 y25.58493363801921 r-0.9131952420709979 p-16.73735552884796 v=0 a=0 b=0 c=0 d=0 e=0 g=0 t=0

#-imgfile 1920 1080 "..\SFM\Left40_03.jpg"

#-metadata -1 -1 -1 0000-00-00T00:00:00 3*8 0 -1 -1 -1 * * * curve -1 * M

#-viewpoint 0 0 0 0 0

#-exposureparams 0 0 0 0

o f0 y24.96290852110656 r-0.7745743265745375 p-8.499812447569184 v=0 a=0 b=0 c=0 d=0 e=0 g=0 t=0

#-imgfile 1920 1080 "..\SFM\Left41_02.jpg"

#-metadata -1 -1 -1 0000-00-00T00:00:00 3*8 0 -1 -1 -1 * * * curve -1 * M

#-viewpoint 0 0 0 0 0

#-exposureparams 0 0 0 0

o f0 y24.58011340207182 r-0.7867702637241223 p-3.564014023912961 v=0 a=0 b=0 c=0 d=0 e=0 g=0 t=0

#-imgfile 1920 1080 "..\SFM\Left42_03.jpg"

#-metadata -1 -1 -1 0000-00-00T00:00:00 3*8 0 -1 -1 -1 * * * curve -1 * M

#-viewpoint 0 0 0 0 0

#-exposureparams 0 0 0 0

o f0 y24.21848773714103 r-0.7596441768724276 p1.245497562103964 v=0 a=0 b=0 c=0 d=0 e=0 g=0 t=0

#-imgfile 1920 1080 "..\SFM\Left44_03.jpg"

#-metadata -1 -1 -1 0000-00-00T00:00:00 3*8 0 -1 -1 -1 * * * curve -1 * M

#-viewpoint 0 0 0 0 0

#-exposureparams 0 0 0 0

o f0 y23.9017640061893 r-0.7201376001849553 p5.644040804366966 v=0 a=0 b=0 c=0 d=0 e=0 g=0 t=0

#-imgfile 1920 1080 "..\SFM\Left45_01.jpg"

#-metadata -1 -1 -1 0000-00-00T00:00:00 3*8 0 -1 -1 -1 * * * curve -1 * M

#-viewpoint 0 0 0 0 0

#-exposureparams 0 0 0 0

o f0 y23.9065012339552 r-0.7223006697804806 p5.65197072705422 v=0 a=0 b=0 c=0 d=0 e=0 g=0 t=0

#-imgfile 1920 1080 "..\SFM\Left46_02.jpg"

#-metadata -1 -1 -1 0000-00-00T00:00:00 3*8 0 -1 -1 -1 * * * curve -1 * M

#-viewpoint 0 0 0 0 0

#-exposureparams 0 0 0 0

o f0 y23.60150048067152 r-0.7369021544339205 p9.99167544870366 v=0 a=0 b=0 c=0 d=0 e=0 g=0 t=0

#-imgfile 1920 1080 "..\SFM\Left47_01.jpg"

#-metadata -1 -1 -1 0000-00-00T00:00:00 3*8 0 -1 -1 -1 * * * curve -1 * M

#-viewpoint 0 0 0 0 0

#-exposureparams 0 0 0 0

o f0 y23.34965273403185 r-0.8029400340232087 p13.67930649139993 v=0 a=0 b=0 c=0 d=0 e=0 g=0 t=0

A.4 Alignment transformations for 3D data fusion

Below are the details for the 3D alignment of the TLS and SfM datasets for the site of Ecab in Mexico. The alignment is computing the 3D transformations using an Iterative Closest Point (ICP) algorithm which minimizes the root mean square (RMS) error, where d_i is the distance between each point in the aligned dataset with the closest point in the reference dataset.

$$RMS = \sqrt{\frac{\sum_{i=1}^{N}(d_i)^2}{N}}$$

The goal of this process is to align three sets of multimodal, multi-resolution data: 1) TLS 2) ground based SfM 3) aerial SfM. The resulting model contains the geometric accuracy of the TLS data, photorealism of SfM and the relative location of the two buildings in their global context utilizing aerial SfM.

- Aerial SfM data to Casa Cural TLS transformation

```
Final RMS: 0.12818
---------------
Transformation matrix
-4.073  -23.513 3.002   -62.863
-23.686 4.156   0.415   38.048
-0.925  -2.887  -23.860 407.523
0.000   0.000   0.000   1.000
---------------
```

- Church TLS to Aerial SfM transformation (no scaling)

```
Final RMS: 0.807425
---------------
Transformation matrix
0.998   -0.010  -0.062  77.383
0.008   0.999   -0.032  196.906
0.062   0.032   0.998   -11.875
0.000   0.000   0.000   1.000
---------------
```

- Ground based SfM data to Casa Cural TLS transformation

Final RMS: 0.0514328

Transformation matrix
0.098 0.017 -0.242 192.837
0.242 -0.010 0.098 255.839
-0.003 -0.261 -0.020 -1.306
0.000 0.000 0.000 1.000

A.5 Example workflow of aligning 2D and 3D data using the information model

This section walks through the alignment of 2D thermal image data (Figure A.1) to the geometric data in the information model for the study of Palazzo Vecchio in Florence. The goal is that this workflow will help others to repeat a similar process in applications in other projects.

Example workflow of aligning 2D and 3D data using the information model:

Figure A.1 High-resolution thermal image mosaic of South Exterior wall of Palazzo Vecchio.

Figure A.2 Virtual camera position within the Palazzo Vecchio point cloud model.

The virtual camera position shown in Figure A.2 is close to where the thermal images were originally taken. Extracted from this virtual camera are the camera projection matrix, position, target vector (where the camera is pointing), and an up vector.

$$\begin{bmatrix} -0.0500157 & 0.998617 & -0.0162021 & -31.5344 \\ 0.571626 & 0.0559267 & 1.68244 & -4.34301 \\ -0.948731 & -0.0422645 & 0.323746 & 46.4714 \\ -0.945574 & -0.0421239 & 0.322668 & 48.3134 \end{bmatrix}$$

Virtual camera projection matrix: this matrix maps points in 3D space to positions within the image (world coordinates to image coordinates)

Up Vector = $[0.3215397371162876 \quad 0.0314587502141263 \quad 0.9463733642121136]$

Camera Position = $[44.89222251714107 \quad 33.60277592339327 \quad -13.788207729480716]$

Target Vector= $[10.157366563075783 \quad 32.05539098545108 \quad -1.9352587003954866]$

Virtual camera parameters extracted in order to reproject the new image layer

Figure A.3 Thermal image aligned to the virtual camera using the homography below.

$$H = \begin{bmatrix} 0.3724 & -0.0544 & -4.7233 * 10^{-5} \\ 0.0140 & 0.4079 & -9.2933 * 10^{-6} \\ 431.4156 & 69.3016 & 1.00 \end{bmatrix}$$

Thermal to Virtual Camera Homography.

The aligned thermal image mosaic is then reprojected onto the geometric model of the building through the inverse of the virtual camera projection matrix, which transforms image coordinates to world coordinates. As seen in Figure A.4 the thermal image data is layered onto the geometry itself allowing for inspection and measurement from any angle in the 3D model.

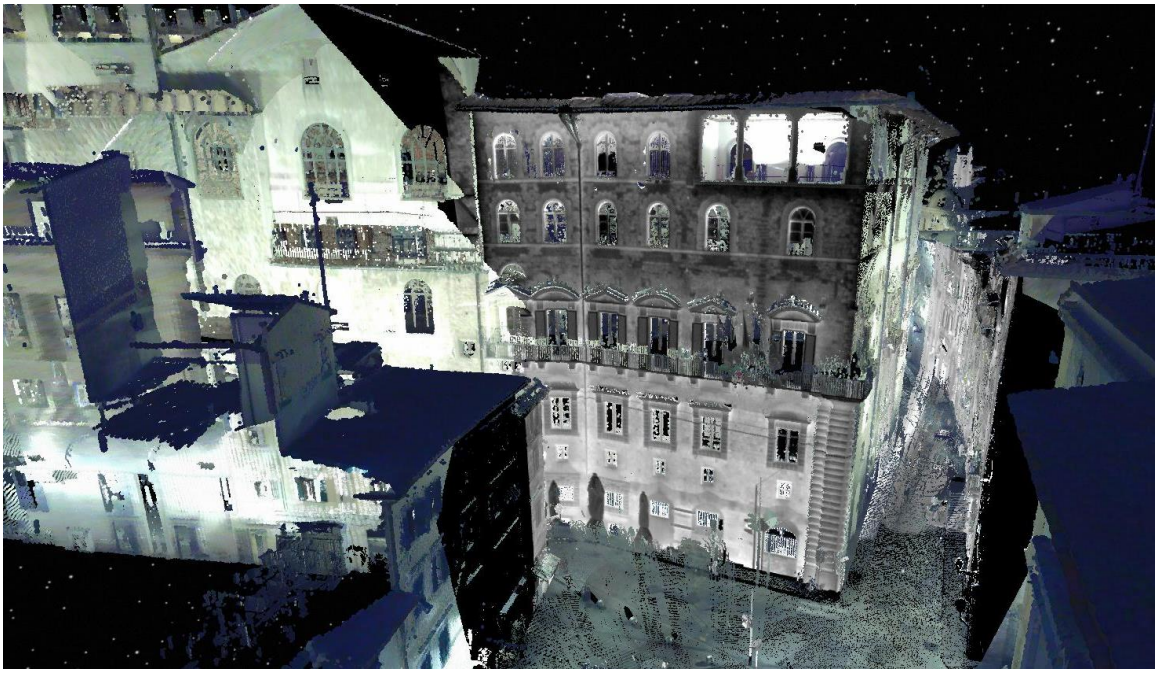

Figure A.4 Thermal image projected onto the geometry of Palazzo Vecchio to enable inspection and measurement.